



Reverse Engineering the SR-71 Blackbird: Flight Stability and Control, and Synthesis

Signatures:

	Name:	Signature:	Dept.:	Date:
Author:	Gayathri Kola		MAE	5/11/2023
Seen:	Dr. Bernd Chudoba		MAE	

Summary:

Aircraft conceptual design is the first step in the design process. It is the foremost planning and evaluation stage that creates a design for a specific purpose. Understanding all aspects of aircraft design is essential to come up with creative yet feasible concepts. This year's Aerospace Engineering senior design course aims to teach students the conceptual design process through the reverse engineering of the SR-71 Blackbird. The iconic Intelligence, Stealth, and Reconnaissance aircraft's design was ahead of its time when introduced back in the 1960s. This high-altitude, long-range, high-speed aircraft was capable of flying at Mach 3+ for hours in the air. This capstone project aims to redesign this aircraft using a sizing methodology known as Hypersonic Convergence. Various sizing methods are evaluated first and compared for pros and cons. A mission profile is created for the flight for a payload of 3000 lb, single pilot using Pratt & Whitney J58 Turbo-Ramjet engines. A total of 9 students work on this project with 7 disciplines. Each student must be responsible for a primary and secondary discipline of the design process. Weekly progress reports are written by the students to record their understanding and findings.

The aircraft conceptual design is split into three sub-phases: Parametric Sizing (PS), Configuration Layout (CL), and Configuration Evaluation (CE). The PS stage utilizes the Hypersonic Convergence methodology to size the vehicle based chosen gross configurations for the vehicle synthesis. For Stability and Control of the aircraft, the control surfaces are sized to meet the flight authority requirements which are further verified using the SR-71 Flight Manual.

The team has taken a different approach where the results from PS are used to grossly size the vehicle. The first configuration focuses on modifying the wing size (the aspect ratio) to perform the first trade study. The configuration is laid out and modified based on takeoff requirements for major disciplines: Performance, Aerodynamics, Propulsion, Weights and Balance and Stability and Control. Wing size is fixed, engines are placed, center of gravity is located, control surfaces are sized, and stability analysis is performed. After which, all teams interact together to calculate necessary parameters for each flight phase. Due to this approach, the CE phase has been only completed up till cruise. Lateral-Directional stability is assessed from takeoff till cruise, and due to the large size of the vertical fins chosen, the vehicle agrees with stability requirements. Although, the methodology can be further refined with higher fidelity methods to yield more accurate results.

Distribution:

Institution:	Dept.:	Name:
The University of Texas at Arlington	MAE	Dr. Bernd Chudoba

 PENGUIN SUPersonic	SENIOR DESIGN: MAE 4351 Project	Ref.: MAE 4351-001-2021 Date: 11. May. 2023 Name: Gayathri Kola Status: In Progress
---	------------------------------------	---

Work Disclosure Statement

The work I performed to document the results presented in this report was performed by me, or it is otherwise acknowledged.

Date: 5/11/2023

Signature:





Table of Contents

WORK DISCLOSURE STATEMENT.....	2
LIST OF FIGURES	5
LIST OF TABLES.....	7
NOMENCLATURE	8
1. INTRODUCTION	10
1.1. HISTORICAL BACKGROUND.....	10
1.2. SR-71 BLACKBIRD	11
1.3. PROJECT SCOPE AND MISSION DETAILS.....	12
1.4. TEAM MANAGEMENT.....	12
2. LITERATURE REVIEW	14
2.1. CONCEPTUAL DESIGN.....	14
2.2. STABILITY AND CONTROL REVIEW.....	16
2.3. SYNTHESIS REVIEW	18
3. DISCIPLINARY ANALYSIS (IDA)	19
3.1. SYNTHESIS MDAS.....	19
3.2. SYNTHESIS IDAS	20
3.3. STABILITY AND CONTROL IDAS.....	21
4. SYNTHESIS.....	22
4.1. BACKGROUND ON SYNTHESIS.....	22
4.2. PARAMETRIC SIZING (PS) FOR SYNTHESIS	26
4.3. CONFIGURATION LAYOUT (CL) FOR SYNTHESIS.....	35
4.4. CONFIGURATION EVALUATION (CE) FOR SYNTHESIS.....	36
4.5. SYNTHESIS CE: MISSION DESCRIPTION.....	37
5. STABILITY AND CONTROL	39
5.1. UNDERSTANDING THE DISCIPLINE	39
5.2. CONFIGURATION LAYOUT (CL) FOR STABILITY AND CONTROL	51
5.3. CONFIGURATION EVALUATION FOR S&C	53
5.4. VERTICAL TAIL SIZING	55
5.5. LATERAL-DIRECTIONAL STABILITY DERIVATIVES FOR CE	64
5.6. LATERAL-DIRECTIONAL STABILITY – MISSION PROFILE DESCRIPTION	66
CONCLUSIONS	ERROR! BOOKMARK NOT DEFINED.
HISTORICAL DEVELOPMENT.....	71
WEEK 1.....	71
WEEK 2.....	71
WEEK 3.....	72
WEEK 4.....	72
WEEK 5.....	72
WEEK 6.....	72
WEEK 7.....	72
WEEK 8.....	72
WEEK 9.....	73
WEEK 10.....	73
WEEK 11.....	73

 PENGUIN SUPersonic	SENIOR DESIGN: MAE 4351 Project	Ref.: MAE 4351-001-2021 Date: 11. May. 2023 Name: Gayathri Kola Status: In Progress
---	------------------------------------	---

WEEK 12.....	73
APPENDIX	73
1. COSTS AND MARKET ESTIMATES APPENDIX.....	73
STABILITY AND CONTROL APPENDIX	74
SYNTHESIS APPENDIX	77
ACKNOWLEDGMENTS	ERROR! BOOKMARK NOT DEFINED.
REFERENCES	93



List of Figures

Fig. 1 The SR-71 Blackbird, during its record-breaking flight in 1990 [1].....	10
Fig. 2 The SR-71 Blackbird and its design features [2].....	11
Fig. 3 The SR-71 Reconnaissance Profile [4].....	12
Fig. 4 Team timeline created by Wesley Junell.....	13
Fig. 5 Penguin Supersonic: Team Roster.....	13
Fig. 6 Stability and Control team breakdown.....	14
Fig. 7 Synthesis team breakdown.....	14
Fig. 8 Aircraft design phases [5].....	15
Fig. 9 Conceptual design phase levels [7].....	15
Fig. 10 Wight and volume budgets for convergence [8].....	16
Fig. 11 Design Team Weekly Meeting Input Categorization.....	16
Fig. 12 Synthesis PS MDA by Wesley Junell [34].....	19
Fig. 13 Synthesis CL MDA by Wesley Junell [34].....	20
Fig. 14 Synthesis CE MDA.....	20
Fig. 15 Synthesis IDA for PS	21
Fig. 16 Stability and Control IDA for CE	21
Fig. 17 Roskam Preliminary Sizing process and Operating Empty Weight estimation [8].....	22
Fig. 18 An example of a matching point diagram to generate a solution space [6].....	23
Fig. 19 Difference between Hypersonic Convergence and classical sizing logic [8].....	24
Fig. 20 Hypersonic convergence design point estimation [8].....	24
Fig. 21 AVD sizing logic [8].....	25
Fig. 22 The SR-71 mission profile created by Phat Nguyen.....	25
Fig. 23 The <i>kw</i> as a function of slenderness ratio for various geometries [19].....	26
Fig. 24 Relationship between slenderness ratio and <i>kw</i> [19].....	26
Fig. 25 The <i>kw</i> as a function of slenderness ratio for various configurations by Austin Prior [35].....	27
Fig. 26 Geometry change based on solution space geometry by Austin Prior [35].....	27
Fig. 27 Fuel fractions for different types of aircraft at various mission phases [29].....	28
Fig. 28 Hypersonic Convergence variables and the relationships [30].....	29
Fig. 29 Coefficient ranges for Weight and Volume Budget equations [33].....	30
Fig. 30 Convergence results from the code written by Wesley Junell [34].....	30
Fig. 31 Initial draft of convergence logic.....	31
Fig. 32 Initial Solution Space (needs to be refined).....	32
Fig. 33 Initial Solution Space (needs to be refined).....	32
Fig. 34 Initial solution space (needs to be refined).....	32
Fig. 35 Convergence Results with landing constraint by Wesley Junell [34]	33
Fig. 36 Redefined Solution Space created by Wesley Junell [34]	34
Fig. 37 3D Solution space generated by Wesley Junell [34]	34
Fig. 38 Initial gross configuration provided by Austin Prior [35]	35
Fig. 39 New Mission Profile by Wesley Junell [34]	37
Fig. 40 Climb Segments by Wesley Junell [34]	37
Fig. 41 Weight change with c.g. location for flight phases by Shiori Jo [38]	38
Fig. 42 Climb profiles for various altitudes [25]	38
Fig. 43 Bank angle versus turn radius for supersonic speeds verification [25]	39
Fig. 44 Neutral point shift from subsonic to supersonic for SR-71 [21].....	40
Fig. 45 Crossflow of streamlines for chines versus a cylindrical fuselage [21].....	40
Fig. 46 Rolling moments of the SR-71 vertical tail with and without canting [21].....	41
Fig. 47 Important non-dimensional parameters and sign convention [5]	41
Fig. 48 Freebody diagram of forces and moments acting on a tailless aircraft [5].....	42
Fig. 49 Flight geometry data for elevon and vertical tail [22]	42
Fig. 50 Translational and rotational stability and control derivatives [9]	43
Fig. 51 Typical vertical tail parameters and geometry [24].....	44
Fig. 52 Control surface design process [24]	45



Fig. 53 Typical values for static and dynamic stability of an aircraft [24].	45
Fig. 54 Horizontal tail setting configurations; (a) Fixed, (b) Adjustable, (c) All-moving [24].	46
Fig. 55 Vertical fin movement of the SR-71 [39].	46
Fig. 56 USAF DATCOM stability equations [26].	46
Fig. 57 MIL-F-8785C Aircraft classes [23].	47
Fig. 58 Stabilizing and de-stabilizing plots with respect to the angle of attack and sideslip [24]	48
Fig. 59 Initial IAO for Stability and Control.	49
Fig. 60 Detailed IAO by the team lead Austin Prior [35].	50
Fig. 61 Parameter breakdown for each phase of Stability and Control [20].	50
Fig. 62 Rolling moment coefficient $Cl\beta VT$ vs. vertical tail area for various vertical c.g. positions.	51
Fig. 63 Vertical tail geometry provided by Austin Prior [35]	52
Fig. 64 Elevon sizing for pitch stability by Noah Blakely [41].	53
Fig. 65 Elevon sizing for pitch stability during cruise by Austin Prior [35]	53
Fig. 66 Yawing moment as a function of sideslip angle for supersonic Mach numbers.....	54
Fig. 67 Static margin as a function of Mach number by Austin Prior [35]	55
Fig. 68 Vertical tail area for different tail configurations by varying tail volume coefficient	56
Fig. 69 Rudder effectiveness chart [24]	57
Fig. 70 Dihedral effect of aspect ratio for given taper ratio and wing sweep angles [27]	58
Fig. 71 Rudder Sizing for One-Engine-Inoperative	59
Fig. 72 Vertical tail geometry variables [24]	59
Fig. 73 Initial vertical tail geometry layout	60
Fig. 74 Right trapezoid for 1st configuration	60
Fig. 75 Generic trapezoid of original SR-71	60
Fig. 76 Trapezoid comparisons	60
Fig. 77 CAD created by Austin Prior based on given estimates of tail geometry [35]	61
Fig. 78 Engine placement dimension given by Austin Prior [35]	61
Fig. 79 Rudder Sizing for OEI	62
Fig. 80 Rudder sizing for Inlet Unstart at Cruise	62
Fig. 81 Rudder sizing for crosswind conditions at takeoff	63
Fig. 82 Weight estimate and C.G. location estimates per flight phase by Shiori Jo [38]	63
Fig. 83 C.G. error based on SR-71 Flight Manual by Shiori Jo [38]	63
Fig. 84 Equations used by NASA LASRE experiment for lateral-directional stability [14]	65
Fig. 85 Baseline SR-71 directional stability derivative for LASRE experiment	66
Fig. 86 Baseline SR-71 dihedral stability derivative for LASRE experiment	66
Fig. 87 Baseline SR-71 rudder effectiveness derivative for LASRE experiment	66
Fig. 88 Baseline SR-71 aileron effectiveness derivative for LASRE experiment	66
Fig. 89 Stability derivatives verification from the LASRE Experiment [14]	66
Fig. 90 SR-71 Turn radius, load factor versus bank angle level 180 turn, provided by Wesley Junell [34]	68
Fig. 91 Yawing moment as a function of sideslip angle for flight phases	70
Fig. 92 Yawing moment as a function of Mach number for flight phases	70
Fig. 93 Rolling moment coefficient as a function of sideslip angle	71
Fig. 94 Initial IAO for Costs and Market Estimates.	74



List of Tables

Table 1. Literature Review for Stability and Control	17
Table 2. Literature Review for Synthesis.	18
Table 3. Parametric Sizing Baseline Configuration and Error by Wesley Junell [Wes, Simon].	33
Table 4. Refined Parametric Sizing Baseline Configuration and Error by Wesley Junell [Wes, Simon].....	34
Table 5. Literature for Synthesis Configuration Evaluation.....	37
Table 6. Important longitudinal and lateral stability derivatives [9].....	44
Table 7. Vertical tail design parameters [27].....	44
Table 8. Lateral-Directional Stability Criteria [5].	48
Table 9. Aircraft similar to SR-71 with delta wings and elevons.	49
Table 10. Airplane Configurations [Chudoba]	52
Table 11. Literature for Stability and Control Configuration Evaluation.....	54
Table 12. Software Review for S&C Configuration Evaluation.....	55
Table 13. Summary of vertical tail sizing for CE.	56
Table 14. Stability and Control Phase Methodology Summary.....	69
Table 15. Aircraft similar to SR-71 with delta wings and elevons.	71
Table 16. Literature Review for Costs and Market Estimates.	73

 PENGUIN SUPersonic	SENIOR DESIGN: MAE 4351 Project	Ref.: MAE 4351-001-2021 Date: 11. May. 2023 Name: Gayathri Kola Status: In Progress
---	--	---

Nomenclature

x	= x-axis distance from aircraft center of gravity to wing aerodynamic center
w	= mean fuselage width
Vol	= fuselage volume
T	= engine thrust
T	= engine thrust
M	= Mach number
h	= mean fuselage depth
d	= maximum fuselage depth
b	= wingspan
z_w	= z-axis distance from the wing root to the fuselage centerline
z_v	= distance of mean aerodynamic chord of the vertical tail to vertical tail projection
q_{VT}	= dynamic pressure of the vertical tail
q_∞	= freestream dynamic pressure
\dot{m}	= engine mass flow rate
l_f	= distance from side force to center of gravity
l_e	= y-axis distance from the fuselage centerline to the engine centerline
l_{VT}	= distance from the center of gravity to the vertical tail center of gravity
c_t	= wing tip chord
c_r	= wing root chord
\bar{c}	= mean aerodynamic chord of the wing
S_{ref}	= wing planform area
S_{refVT}	= reference area of the vertical tail
L_f	= side force on the fuselage
L_{VT}	= side force on the vertical tail
D_e	= engine drag
$C_{n\beta}$	= yawing moment due to side slip angle
$C_{n\beta wing}$	= yawing moment due to the side slip angle of the wing
$C_{n\beta fus}$	= yawing moment due to the side slip angle of the fuselage
C_L	= wing lift coefficient
C_{LaVT}	= lift curve slope of vertical tail based on the vertical tail planform area
$C_{l\beta wing}$	= rolling moment due to the side slip angle of the wing
$C_{l\beta fus}$	= rolling moment due to the side slip angle of the fuselage
\bar{V}_{VT}	= vertical tail coefficient
$C_{l\beta}$	= rolling moment due to side slip angle
$C_{L\alpha}$	= lift coefficient due to the angle of attack
$C_{D\alpha}$	= drag coefficient due to the angle of attack
$C_{m\alpha}$	= pitching moment coefficient due to the angle of attack
C_{Lq}	= lift coefficient due to pitch rate
C_{mq}	= pitching moment coefficient due to pitch rate
$C_{Y\beta}$	= sideforce coefficient due to the angle of sideslip
C_{Yp}	= sideforce coefficient due to roll rate
C_{lp}	= rolling moment coefficient due to roll rate
C_{np}	= yawing moment coefficient due to roll rate
C_{Yr}	= sideforce coefficient due to yaw rate
C_{lr}	= rolling moment coefficient due to yaw rate

 PENGUIN SUPersonic	SENIOR DESIGN: MAE 4351 Project	Ref.: MAE 4351-001-2021 Date: 11. May. 2023 Name: Gayathri Kola Status: In Progress
---	--	---

C_{n_r} = yawing moment coefficient due to yaw rate

Greek symbols

$\Lambda_{c/4}$	= sweep angle at quarter chord
δ_a	= aileron deflection angle
δ_e	= elevator deflection angle
δ_r	= rudder deflection angle
Λ	= wing sweep angle
T	= engine thrust
T	= engine thrust
α	= angle of attack
β	= side slip angle

Acronyms

<i>a.c.</i>	= aerodynamic center
<i>AR</i>	= Aspect Ratio
<i>c.g.</i>	= center of gravity
<i>CD</i>	= Conceptual Design
<i>CL</i>	= Configuration Layout
<i>DD</i>	= Detailed Design
<i>HTHL</i>	= Horizontal Takeoff and Horizontal Landing
<i>IAO</i>	= Input Analysis Output
<i>IDA</i>	= Individual Disciplinary Analysis
<i>LCC</i>	= Life Cycle Cost
<i>MDA</i>	= Multidisciplinary Analysis
<i>np</i>	= neutral point
<i>O&S</i>	= Operations and Support
<i>PD</i>	= Preliminary Design
<i>PS</i>	= Parametric Sizing
<i>S&C</i>	= Stability and Control
<i>SAS</i>	= Stability Augmentation System
<i>SM</i>	= Static Margin
<i>FH</i>	= Flying Hours
<i>MMH</i>	= Maintenance Man Hours
<i>VLM</i>	= Vortex Lattice Method



1. Introduction

Since the 1960s, the Soviet Union, the United States, and the European Union have been competing vigorously in making the fastest, deadliest fighter jets and surveillance aircraft mankind has ever seen. This “arms race” as we call it today, has been an ongoing show of a country’s military strength and rate of innovation in the aerospace and defense industry. To date, one such aircraft has captured the attention of many airplane design enthusiasts. The plane is the iconic SR-71 *Blackbird*, a strategic reconnaissance aircraft designed for stealth during the cold war, back in the 1960s. It flew so fast, to date it’s the fastest Horizontal-Takeoff-Horizontal-Landing (HTHL) aircraft ever built. This was a consequence of the many previous iterations created in order to build a strong, undetectable spy plane.



Fig. 1 The SR-71 Blackbird, during its record-breaking flight in 1990 [1].

1.1. Historical Background

In 1955, the U-2, United States spy plane was shot down by the Soviet Union’s surface-to-air missile, DVINA SA-2 [1]. Until then, the plane was known to reach a high altitude of 70,000 ft which enabled it to escape Russian radars. However, the plane was not as invulnerable as the US government hoped. The plane was already detected by the Soviets, and it was a matter of time before they caught up with deadlier missiles. The need for a special, reconnaissance plane emerged that could stay invisible while it flew along the Soviet Union’s airspace.

Amidst the cold war in 1957, US intelligence obtained news on Soviet Union’s secret Inter-Continental Ballistic Missile development program. This program could hurt US surveillance aircraft like the U-2 with its advanced tracking capabilities. The CIA contracted Lockheed Martin’s Advanced Development Program nicknamed “Skunk Works” for the development of a new, high-speed reconnaissance aircraft, emphasizing a reduced radar signature [2].

This project, led by the infamous aircraft designer, Clarence (Kelly) Johnson, was secretly codenamed Archangel. The plane was to replace the U-2 with higher stealth capability, flying to higher altitudes at supersonic speeds. Initially, the design team at Skunk Works produced 11 different designs: A-1 through A-11 [2]. The best design A-10 was chosen by Kelly Johnson to convince the CIA. However, there was one caveat. The plane A-10 would be bigger, and faster, flying at Mach 3.0 but 100% visible to radar. The CIA pushed back on this design and enforced a strong need for an undetectable spy plane. Kelly Johnson and his design team spent the next several months coming up with a new design that combined some of the stealth aspects from previous iterations.

This new design later went on to have three variants. One for the CIA named A-12, one interceptor prototype with armed air-to-air missiles named YF-12 for the Air Force, and lastly, an unmanned reconnaissance drone to be mounted known as the M-21.



1.2. SR-71 Blackbird

The aircraft we now call the SR-71 was another US Air Force variant of the highly classified A-12 fleet. To reduce the radar signature, engineers at Lockheed had to modify conventional round fuselage designs.

The new SR-71 had a flattened underbelly. This shape deflected the radar signals away from the plane rather than reflecting them to any radar. Chines were added along the fuselage to prove additional lift and stability [2]. This gave the plane the radar profile of a large bird. To reach high altitudes, the plane has to be lightweight and have high strength to withstand temperatures at Mach 3-plus. In those days, Titanium was the only lightweight material that could withstand such high temperatures at approximately 600°C without melting. Completely new forging, refinement, and manufacturing facilities had to be built to allow for the development of SR-71. This made the program very expensive to operate.

For stability, the plane now had elevons with combined aileron and elevator functionality in a single control surface. A single rudder was replaced by two all-moving vertical fins atop the engine nacelles. These fins were canted inward to further reduce radar cross-section.

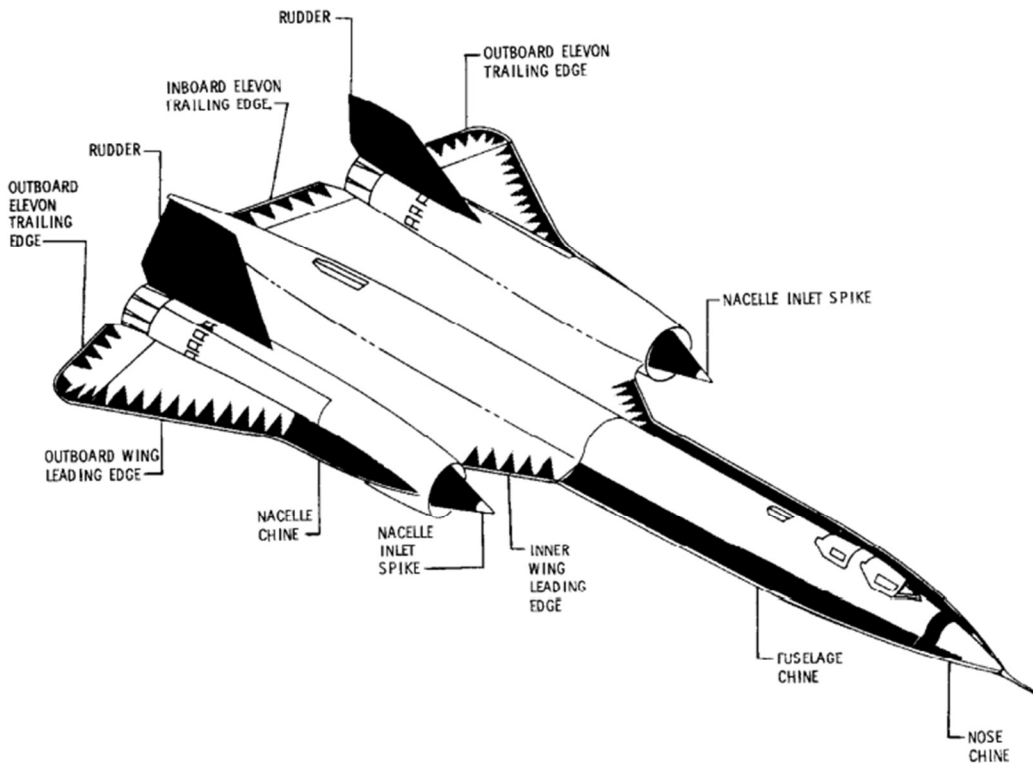


Fig. 2 The SR-71 Blackbird and its design features [2].

To gain more reduction, the wing edges, and control surfaces were made of composite plastic laminates illustrated by triangle patterns in [2]. Since the plane's main purpose is for surveillance operation, there were no onboard air-to-air missiles, and the extra space was used for storing massive amounts of low volatility fuel named JP-7.

The SR-71 used a dual propulsion system resting in a single-engine nacelle. Its Pratt and Whitney J-58 engines behaved like a conventional turbojet below Mach 2.0, enabling takeoff and landing for the aircraft. Once there was enough forward movement of air at the inlet, the engines switched to a ramjet and bypassed the air straight to the afterburner to cruise at supersonic speeds of Mach 3+.

Although detectable, the aircraft was so fast that it could outmaneuver any missile by simply changing its course or climbing higher. This made the SR-71 invulnerable at its time.



1.3. Project Scope and Mission Details

1.1.1. Key Mission Design Parameters

Throughout the semester, the team will perform a literature review and record all the progress in the form of individual/midterm reports. The goal is to reverse engineer the SR-71 through synthesis-based design architecture. The geometry is held constant, but other parameters such as material and propulsion system are to be updated to fit the requirements of modern times. A comparison study is to be performed between the original versus modern design. The mission is to design the aircraft to reach a target altitude of 85,000 ft, taking off from the Edwards Air Force Base main runway with a length of 15,024 ft [3].

1.1.2. Mission Deliverables

The aircraft must be capable of carrying out both single-legged and multi-legged missions carrying a payload of 3,000 lbs and a single pilot with minimum equipment. For a single-legged mission, the aircraft will have to take off, climb, and fly at a target area for one hour and then land safely. In a multi-legged mission, the aircraft will be refueled mid-air at a lower subsonic altitude multiple times before climbing back to the target altitude, thereby increasing its range. A typical SR-71 mission profile is outlined in Fig. 3. The vehicle has to be capable of performing a Horizontal-Takeoff-Horizontal-Landing (HTHL) at the Edwards Air Force base using the original Pratt & Whitney J-58 (JT11D-20) turbo-ramjet engines.

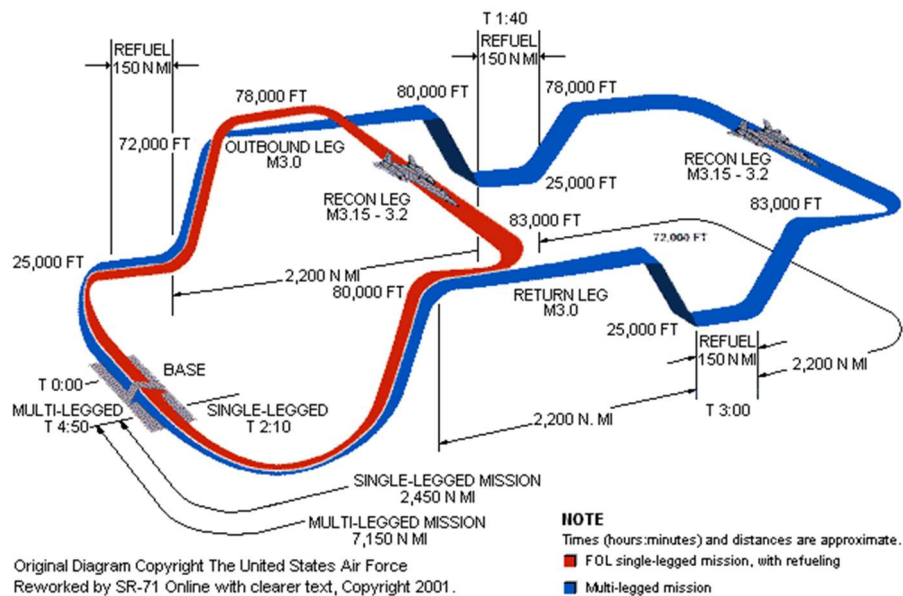


Fig. 3 The SR-71 Reconnaissance Profile [4].

1.4. Team Management

This semester, our senior design team Penguin Supersonic will be reverse-engineering the SR-71 Blackbird to familiarize ourselves with the conceptual design phase of aircraft design. The focus is to recreate the high-speed, high-altitude, long-range SR-71 through detailed analysis and data comparison.

1.4.1. Team Structure

Our team is split into seven divisions, each focusing on different categories of aircraft analysis shown in Fig. 5. The names highlighted in bold are the respective team leads. Each team consists of 2-3 engineers, and each chooses a primary and secondary discipline to focus on.

 PENGUIN SUPersonic	SENIOR DESIGN: MAE 4351 Project	Ref.: MAE 4351-001-2021 Date: 11. May. 2023 Name: Gayathri Kola Status: In Progress
---	--	---

1.4.2. Team Timeline

The Fig. 4 shows the tentative team timeline. The majority of the semester will be spent performing a literature review to find convergence methods, and resources to verify these methods.



Fig. 4 Team timeline created by Wesley Junell.

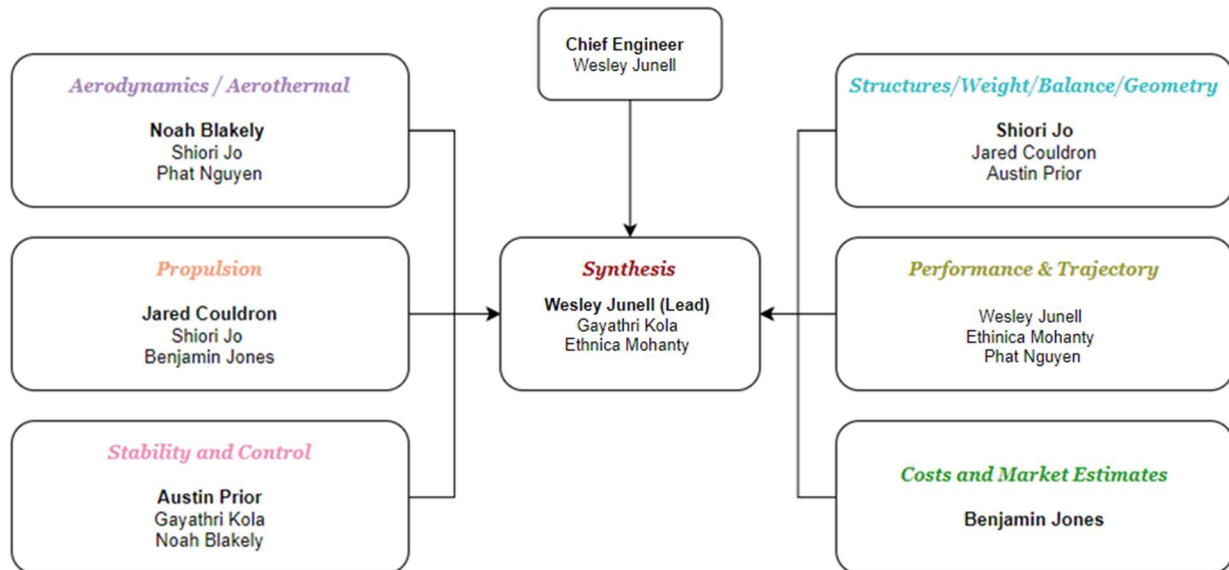


Fig. 5 Penguin Supersonic: Team Roster.

This report will primarily focus on two disciplines: Stability and Control, and Synthesis of SR-71. This section will elaborate on each of the team's responsibilities, references gathered and reviewed literature. Due to a team member dropping out of the course in week 4, the entire team was restructured. The author of this report has been moved from the Costs team to the Synthesis team, due to the current workload.

1.4.3. Stability and Control Team Structure

The primary discipline this report will cover is Stability and Control. Within the discipline, each member of our team is individually focusing on three different topics: longitudinal stability, lateral-directional stability, and controls. This report will focus on categorizing and understanding the lateral and directional stability aspects of SR-71. The breakdown of the Stability and Control team is given below in Fig 6, with the names highlighted in blue. The weekly team meetings will occur on Wednesdays.

 PENGUIN SUPersonic	SENIOR DESIGN: MAE 4351 Project	Ref.: MAE 4351-001-2021 Date: 11. May. 2023 Name: Gayathri Kola Status: In Progress
---	--	---

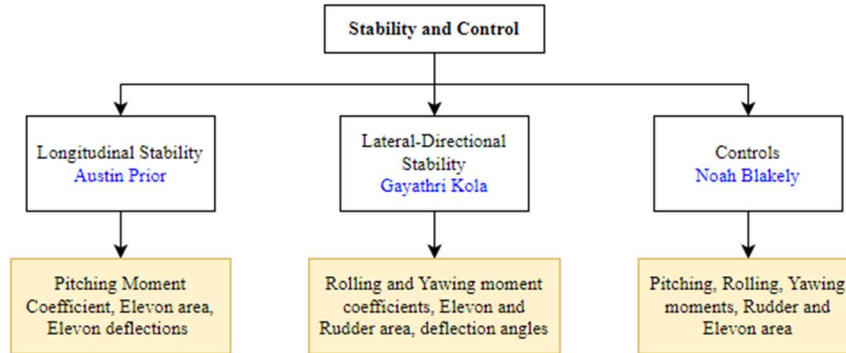


Fig. 6 Stability and Control team breakdown.

1.4.4. Synthesis Team Structure

The secondary discipline this report will cover is Synthesis. The author has been moved to Synthesis due to a lack of team members needed for the current workload. This team's primary goal is to finalize a sizing method for the Parametric Sizing (PS) stage of the Conceptual Design (CD) phase. The author of this report is responsible for the Configuration Evaluation (CE) phase of CD.

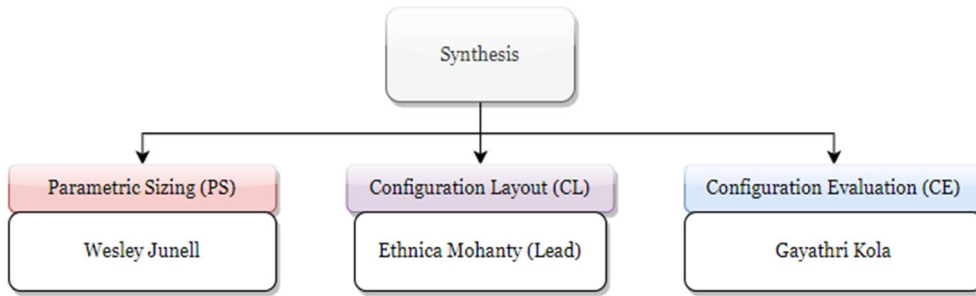


Fig. 7 Synthesis team breakdown.

2. Literature Review

To start, a literature review is performed amongst all disciplines to identify parameters within the team needed for an Input-Analyse-Output (IAO) formation. The section will briefly cover phases of aircraft design and convergence methodology called "Hypersonic Convergence" being considered by the Synthesis team. This will help in developing a base knowledge for the Synthesis team later once the convergence process starts.

2.1. Conceptual Design

Once an aircraft company receives an order from a customer or the military, the design team goes through the first step of assessing the feasibility of the concept. This phase of design where a design is generated, and its feasibility is studied by performing important base calculations is called Conceptual Design (CD). A methodology is developed based on all gathered data from various disciplines and a list of all possible designs is generated. This is the first phase of an aircraft design process followed by Preliminary Design (PD) and Detailed Design (DD).

As the names suggest, PD is a more comprehensive analysis through wind tunnel tests. The engines are selected, and structural loads and stresses are determined. Detailed trade studies are performed. In the DD phase, the best design is finalized and sent to shop rooms to be built. Prototype models are fabricated, and the required hardware is identified. Interiors are laid out; blueprints of hydraulic lines are made, and equipment is mounted in place [5].



Phase 1 Conceptual Design		Phase 2 Preliminary Design	Phase 3 Detail Design
vs		vs 3 deg vs 5 deg	
Known	Basic Mission Requirements Range, Altitude, & Speed Basic Material Properties σ/p E/p $\$/lb$	Aeroelastic Requirements Fatigue Requirements Flutter Requirements Overall Strength Requirements	Local Strength Requirements Producibility Functional Requirements
Results	Geometry Airfoil Type R t/c λ Δ	Design Objectives Drag Level Weight Goals Cost Goals	Basic Internal Arrangement Complete External Configuration <i>Camber & Twist Distribution</i> <i>Local Flow Problems Solved</i> Major Loads, Stresses, Deflections
Output	Feasible Design	Mature Design	Shop Designs
TRL	2 – 3	4 – 5	6 – 7

Fig. 8 Aircraft design phases [5].

The literature review is performed in an effort to identify all the parameters for deriving IDA/MDA methodologies. The CD phase has three levels – Parametric Sizing (PS), Configuration Layout (CL), and Configuration Evaluation (CE). First, in PS, the feasibility of the mission and the size of the vehicle are determined. Second, in CL, different vehicle configurations are addressed, and trade studies are assessed. Lastly in CE, all the selected design concepts and the trade studies are evaluated at current markets [6].

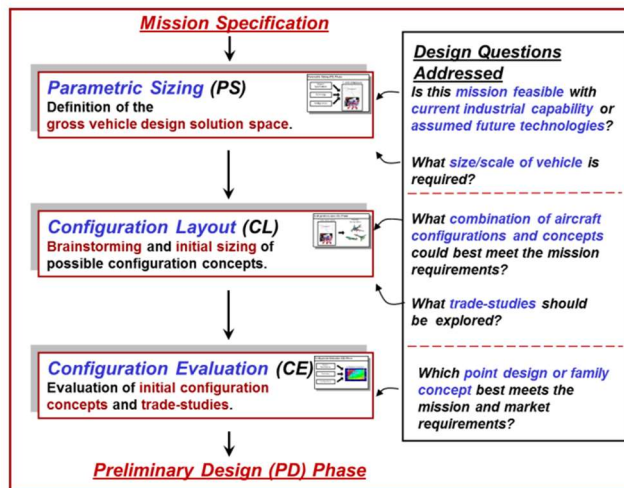


Fig. 9 Conceptual design phase levels [7].

2.1.1. Parametric Sizing

In Parametric Sizing (PS), a design solution space is created. This is categorized as physical, technical, and economical. Next, various tools are identified for carrying out sizing. The most commonly known methods are Loftin Sizing, Roskam Sizing, and hypersonic convergence [8]. These are methods the Synthesis team has to choose from for initial sizing. The last step is to obtain deliverables by making plots that aid in solution space visualization. Each discipline will have to make constraint charts, clearly specifying which region is allowable and where it is unacceptable. The synthesis team will weigh all these discipline constraints together to come up with the size and scale of the prospective vehicle [7]. More details on PS will be discussed in the Synthesis section.

2.1.2. Configuration Layout

In Configuration Layout, alternative designs are identified and narrowed down to the solution space. Then, several creative solutions are tested based on available technology, knowledge, and past experience. Lastly, the prioritized technology matrix, configuration trade matrix, and concept trade matrix are made. This phase will generate a list of possible configurations to be evaluated [7].

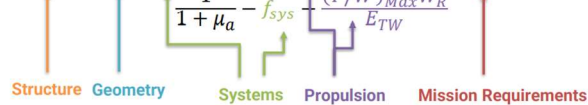
2.1.3. Configuration Evaluation

Lastly, in Configuration Evaluation, as the name suggests different configurations are evaluated to come up with a finalized baseline aircraft. Many tools are used such as computer-integrated synthesis, Roskam II, etc.

Once all methodology is set in place for all disciplines, the Synthesis team will perform a convergence analysis of varying key parameters to obtain a *solution space*. A solution space would be a list of feasible designs that fit within the mission criteria. The goal is to obtain the design with the least weight. Higher fidelity methods are used for accurate analysis.

Weight budget

$$W_{OEW} = \frac{I_{str} K_w S_{pln} + C_{sys} + \frac{(T/W)_{Max} W_R}{E_{TW}} (W_{pay} + W_{crew}) + W_{cprv}}{1 + \mu_a - f_{sys}}$$



Volume budget

$$W_{OWE} = \frac{\tau S_{pin}^{1.5} (1 - k_{vv} - k_{vs}) - v_{fix} + N_{crw}(v_{crw} - k_{crw}) - W_{pay}/\rho_{pay}}{\frac{W_R - 1}{\rho_{ppl}} + (k_{ve} (T/W)_{Max} W_R)}$$

Where:

$$W_{OWE} = W_{OEW} + W_{pay} + W_{crew}$$

Fig. 10 Weight and volume budgets for convergence [8].

During the second week's design team meeting, an attempt was made to categorize inputs required based on range, altitude, speed, endurance, takeoff, and landing in Fig. 11. The goal is to find relevant references for each level of PS, CL, and CE for each sub-discipline.

	Range	Altitude (85,000 ft)	Speed	Endurance	Takeoff and Landing (Edwards AFB)
<i>Weight Change</i>	✓	✓	✓	✓	✓
<i>Lift-to-Drag Ratio (L/D)</i>	✓		✓	✓	
<i>Vehicle Geometry/Materials</i>	✓	✓	✓		✓
<i>Thrust Specific Fuel Consumption</i>	✓			✓	
<i>Lift-curve-slope</i>					✓
<i>Propulsion</i>		✓	✓		

Fig. 11 Design Team Weekly Meeting Input Categorization.

2.2. Stability and Control Review

For the initial references collected, a broad search was performed with keywords such as: 'SR-71', 'Supersonic', 'Stability and Control', 'Trim drag', 'Lateral Stability', 'Airplane Design', etc. Currently, textbooks on stability and control are being reviewed to identify key parameters needed for deriving an Intra-Disciplinary-Analysis/Multi-Disciplinary-Analysis (IDA/MDA) [5,7,18]. Additionally, Table 1 lists all the literature collected so far on this topic.

 PENGUIN SUPERSONIC	SENIOR DESIGN: MAE 4351 Project	Ref.: MAE 4351-001-2021 Date: 11. May. 2023 Name: Gayathri Kola Status: In Progress
---	--	---

Table 1. Literature Review for Stability and Control.

Serial No.	Title	Author	Year	Category
1	Stability & Control of Conventional & Unconventional Aerospace Vehicle Configurations [9]	Chudoba, B.	2019	Book
2	A Generic Stability and Control Tool for Conceptual Design, Prototype Styem Overview [10]	Coleman, G. Chudoba, B.	2007	Book Section
3	Airplane Design Part VII: Determination of Stability, Control, and Performance Characteristics [11]	Roskam, J.	2017	Book
4	Design and Development of the Blackbird: Challenges and Lessons Learned [12]	Merlin, P. W.	2009	Conference Paper
5	Stability and Control Estimation Flight Test Results for the SR-71 Aircraft with Externally Mounted Experiments [2]	Moes, T. R.	2002	Book
6	The Lockheed SR-71 Blackbird – A Senior Capstone Re-Engineering Experience [13]	Mixon, B. Chudoba, B.	2007	Book Section
7	Flight Stability and Control and Performance Results from the Linear Aerospike SR-71 Experiment (LASRE) [14]	Moes, T. Et al.	1998	Conference Paper
8	Supersonic Flying Qualities Experience Using the SR-71 [15]	Cox, T. H. Jackson, D.	1997	Conference Paper
9	The SR-71 Test Bed Aircraft: A Facility for High-Speed Flight Research [16]	Corda, S. Et al.	2000	Technical Paper
10	Examination of Recent Lateral-Stability Derivative Data [17]	Malvestuto, F.	1953	Technical Report
11	Longitudinal Handling Qualities of the Tu-144LL Airplane and Comparisons with Other Large, Supersonic Aircraft [18]	Kuhn, R. E.		Journal
12	Future Spacecraft Propulsion Systems and Integration: Enabling Technologies for Space Exploration [19]	Cox, T. H. Marshall, A.	2000	Article
13	Development of the Vehicle Configuration Compendium: A Comprehensive Data-Information-Knowledge System to Aid in High-Speed Vehicle Design [20]	Czysz, P. Et al.	2018	Book
14	Subsonic Aircraft: Evolution and the Matching of Size to Performance [6]	Simon, S.	2021	Master's Thesis
15	Fundamentals of Aircraft and Airship Design. Volume I – Aircraft Design [5]	Nicolai, L. M.	2010	Book
16	Aircraft Performance and Design [21]	Loftin, L. K.	1980	Book
17	Lockheed SR-71 Blackbird: Flight Manual [22]	Carichner, G.		Webpages
18	Introduction to Aircraft Flight Mechanics, Performance, Static Stability, Dynamic Stability, and Classical Feedback Control [23]	Anderson, J.D. Kucher, P. R. Yechout, T. R. Et al.	1999 2010 2003	Book

2.2.1. Nicolai “Stability and Control” [5]

This book was used as the main textbook for the course. It was used for majority of initial literature understanding of stability and control, from control surface sizing to lateral-directional stability build-up. The chapters of interest are 11, 21, 22, 23. However, the methods mentioned here are too simplistic to apply for a supersonic aircraft that flies above Mach 3. Due to this, additional sophisticated methods were explored in conjunction with this textbook. Many of these design texts have similar methods build-up with slightly different equations. This becomes a challenge if a proper distinction between the methods is not noted since the start.

2.2.2. Aircraft Design – Systems Engineering approach [24]

This book has two excellent chapters on vertical tail design and control surface sizing, namely chapters 16 and 23. The chapter 16 was essential for distinguishing between various tail configurations, tail geometry, and methods for laying out the hinge line for the all-moving vertical tails. Chapter 23 was consulted for control surface sizing criteria, MIL-SPEC regulations summaries, critical conditions that the control surfaces must be sized for. Additionally, this chapter contains methods for dynamic stability analysis that could be utilized.

2.2.3. SR-71 Researcher’s Handbook [25]

This book, along with SR-71 Flight Manual, was mainly used for verification purposes [22]. It has abundant information on the flight operational limits, center of gravity locations, typical mission profile etc. The operational limits section was utilized for getting base estimates of ideal angle of attack ranges, sideslip angle ranges, maximum elevons and rudder deflection angles for various flight phases.

 PENGUIN SUPersonic	SENIOR DESIGN: MAE 4351 Project	Ref.: MAE 4351-001-2021 Date: 11. May. 2023 Name: Gayathri Kola Status: In Progress
---	--	---

2.2.4. USAF Stability and Control DATCOM [26]

This document was initially chosen for its extensive database methods for calculating stability derivatives for various kinds of aircraft configurations, be it total wing, wing-body, wing-body-tail, all-body. Additionally each derivative calculation was split into subsonic, supersonic, transonic and hypersonic regimes. This helps in gaining higher accuracy of the stability calculations. However, the one downside is it requires a large number of inputs and precise geometry knowledge which might not apply to every aircraft. Although initially chosen, this method proved to be tedious, and with limited amount of time, other simpler methods outlined in Nicolai and Raymer were chosen instead [5,27].

2.2.5. Aircraft Design: Conceptual Approach [27]

This text by the author Daniel Raymer has been used primarily for lateral coefficients build-up along with Jan Roskam's Fight Dynamics design text [28]. The text by Raymer appeared to have a more consistent, simpler methodology buildup. There are methods for calculating the tail volume coefficients are different vertical tail configurations from semi-moving to all-moving tails. This has been used initially to estimate the original SR-71's tail volume coefficients and compare it with other types of fighter aircraft.

2.3. Synthesis Review

Below in Table 2 are the references the author has gathered for the Synthesis literature review. The current focus is to obtain enough information on Parametric Sizing (PS). A lot of progress what made during the team meeting of week 4, and attempts were made to obtain a rough constraint diagram by making plots on MATLAB. More about constraint diagrams and synthesis literature is discussed in section IV.

Table 2. Literature Review for Synthesis.

Serial No.	Title	Author	Year	Category
1	Fundamentals of Aircraft and Airship Design. Volume I – Aircraft Design [5]	Nicolai, L. M. Carichner, G.	2010	Book
2	Subsonic Aircraft: Evolution and the Matching of Size to Performance [6]	Loftin, L. K	1980	Book
3	Development of the Vehicle Configuration Compendium: A Comprehensive Data-Information-Knowledge System to Aid in High-Speed Vehicle Design [20]	Simon, S.	2021	Master's Thesis
4	Future Spacecraft Propulsion Systems and Integration: Enabling Technologies for Space Exploration [19]	Czysz, P. Et al.	2018	Book
5	Hypersonic Convergence: Background and Methodology [8]	Ledford, T. Harris, C	2023	Guest Lecture
6	Aircraft Design Part I – Preliminary Sizing of Airplanes [29].	Roskam, J	2012	Series
7	Aircraft Conceptual Design – An Adaptable Parametric Sizing Methodology [30]	Coleman, G	2010	Thesis
8	Synthesis of Subsonic Airplane Design [31]	Torenbeek, E	1982	Book
9	General Aviation Aircraft Design: Applied Methods and Procedures [32].	Gudmundsson, S	2014	Book
10	Scramjet Propulsion: Trans-atmospheric Launcher Sizing [33]	Czysz, P	2013	Book Chapter

2.3.1. Hypersonic Convergence Lecture [8]

This resource is a presentation that encompasses all the required details required for parametric sizing convergence methodologies. It begins by comparing conventional design sizing processes such as Roskam sizing, Loftin sizing, and derives the differences between them and Hypersonic Convergence by Paul. S. Czysz. Additionally, it builds upon this method by introducing AVD sizing that essentially allows for integration of trade studies inclusion within the sizing methodology. This lecture was used primarily for getting started with implementing hypersonic convergence for PS.

2.3.2. Scramjet Propulsion [33]

The original text contains Hypersonic Convergence methodology, this book explains in detail about the methods, its application to different modern aircraft configuration and descriptions of coefficients used. The Synthesis team used this text to obtain ways to calculate the coefficients used in the weight and volume budget equations. More clear definitions of the constants used in the calculations are presented here along with approximate ranges for said constants.

 PENGUIN SUPERSONIC	SENIOR DESIGN: MAE 4351 Project	Ref.: MAE 4351-001-2021 Date: 11. May. 2023 Name: Gayathri Kola Status: In Progress
---	--	--

2.3.3. Future of Spacecraft Propulsion Integration Systems [19]

This text is a more refined version of the Scramjet Propulsion book, contains clear images and relationships for different parameters used in hypersonic convergence such as slenderness ratio for different aircraft geometries. This text was used for the majority of graphical relations for slenderness ratio, structural index, weight and volume budget equations, aerodynamics L/D estimations, etc., to grossly size the vehicle.

2.3.4. Simon's Thesis [20]

This thesis contains many useful comparisons of modern highspeed vehicles, has been especially helpful in gathering resources compiled for SR-71 in the conceptual design phase. For Stability & Control and Synthesis, this paper gives the list of various that are needed for consideration. Specifically for Synthesis, the paper discusses the important aspects of parametric sizing, configuration layout procedure, and configuration evaluation based on each discipline. Further, for configuration evaluation (CE) phase, the paper breakdowns each discipline's important parameters of interest. This paper was consulted for an overall picture of the CE phase in conjunction with Coleman's thesis.

2.3.5. Coleman's thesis [30]

This thesis was used to get a detailed background of the Parametric Sizing (PS) process when Hypersonic Convergence methodology was opted. This paper has helpful function cards, overview cards that give concise description of needed requirements for each discipline. It mainly builds upon AVD sizing, but it can also be used for obtaining coefficient descriptions for Hypersonic Convergence. Important transonic and highspeed commercial aircraft case studies have also been presented in this paper.

3. Disciplinary Analysis (IDA)

3.1. Synthesis MDAs

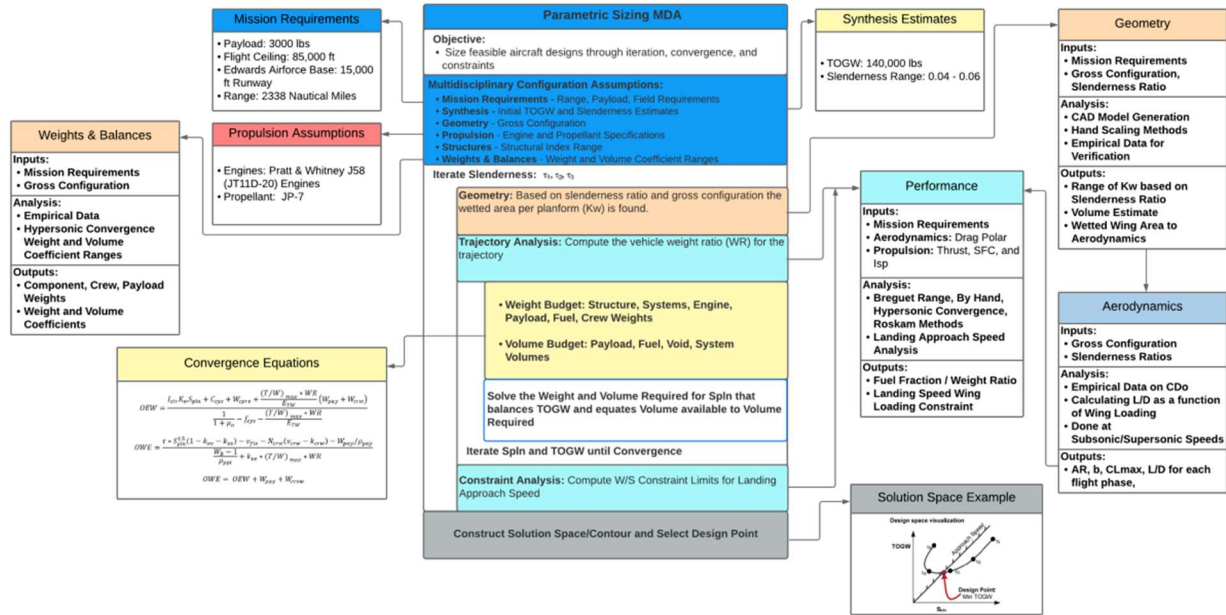


Fig. 12 Synthesis PS MDA by Wesley Junell [34].

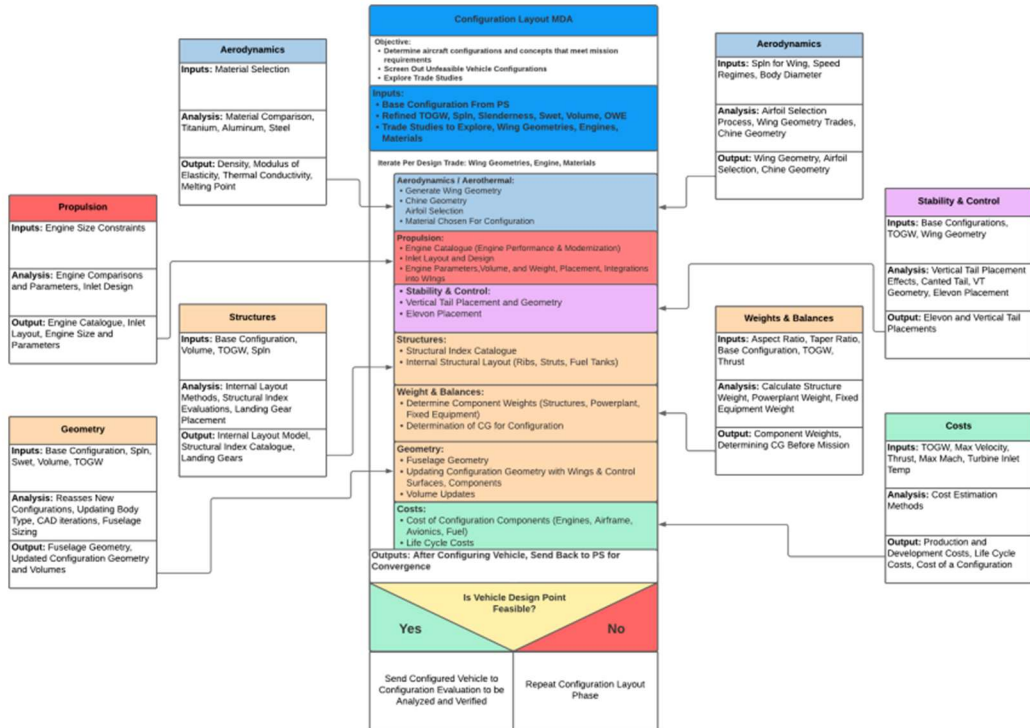


Fig. 13 Synthesis CL MDA by Wesley Junell [34].

Configuration Evaluation (MDA)					
Takeoff	Climb	Cruise	Descent	Landing	
Aircraft geometry refinement					
TO Speed Lift coefficients Drag coefficients Maximum Lift-to-Drag ratio	L/D max Lift curve slopes Drag polaris	CL^1.5/CD cruise angle of attack Lift, drag coefficients	L/D max Lift curve slopes Drag polaris	Maximum angle of attack Landing distance	
Takeoff angle of attack Takeoff rotation Takeoff speed Thrust required	Max nose, inlet temperature Climb angle of attack Climb velocity Stall speed Thrust required	Max nose, inlet temperature Max range, endurance Cruise range, cruise endurance Cruise velocity Thrust required	Descent angle of attack Descent speed Thrust required	Lift coefficients Drag coefficients Maximum Lift-to-Drag ratio	
Engine placement Engine thrust, drag Engine fuel, weight C.G. location Maximum rudder deflection Maximum elevon deflection Elevon, rudder sizing Trim drag Stability Analysis	Engine placement Engine thrust, drag Engine fuel, weight C.G. location Maximum rudder deflection Maximum elevon deflection Elevon, rudder sizing Trim drag Stability Analysis	Engine placement Engine thrust, drag Engine fuel, weight C.G. location Maximum rudder deflection Maximum elevon deflection Elevon, rudder sizing Trim drag Stability Analysis	Engine placement Engine thrust, drag Engine fuel, weight C.G. location Maximum rudder deflection Maximum elevon deflection Elevon, rudder sizing Trim drag Stability Analysis	Engine placement Engine thrust, drag Engine fuel, weight C.G. location Maximum rudder deflection Maximum elevon deflection Elevon, rudder sizing Trim drag Stability Analysis	
Cost Analysis					

Fig. 14 Synthesis CE MDA.

3.2. Synthesis IDAs

 PENGUIN SUPERSONIC	SENIOR DESIGN: MAE 4351 Project	Ref.: MAE 4351-001-2021 Date: 11. May. 2023 Name: Gayathri Kola Status: In Progress
---	--	---

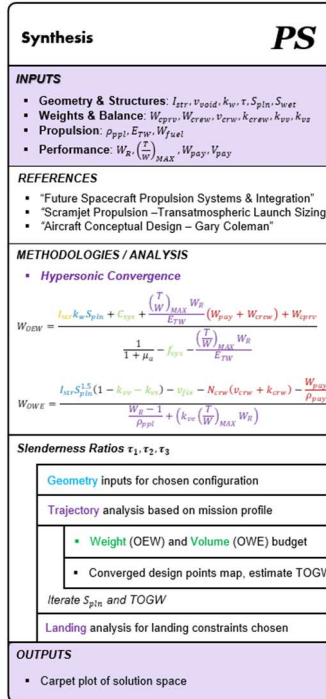
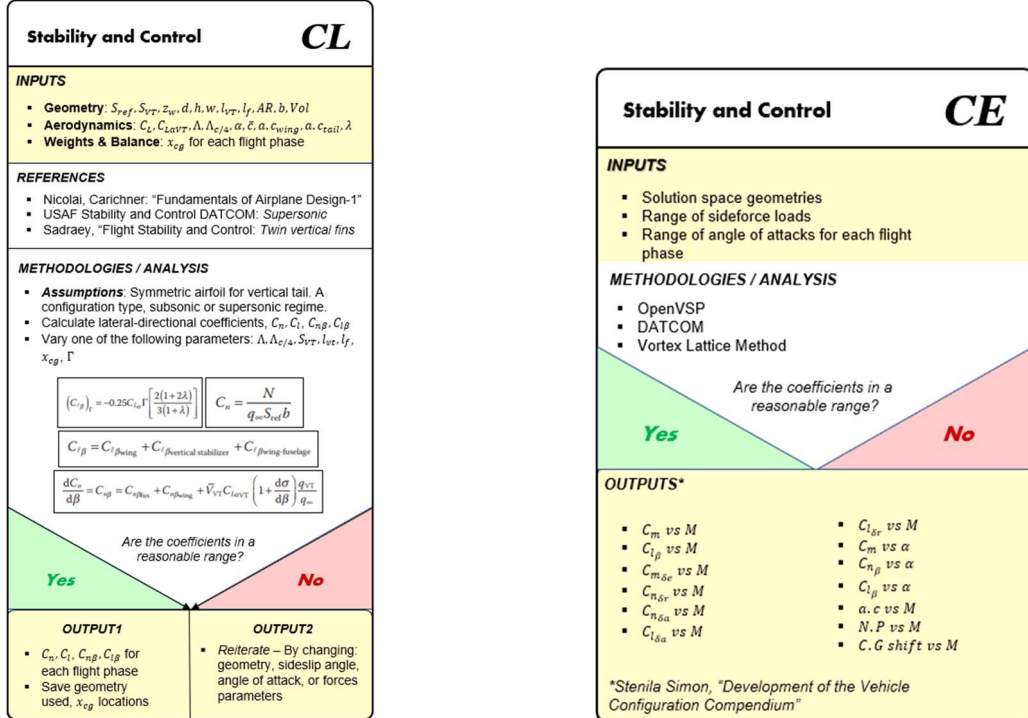


Fig. 15 Synthesis IDA for PS

3.3. Stability and Control IDAs



Stability and Control IDA for CL

Fig. 16 Stability and Control IDA for CE

Stability and Control IDA for CE

Fig. 16 Stability and Control IDA for CE



4. Synthesis

4.1. Background on Synthesis

4.1.1. Understanding the Discipline

Before the author joined this team, the synthesis team was weighing between AVD sizing and Roskam to choose a sizing method. This week, the Synthesis team had chosen Roskam to be the appropriate sizing method. Hence, this section will go into detail about Roskam first and lay out the methodology being tested.

4.1.2. Reference 1: Roskam [29]

Roskam has a simple methodology for the convergence process. It starts by first establishing the mission requirements, design trades, and a mission profile. The mission profile usually consists of phases in this order: takeoff, climb, cruise, loiter/descent, and landing. A broad search is made on similar concepts that were already made. Then, an empirical method is used to estimate the Takeoff-Gross-Weight (TOGW) of the airplane. Roskam presents the following Eq. (1) to estimate TOGW.

$$W_{TO} = W_{OE} + W_F + W_{PL} \quad (1)$$

Where W_{OE} is the Operating Weight Empty (OWE), W_F is the fuel weight and W_{PL} is the weight of the payload. According to Roskam, there is a linear relationship between $\log W_{TO}$ and $\log W_E$ for supersonic cruise airplanes. The initial payload weight needs to be determined. Here, the initial payload weight is given to be 3,000 lb for the mission. Then, an initial guess is made for the takeoff weight, which is later used to determine OWE. This value of OWE is plugged back into Eq. (1) to obtain a new value of TOGW. This TOGW is then iterated until there is a converged solution. The Fig. 17 below illustrates the empirical method used for estimating W_{OE} . Once the TOGW is estimated, a set of constraints are selected for analysis, namely stall, landing distance, takeoff field length, climb gradient, cruise conditions, and maneuvering flight. These constraints are calculated as a function of the wing loading (W/S) and/or thrust loading (T/W). A performance matching diagram is generated with all the constraint plots from which the solution space can be visualized as seen in Fig. 38. The match point is chosen for minimum thrust loading (T/W) to get an estimate of the maximum TOGW needed.

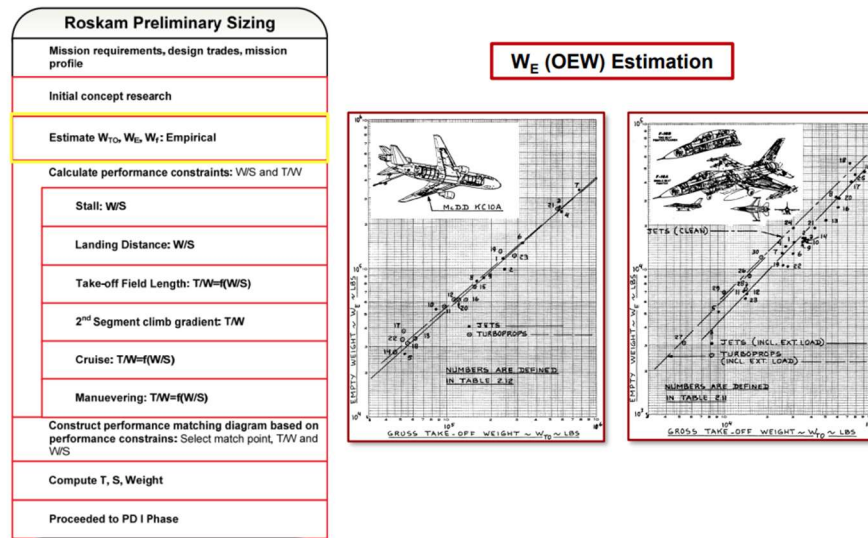


Fig. 17 Roskam Preliminary Sizing process and Operating Empty Weight estimation [8]

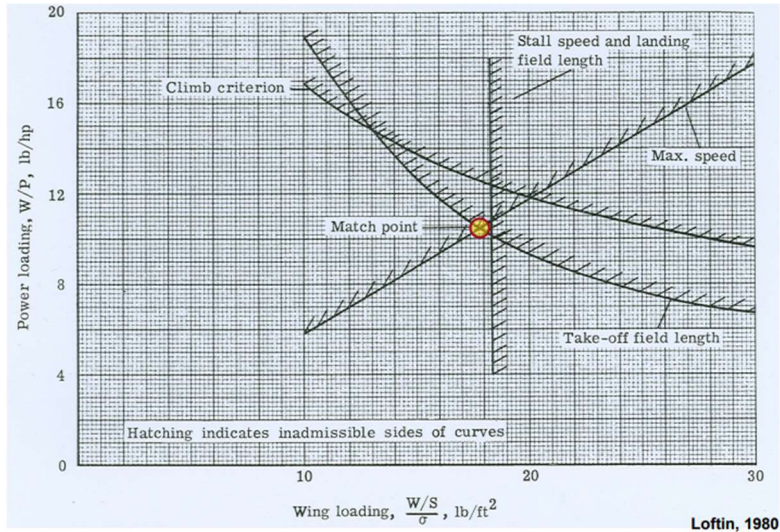


Fig. 18 An example of a matching point diagram to generate a solution space [6].

Once the design match point is chosen, the W/S and T/W are chosen for a TOGW. The new OEW is calculated as a function of TOGW. A new estimate was made for TOGW based on payload weight, fuel weight, and the value of OEW. The convergence will happen when the difference between old TOGW and new TOGW is less than or equal to a specified tolerance. The convergence process for Roskam sizing is long and difficult since a single change in a parameter requires the whole process to be restarted again.

$$|TOGW_{old} - TOGW_{new}| \leq tolerance \quad (2)$$

4.1.3. Reference 2: Hypersonic Convergence [8]

Another method named Hypersonic Convergence was developed by Paul A. Czysz back in 1980. Traditionally, the sizing logic involves first sizing the wing and propulsion system first and later adding fuselage and empennage sizing using empirical methods laid out in methods such as Roskam [29]. However, hypersonic convergence combines the volume of the body into its convergence process. This is done by utilizing two core equations solving for the weight (OEW) and volume (OWE) budget equations given in Eq. (6)-(8). This method introduces a new variable called the slenderness ratio τ . This equates the volume of the vehicle to its planform area. This ratio can be used to estimate how slender an aircraft body is. The higher the value of τ , the larger the vehicle is.

$$\tau = \frac{Vol}{S_{plan}^{1.5}} \quad (3)$$

The following Fig. 39 shows the difference in the process for hypersonic convergence and traditional sizing logic. First, geometry is chosen from a family of configurations outlined by Paul. A. Czysz as seen in Fig. 23. The propulsion system is chosen along with the gross configuration, and other necessary constraints are defined. For the iteration process, first, the geometry is developed based on the chosen slenderness ratio τ . The wetted area per planform area k_w is computed to use in the weight budget equation (Eq. 12). This is different from the classical sizing logic where the thrust loading and wing loading are both iterated to estimate OEW. This would result in a large amount of data to process. For trajectory analysis, the total weight ratio (WR) is obtained by performing calculations for fuel fractions for segments of the flight trajectory. This is an independent analysis that can be performed using methods set out by Roskam, and Loftin, depending on mission requirements and speed regime [6,29].

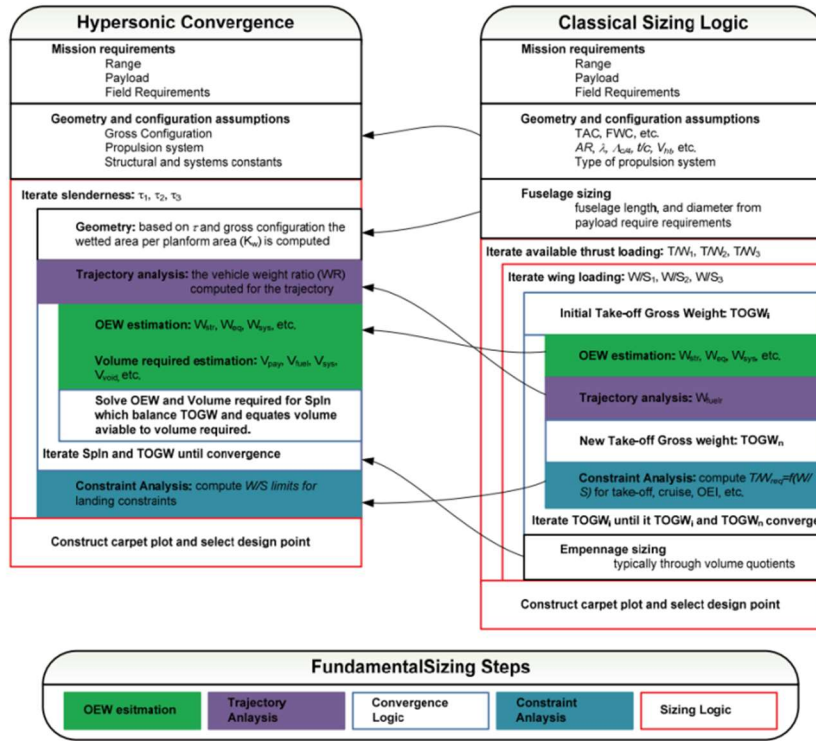


Fig. 19 Difference between Hypersonic Convergence and classical sizing logic [8].

The whole process is iterated for a range of slenderness ratios depending on chosen geometry. Each value of τ has a specific wing loading associated with it. The map of converged design points is produced for each value of τ . Then, the landing constraint analysis is performed such as approach speed for maximum wing loading. For a given planform area, the minimum TOGW is used as the main design point (seen in Fig. 20) and a carpet plot is made showing the solution space.

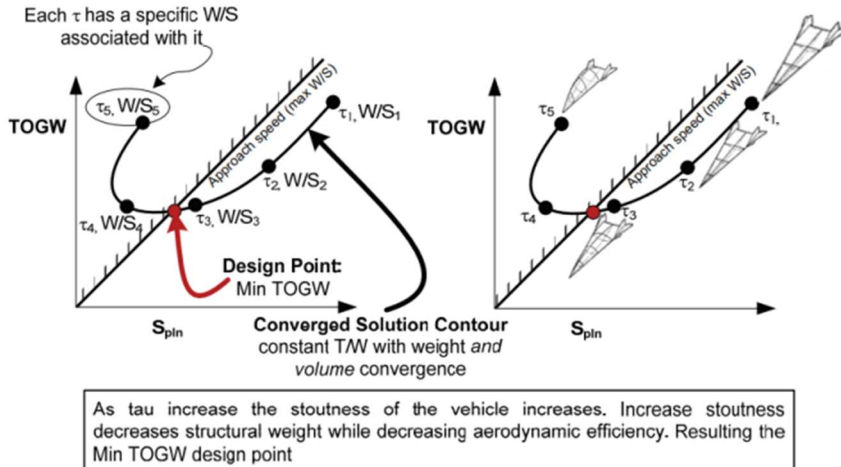


Fig. 20 Hypersonic convergence design point estimation [8].

4.1.4. Reference 3: AVD Sizing [8,20,30]

This method is similar to hypersonic convergence, but it combines the constraint analysis within the convergence logic. This allows for varying a specific independent design parameter such as aspect ratio, taper ratio, leading-edge



sweep, or critical Mach number before iterating for τ . The slenderness ratio is held constant, and the geometry, trajectory, and constraint analysis is performed. The weight and volume budget equations are computed independently, with the planform area being iterated until they converge.

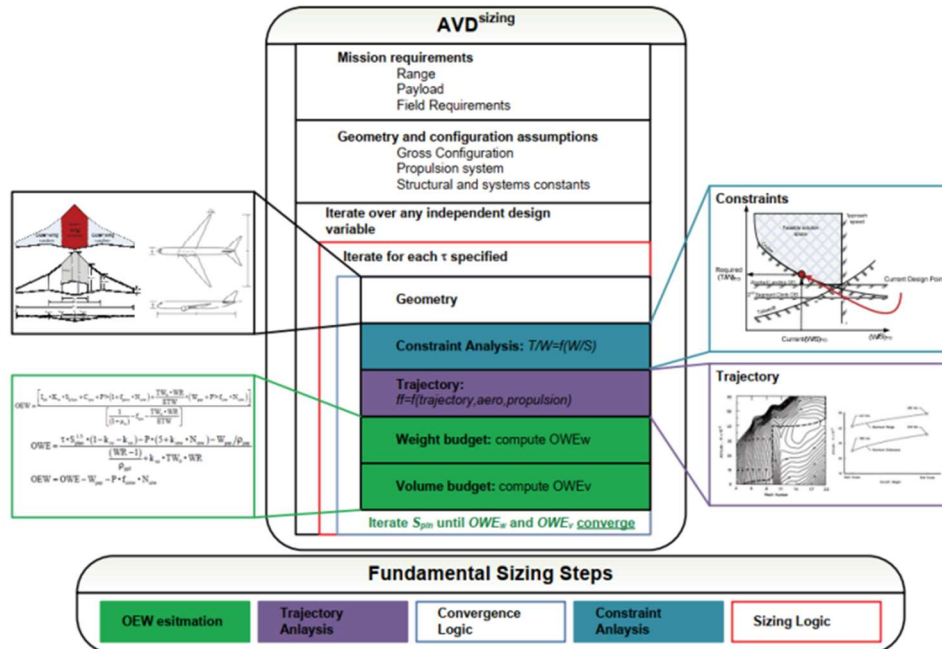


Fig. 21 AVD sizing logic [8].

The Synthesis team has elected to use Hypersonic convergence for the sizing methodology. This methodology was chosen since it is the best way to size the aircraft quickly and reliably. The mission profile was updated after discussing with competing teams to add an accelerated climb segment after takeoff. The PS stage involves constraints analysis where the performance is calculated as a function of W/S (wing loading) and T/W (thrust loading).

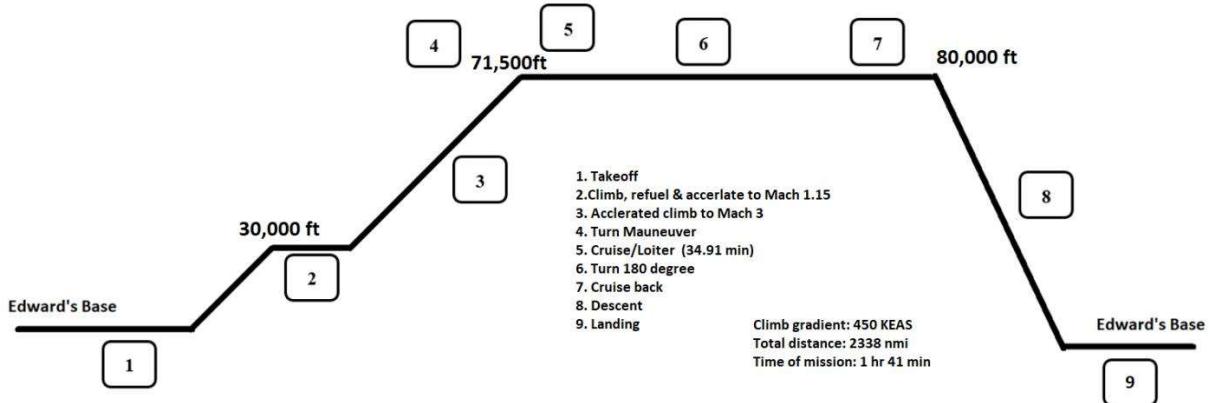


Fig. 22 The SR-71 mission profile created by Phat Nguyen.

4.1.5. Segregating tasks among disciplines

For convergence, the variables in the OWE and OEW equations are identified and segregated among disciplines. The variable names and ranges are given in the Fig. 48. Each discipline must conduct its independent analysis of the required variables to provide a range of suitable values to the Synthesis team. The Synthesis team will use these values by iterating the slenderness ratio to obtain values of TOGW and S_{pln} . A solution space will be obtained for a chosen configuration (examples given in Fig. 20).



4.2. Parametric Sizing (PS) for Synthesis

4.2.1. Estimating Slenderness Ratio (τ)

An initial TOGW guess was taken to be 140,000 lb based on the previous Roskam sizing method. The slenderness ratio can be estimated based on various families of geometries given in the Hypersonic Convergence methodology by Paul A. Czysz [19]. The Fig. 23 below shows the slenderness ratio as a function of the ratio between the wetted area and planform area k_w for multiple geometric configurations.

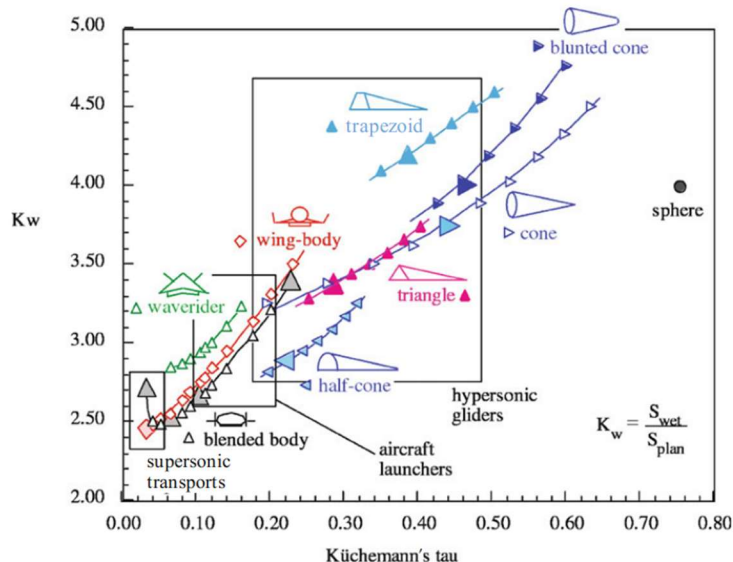


Fig. 23 The k_w as a function of slenderness ratio for various geometries [19].

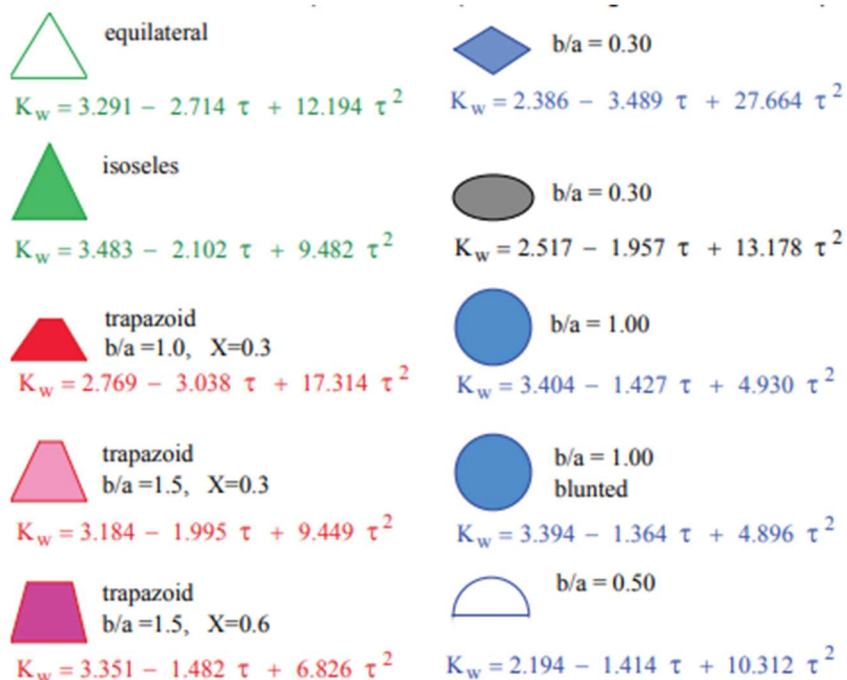


Fig. 24 Relationship between slenderness ratio and k_w [19].

The Geometry team member, Austin, has produced an analysis of slenderness ratio τ for various configurations along with an estimated value of τ based on his CAD model of the SR-71. The Fig. 25 below shows k_w as a function



of τ for various configurations. This is very helpful for having a starting guess of the τ range to be iterated for sizing. Currently, the diamond, half-diamond, and elliptical appear to be the closest to the estimated SR-71 value. The τ range chosen for initial sizing will be from 0 to 0.06. This appears to be falling in the supersonic range as seen in Fig. 23.

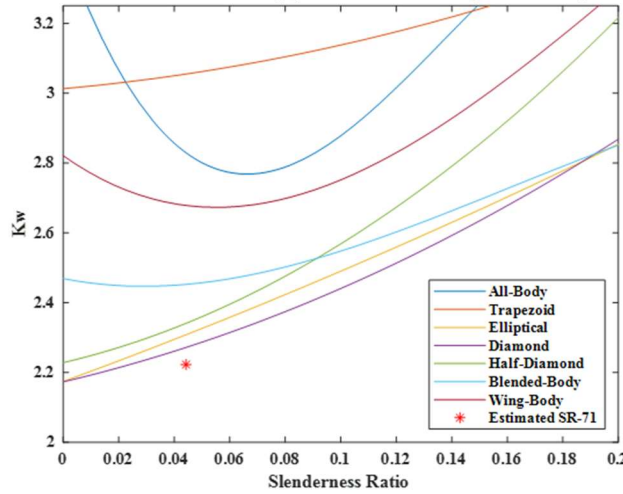


Fig. 25 The k_w as a function of slenderness ratio for various configurations by Austin Prior [35].

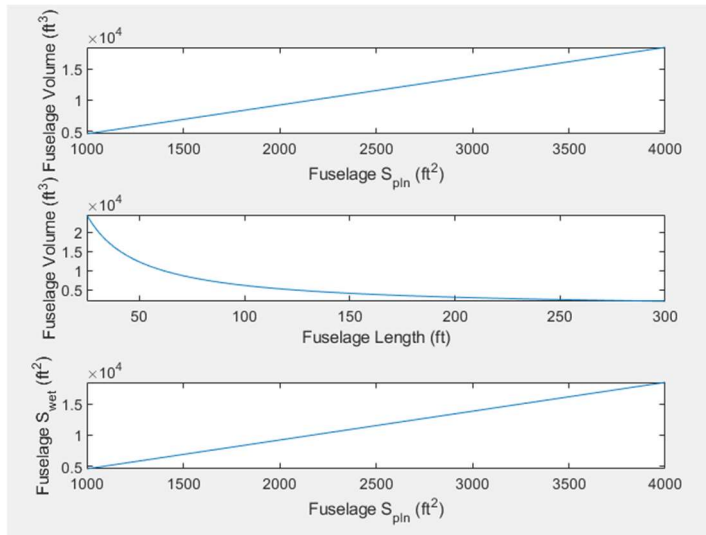


Fig. 26 Geometry change based on solution space geometry by Austin Prior [35].

4.2.2. Trajectory Analysis

The Performance team is tasked with conducting a trajectory analysis based on the chosen mission profile and providing the Synthesis team with the overall Weight-Ratio (WR) for the mission. The performance team is using Roskam as the methodology for performing this analysis. The overall WR will be calculated using the overall fuel fraction using Eq. (4) below.

$$WR = \frac{1}{1 - ff} \quad (4)$$

First, the takeoff weight is estimated using Eq. (4)-(5) below is used to estimate OWE.

$$W_{OE} = W_E + W_{tfo} + W_{crew} \quad (5)$$

 PENGUIN SUPERSONIC	SENIOR DESIGN: MAE 4351 Project	Ref.: MAE 4351-001-2021 Date: 11. May. 2023 Name: Gayathri Kola Status: In Progress
---	--	---

Where W_E is the empty weight, W_{tfo} is the trapped fuel and oil, and W_{crew} is the weight of the crew. The fuel weight W_F is estimated using the fuel-fraction method outlined in Roskam [29]. A MATLAB code was made by the chief engineer Wesley Junell to estimate the overall fuel fraction based on methods given in Roskam [34]. The Fig. 27 below can be used to estimate fuel fractions for a supersonic cruise based on mission phases. The numbers associated with each flight phase can be used to calculate the beginning and end weights.

Table 2.1 Suggested Fuel-Fractions For Several Mission Phases

Mission Phase No. (See Fig. 2.1)	1	2	3	4	7	8
Airplane Type:	Engine Start, Warm-up	Taxi	Take-off	Climb	Descent	Landing Taxi, Shutdown
1. Homebuilt	0.998	0.998	0.998	0.995	0.995	0.995
2. Single Engine	0.995	0.997	0.998	0.992	0.993	0.993
3. Twin Engine	0.992	0.996	0.996	0.990	0.992	0.992
4. Agricultural	0.996	0.995	0.996	0.998	0.999	0.998
5. Business Jets	0.990	0.995	0.995	0.980	0.990	0.992
6. Regional TBP's	0.990	0.995	0.995	0.985	0.985	0.995
7. Transport Jets	0.990	0.990	0.995	0.980	0.990	0.992
8. Military Trainers	0.990	0.990	0.990	0.980	0.990	0.995
9. Fighters	0.990	0.990	0.990	0.96-0.90	0.990	0.995
10. Mil. Patrol, Bomb, Transport	0.990	0.990	0.995	0.980	0.990	0.992
11. Flying Boats, Amphibious, Float Airplanes	0.992	0.990	0.996	0.985	0.990	0.990
12. Supersonic Cruise	0.990	0.995	0.995	0.92-0.87	0.985	0.992

Fig. 27 Fuel fractions for different types of aircraft at various mission phases [29].

4.2.3. Weight and Volume budgets

The weight and volume budget equations, OEW and OWE are solved for the planform area for a specific TOGW. The following are the weight W_{OEW} and volume W_{OWE} budget equations used in the convergence process. The variables are color-coded to indicate the category associated with them.

$$W_{OEW} = \frac{I_{str} k_w S_{pln} + C_{sys} + \frac{\left(\frac{T}{W}\right)_{MAX} W_R}{E_{TW}} (W_{pay} + W_{crew}) + W_{cprv}}{\frac{1}{1 + \mu_a} - f_{sys} - \frac{\left(\frac{T}{W}\right)_{MAX} W_R}{E_{TW}}} \quad (6)$$

$$W_{OWE} = \frac{I_{str} S_{pln}^{1.5} (1 - k_{vv} - k_{vs}) - v_{fix} - N_{crw} (v_{crw} + k_{crw}) - \frac{W_{pay}}{\rho_{pay}}}{\frac{W_R - 1}{\rho_{ppl}} + \left(k_{ve} \left(\frac{T}{W}\right)_{MAX} W_R \right)} \quad (7)$$

$$W_{OWE} = W_{OEW} + W_{pay} + W_{crew} \quad (8)$$

The variable I_{str} is the structural index, the ratio between structural weight W_{str} and wetted area S_{wet} of the aircraft. The structural weight can be calculated using the following equation below:

$$W_{str} = k_{str} * S_{pln}^{1.38*OEW} \quad (9)$$

The list of variables and their relations to hypersonic convergence are given in Fig. 28. The coefficients with no relationship such as the fuel density, payload density, etc, are estimated based on the type of vehicle.



Table 4-1: Weight and Volume Budget Terms from Hypersonic Convergence⁽⁶⁴⁾

Variable	Description	Hypersonic Convergence Relationship
Weight Budget		
W_{str}	Structural weight	$W_{str} = I_{str} S_{wet}$
W_{sys}	Systems weight	$W_{sys} = C_{sys} + f_{sys} W_{OWE}$
W_{eng}	Engine weight	$W_{eng} = \frac{T/W \cdot WR}{E_{TW}} OWE$
C_{sys}	Constant systems weight	-
f_{sys}	Variable systems weight	-
E_{TW}	Engine thrust to weight ratio	
I_{str}	Structural index	See methods library
Volume Budget		
V_{fuel}	Fuel volume	$V_{fuel} = \frac{OWE \cdot (WR - 1)}{\rho_{fuel}}$
V_{fix}	Fixed system volume	$V_{fix} = V_{un} + V_{options}$
V_{sys}	Total system volume	$V_{sys} = V_{fix} + k_{vs} V_{tot}$
V_{eng}	Engine volume	$V_{eng} = k_{ve} \cdot T / W \cdot WR \cdot OWE$
V_{void}	Void volume	$V_{void} = k_{vv} V_{tot}$
V_{pay}	Payload volume	$V_{pay} = W_{pay} / \rho_{pay}$
V_{crw}	Crew volume	$V_{crw} = k_{crw} N_{crw}$
V_{tot}	Total volume	$V_{tot} = \tau \cdot S_{pln}^{1.5}$
V_{un}	Unused volume	-
$V_{options}$	Operational items volume	-
ρ_{fuel}	Fuel density	-
ρ_{pay}	Payload density	-
k_{ve}	Engine volume coefficient	-
k_{vv}	Void volume coefficient	-
k_{vs}	Variable systems volume	-

Fig. 28 Hypersonic Convergence variables and the relationships [30]

For an initial estimate of the values, Fig. 29 helped obtain some of the ranges.

$$W_{str} = I_{str} \cdot K_w \cdot S_{pln} + W_{cpnv} \quad 17 \leq I_{str} \leq 23 \text{ kg/m}^2$$

$$W_{sys} = C_{sys} + f_{sys} \cdot W_{dry} \quad 0.16 \leq f_{sys} \leq 0.24 \text{ ton/ton}$$

$$C_{sys} = C_{un} + f_{mnd} \cdot N_{crw} \quad 1.9 \leq C_{un} \leq 2.1 \text{ ton}$$

$$1.45 \leq f_{mnd} \leq 1.05 \text{ ton/person}$$

$$W_{eng} = \frac{TW_0 \cdot WR}{E_{TW}} \cdot (W_{dry} + W_{pay} + W_{crw}) \quad 10 \leq E_{TW} \leq 25 \text{ kg thrust/kg weight}$$

$$W_{cpnv} = f_{cpnv} \cdot N_{crw} \quad 0.45 \leq f_{cpnv} \leq 0.50 \text{ ton/person}$$

$$W_{crw} \cdot N_{crw} \quad 0.14 \leq f_{crw} \leq 0.15 \text{ ton/person}$$

 PENGUIN SUPersonic	SENIOR DESIGN: MAE 4351 Project	Ref.: MAE 4351-001-2021 Date: 11. May. 2023 Name: Gayathri Kola Status: In Progress
---	------------------------------------	---

$V_{\text{tot}} = \tau \cdot S_{\text{pln}}^{1.5}$	$0.032 \leq \tau \leq 0.20$
$V_{\text{ppl}} = W_{\text{OE}} \cdot \frac{(WR - 1)}{\rho_{\text{ppl}}}$	$5.0 \leq V_{\text{un}} \leq 7.0 \text{ m}^3$
$V_{\text{fix}} = V_{\text{un}} + f_{\text{crw}} \cdot N_{\text{crw}}$	$11.0 \leq f_{\text{crw}} \leq 12 \text{ m}^3 / \text{person}$
$V_{\text{sys}} = V_{\text{fix}} + K_{\text{vs}} \cdot V_{\text{tot}}$	$0.02 \leq k_{\text{vs}} \leq 0.04 \text{ m}^3/\text{m}^3$
$V_{\text{eng}} = k_{\text{ve}} \cdot TW_0 \cdot W_R \cdot W_{\text{OE}}$	$0.25 \leq k_{\text{ve}} \leq 0.75 \text{ m}^3/\text{ton thrust}$
$V_{\text{void}} = k_{\nu\nu} \cdot V_{\text{tot}}$	$0.10 \leq k_{\nu\nu} \leq 0.20 \text{ m}^3/\text{m}^3$
$V_{\text{pay}} = W_{\text{pay}}/\rho_{\text{pay}}$	$48 \leq \rho_{\text{pay}} \leq 130 \text{ kg/m}^3$
$V_{\text{crw}} = (V_{\text{pcrv}} + k_{\text{crw}}) \cdot N_{\text{crw}}$	$0.9 \leq k_{\text{crw}} \leq 2.0 \text{ m}^3/\text{person}$
	$6.0 \leq V_{\text{pcrv}} \leq 5.0 \text{ m}^3/\text{person}$

Fig. 29 Coefficient ranges for Weight and Volume Budget equations [33].

4.2.4. Solution Space for PS – Iteration 1

A baseline code was developed using the lowest values in the coefficient ranges with no iterations. The Synthesis team has been developing code to make a solution space for PS stage. A convergence was achieved from the code written by the chief engineer, Wesley Junell [34]. The code is further being developed to make a solution space with all possible design by the author. Following are the main assumptions and inputs used (rest is listed in the code in Appendix C):

- TOGW(initial) = 140,000 lb
- Tau = 0.05
- Splt = 2396 ft² from Geometry
- Payload Weight (W_{pay}) = 3,000 lb
- Crew Weight (W_{crew}) = 258 lb
- Thrust Required (T_{req}) = 40,000 lb (refine)
- No. of crew = 1

```

For given tau: 0.05

The TOGW is: 140592 lbs and the Planform Area is: 2871 ft^2

```

Fig. 30 Convergence results from the code written by Wesley Junell [34].

The code has a long runtime for a τ value of 0.04 and the Thrust Required value of 19,318 lb. The issue is unknown and needs to be refined further. It is assumed that the while loop is executing continuously due to the MATLAB function fzero(). This function is similar to goal seek where it guesses a single variable until a condition is met.

Below is the layout for convergence logic. The author was having difficulty in stopping the while loop, even with break/continue statements. The Required Thrust was changed to 19,318 lb, more suited for the mission. The initial Thrust Required of 40,000 lb no longer works with the solution space code. More modifications were made to the values to suit the configuration's needs.

The following was the buildup used for generating the solution space code.

- OEW (Weight budget) = TOGW(old)
- OWE (Volume budget)
- OEW1 = OEW + $W_{\text{pay}} + W_{\text{fuel}}$
- $OEW = f(I_{\text{str}}, k_w, S_{\text{pln}}, C_{\text{sys}}, \left(\frac{T}{W}\right), W_R, E_{\text{TW}}, W_{\text{pay}}, W_{\text{crew}}, W_{\text{cpnv}}, f_{\text{sys}})$



- $OWE = f \left(\tau, S_{pln}, k_{vv}, k_{vs}, v_{fix}, N_{crew}, V_{crew}, k_{crew}, W_{pay}, \rho_{pay}, W_R, \rho_{ppl}, k_{ve}, \left(\frac{T}{W} \right) \right)$
- Tolerance = 0.00001
- $OWE = OEW + W_{pay} + W_{crew}$, (OEW has new S_{pln})
- $TOGW_{new} = W_{pay} + W_{fuel} + OEW$
- $TOGW_{new} = W_{pay} + W_{fuel} + (ff * TOGW)$
- $TOGW = OWE * W_R$
- $TOGW_{new} = (OEW + W_{pay})W_R$
- $(TOGW_{new} - TOGW_i) > 0.005 TOGW_i$
- Either choose an error of 0.5 % or 0.01%

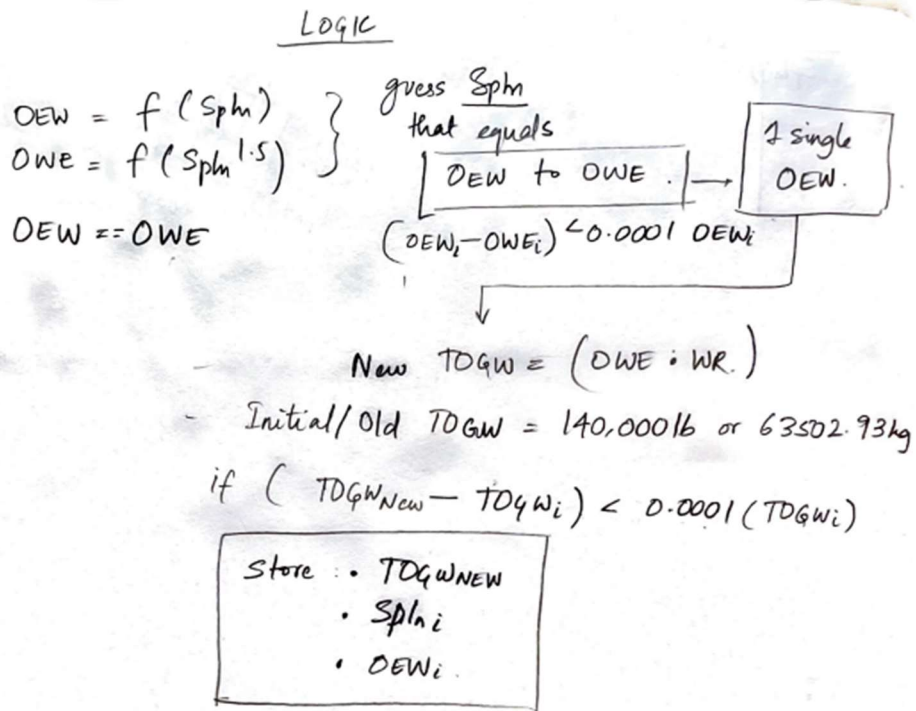


Fig. 31 Initial draft of convergence logic.

The author was looking into ways to debug the code. At first, the solution was to pause the code and plot the results. Following are the assumptions made for the code:

- $TOGW(\text{initial}) = 140,000 \text{ lb}$
- τ range = 0.04 to 0.06, 0.001 increments
- $Spln$ = 2,200 to 2,600 ft^2 , 100 increment
- Payload Weight (W_{pay}) = 3,000 lb
- Crew Weight (W_{crew}) = 258 lb
- Thrust Required (T_{req}) = 19,318 lb (refine)
- No. of crew = 1

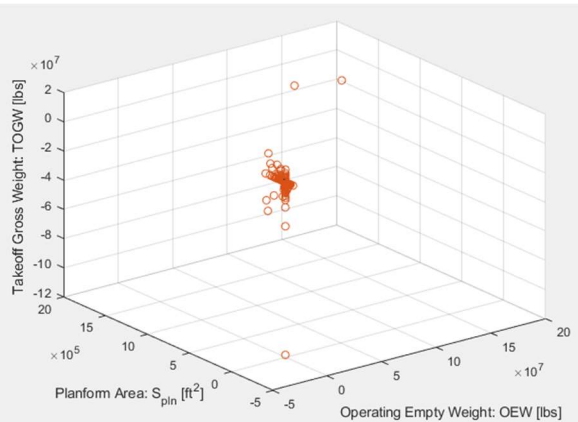


Fig. 32 Initial Solution Space (needs to be refined).

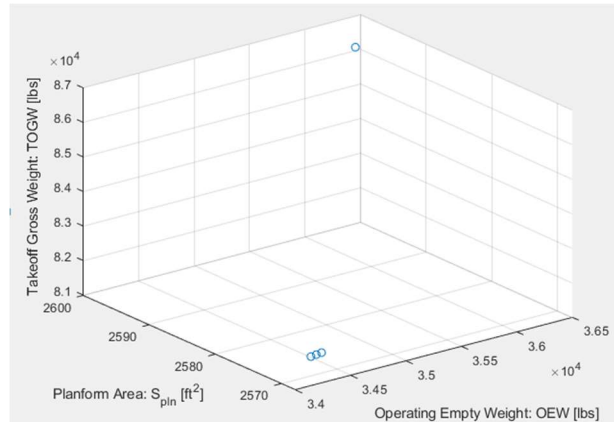


Fig. 33 Initial Solution Space (needs to be refined).

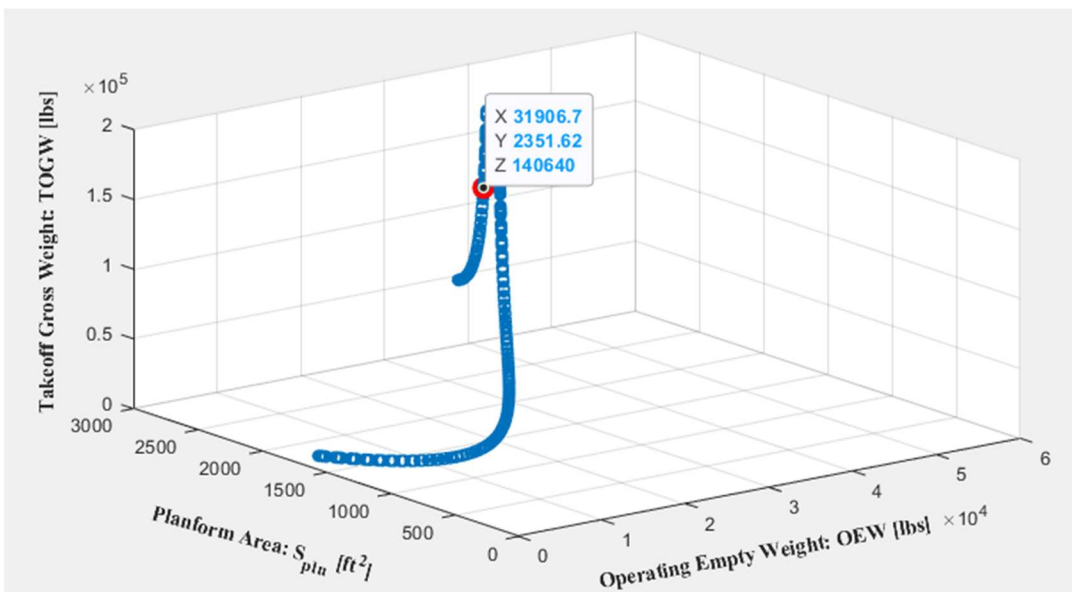


Fig. 34 Initial solution space (needs to be refined).

Some of the concerns with solution space above is that the OEW is quite low compared to initial values. The following are the verification numbers of the original SR-71.

- TOGW = 170,000 lbs
- Engine thrust = 34,000 lbs
- OEW = 59,000 lbs

The Fig. 32-Fig. 34 are not the anticipated form of a solution spaces. The plots are suspected to be wrong, and the code needs to be rechecked and updated so that the points are in the form of slightly curved lines. The Fig. 32 shows the initial solution space without any axis bounds. The values of TOGW are even largely negative, which is not realistic and further clarifies it is wrong.

4.2.5. Solution Space for PS – Iteration 2

The initial solution space was corrected by removing the loops and making the convergence logic produced by Wesley Junell into a function file. A main script was made to iterate slenderness ratio and planform area. A landing constraint code was produced by Performance team member Phat Nguyen [36]. However, initially the constraint appeared to have very high TOGW starting number of 150,000 lbs, which was not feasible since convergence code results barely reached upto 150,000 lbs. The code was further modified to produce the results below. This plot does not appear to be right since the landing constraint (wing loading) appears to have fairly low numbers compared to



TOGW. The intersection point was extrapolated by Wesley and the percentage errors were assessed using SR-71 data from Stenila Simon's [20,34].

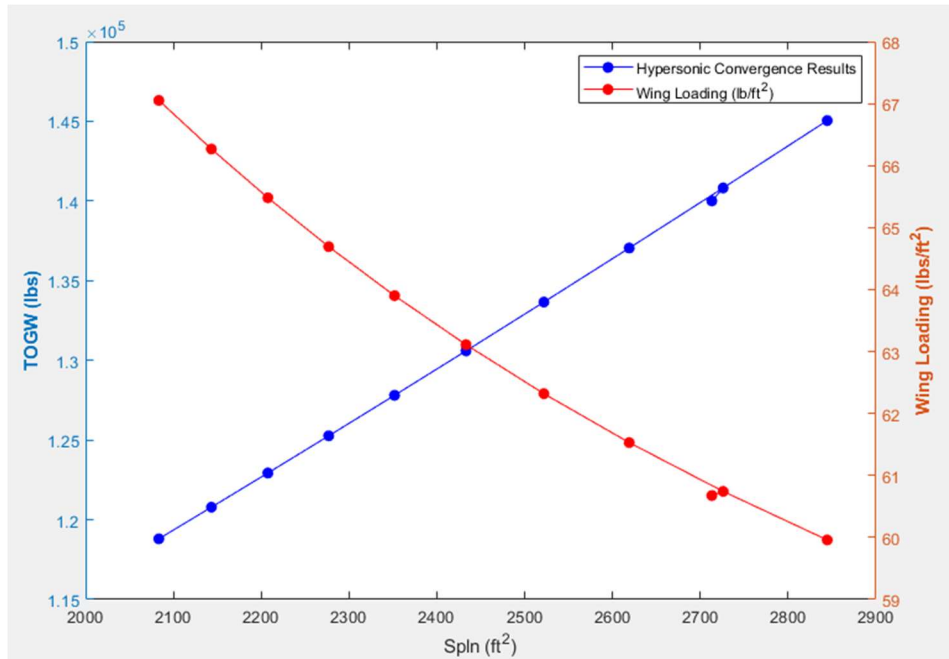


Fig. 35 Convergence Results with landing constraint by Wesley Junell [34].

Table 3. Parametric Sizing Baseline Configuration and Error by Wesley Junell [34].

Variable	Current Value	SR-71 Data	Percent Error %
TOGW	130,592 lbs	140,853 lbs	7.29
Splt	2,433 ft ²	2,491 ft ²	2.33
tau	0.049	0.0442	10.85
Swing	1,763 ft ²	1.795 ft ²	1.78
OEW	58,835 lbs	56,203 lbs	4.68
OWE	55,335 lbs	60,203 lbs	8.08
Kw	2.34	2.6	10
Wing Loading	63.11 lbs/ft ²	78.5 lbs/ft ²	19.61
Stall Speed	369.54 ft/s	-	-

4.2.6. Solution space for PS – Iteration 3

A new solution space was produced by the chief engineer Wesley. The landing constraint was corrected to being at a TOGW of 50,000 lbs. Below in Fig. 36 is the new solution space with the updated landing constraint.

To make a solution space with carpet plots, the last chapter of Nicolai book was referenced for build-up [5].The carpet plots are made by changing one constant value and plotting multiple curves.

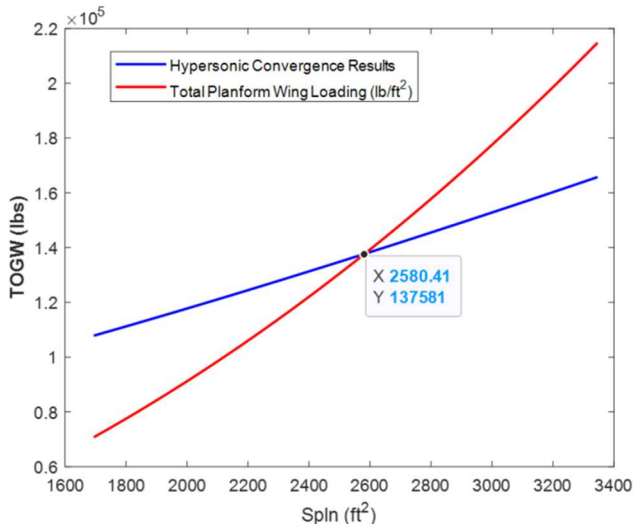


Fig. 36 Redefined Solution Space created by Wesley Junell [34].

Table 4. Refined Parametric Sizing Baseline Configuration and Error by Wesley Junell [20,34].

Variable	Current Value	SR-71 Data	Percent Error %
TOGW	137,581 lbs	140,853 lbs	2.32
Spln	2,580 ft ²	2,491 ft ²	3.57
tau	0.0457	0.0442	3.39
Swing	1,869 ft ²	1,795 ft ²	4.12
OEW	61,012 lbs	56,203 lbs	8.56
OWE	57,512 lbs	60,203 lbs	4.47
Kw	2.33	2.60	10.38
Wing Loading	73.61 lbs/ft ²	78.5 lbs/ft ²	6.23
Total Planform Wing Loading	53.3 lbs/ft ²	56.5 lbs/ft ²	5.66
Stall Speed	339.47 ft/s	-	-

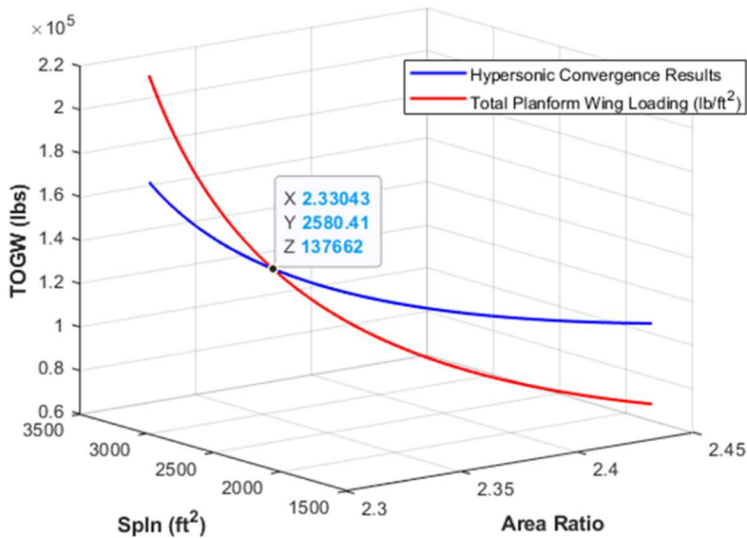


Fig. 37 3D Solution space generated by Wesley Junell [34].



4.3. Configuration Layout (CL) for Synthesis

4.3.1. Background

This section will briefly cover Configuration Layout phase for Synthesis. The main focus of this report is dedicated to Parametric Sizing (PS) and Configuration Evaluation (CE) phases. The CL phase is being researched in depth by fellow Synthesis engineer, Ethnica Mohanty [37]. The Synthesis MDA for CL gives the details required for trade studies.

4.3.2. Understanding Synthesis Configuration Layout: Coleman's Thesis [30]

The following are the trade studies selected by the entire team to be performed during the CL phase:

- wing geometry,
- modern materials,
- modern engine configurations.

4.3.3. Trade Study 1: Wing Geometry

Inputs: from geometry and Aerodynamics. The aspect ratio was chosen to be 2.0 based off of a compromise between the Aerodynamics and Performance team. The ideal aspect ratio needed by aerodynamics based of the PS results is 1.5 for aerodynamic efficiency, with the maximum being 2.0. An aspect ratio of 1.5 is too small for performance as the aircraft cannot takeoff, which is why a starting value of 2.0 was chosen.

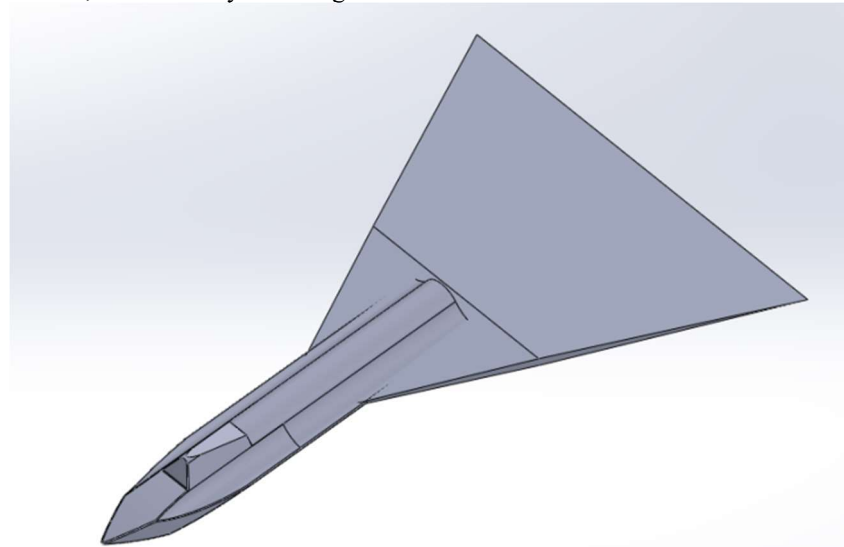


Fig. 38 Initial gross configuration provided by Austin Prior [35].

The minimum fuselage length required by aerodynamics for a nose sweep angle $\Lambda = 63.4^\circ$, aspect ratio of 2.0 is 27.7 ft. The wingspan and root chord given by aerodynamics for these numbers are $b = 61.2$ ft and $c_r = 61.1$ ft. The fuselage length would then become 88.8 ft at a minimum. The propulsion team is currently finding the length and width of the J-58 engine that includes both the ramjet and turbojet, and nacelles. Once the engine lengths are obtained, the fuselage length can be extended to fit them within the nose shock. The engine's lateral placement will be determined by stability and control OEI condition at takeoff. If the engine cannot be placed any further away from the fuselage centerline, the vertical tails must be sized accordingly. The elevon geometry is based on the diameter of the engines and wingspan. It has been decided that the elevons will be an extension of the wing with a hinge line slightly separating the wing and the control surface.

- Analysis: No analysis, gross wing configuration: Diamond body
- Aerodynamics: Configuration layout ranges necessary:
 - Aspect ratio: 1.5 to 2.5
 - Thickness (t/c): 0.03 to 0.06
 - Taper ratio: 0

 PENGUIN SUPersonic	SENIOR DESIGN: MAE 4351 Project	Ref.: MAE 4351-001-2021 Date: 11. May. 2023 Name: Gayathri Kola Status: In Progress
---	---	---

- Max thickness: 50% chord
- Sweep angle: 63.4 degrees.
- Stability and Control: Configuration layout ranges necessary:
 - Vertical tail area: 200 ft² to 400 ft².
 - Vertical tail volume coefficient: 0.06 to 0.07
 - Two vertical tails
- Output: Redo PS to assess if the design is feasible. If feasible, add to the list of feasible designs to be sent to CE.
- Choose the best configuration of geometry to send to materials.

4.3.4. Trade Study 2: Materials

- Inputs: Aerothermal, weights and balances (new material weights)
- Analysis: Different materials list, coefficients calculated to go into OEW and OWE.
- Output: Redo PS to assess if the design is feasible. If feasible, add to the list of feasible designs to be sent to CE.
- Choose the best feasible designs.

4.3.5. Trade Study 3: Engine Change

- Inputs: Propulsion Engine configurations + Thrust-to-weight ratios
- Analysis: no analysis: engine configurations laid out
- Outputs: Redo PS to assess if the design is feasible, add to list of feasible designs to be sent to CE.
- Send thrust data to stability and control for their control surface sizing.

Send all these designs to CE phase. CE will assess Stability and Control, Costs and Estimates, and Mission profile performance. Due to time constraints and the given nature of sizing and geometry change for each configuration, only the first configuration could be evaluated.

4.4. Configuration Evaluation (CE) for Synthesis

This report will go over the details for the CE phase. The Synthesis team is broken down such that each person is responsible for PS, CL, and CE. The Synthesis team has decided to have one person focus on two phases each. The author will be focusing on PS and CE phase.

4.4.1. Goals

The purpose of CE for Synthesis is to perform detailed trade studies, further refine the methodologies and analyze the performance of the generated aircraft for the entire mission. For each flight phase, there is usually one critical discipline that dominates the requirements to be met. It is the job of Synthesis team and the chief engineer to evaluate these tradeoffs between disciplines and land on a compromise that fulfills majority of the requirements for all disciplines. Here, the task will be to identify the requirements for each flight phase from every discipline for the chosen trade studies. The inputs, methodology, and outputs of each discipline must be laid out, so it can be integrated into the ongoing solution space code to further refine it. The IAOs must be identified for each flight phase for all disciplines and a code format must be communicated to easily combined into the Synthesis code. Analysis is performed by the majority of disciplines in CE namely: Stability and Control, Costs and Market Estimates, Performance and Trajectory. These three disciplines are reliant on other disciplines to perform mission analysis for the entire mission profile. The inputs come from the disciplines - Propulsion, Aerodynamics/Aerothermal, Structures-Weight and Balance. The Synthesis team will take the trade study design from CL and assess the design's performance with original SR-71 metrics. The author will be looking into methods to compare the SR-71 generated designs to other aircraft.

Following are things to-do (ongoing):

- Ask teams for their CE IAOs
- Ask for IAOs for each mission phase
- Make MDA including mission phases

4.4.2. Characterizing requirements from disciplines

 PENGUIN SUPERSONIC	SENIOR DESIGN: MAE 4351 Project	Ref.: MAE 4351-001-2021 Date: 11. May. 2023 Name: Gayathri Kola Status: In Progress
---	--	---

4.4.3. Function formats

The teams have been asked to make functions with respective inputs and outputs that can be integrated to the main synthesis code during CE. The function format is to start with flight phase and the discipline name. For example, the takeoff function from Aerodynamics team would look like: TO_Aero(Inputs).

4.4.4. Verification sources

The verification for SR-71 comes from established sources such as “The SR-71 Researcher’s Handbook”, “The Declassified SR-71 Flight Manual” and comparison to other aircraft numbers [25].

- Exact verification plots needed.

Table 5. Literature for Synthesis Configuration Evaluation.

Title	Author	Year	Application
SR-71 Researcher’s Handbook [25]		2010	Mission Profile verification numbers
SR-71 Flight Manual [22]	Loftin, L. K	1980	SR-71 Verification data (main source)
Development of the Vehicle Configuration Compendium: A Comprehensive Data-Information-Knowledge System to Aid in High-Speed Vehicle Design [20]	Simon, S.	2021	SR-71 Verification Data

The mission profile mistakenly had a turn maneuver (previously during phase 4) which has been removed from our segment analysis and replaced with accelerated climb to Mach 3.0.

4.5. Synthesis CE: Mission Description

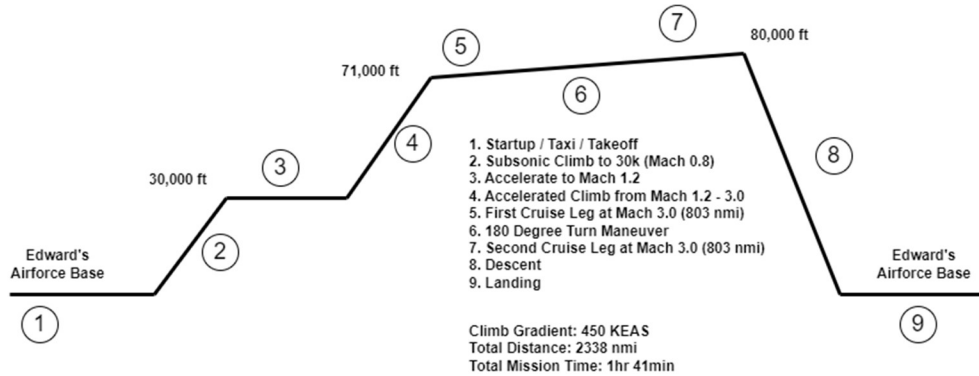


Fig. 39 New Mission Profile by Wesley Junell [34].

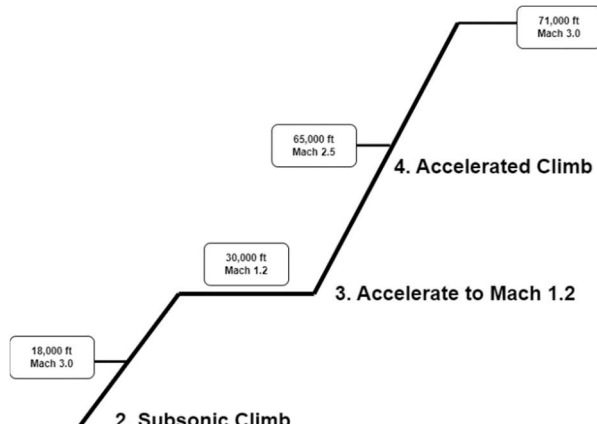


Fig. 40 Climb Segments by Wesley Junell [34].

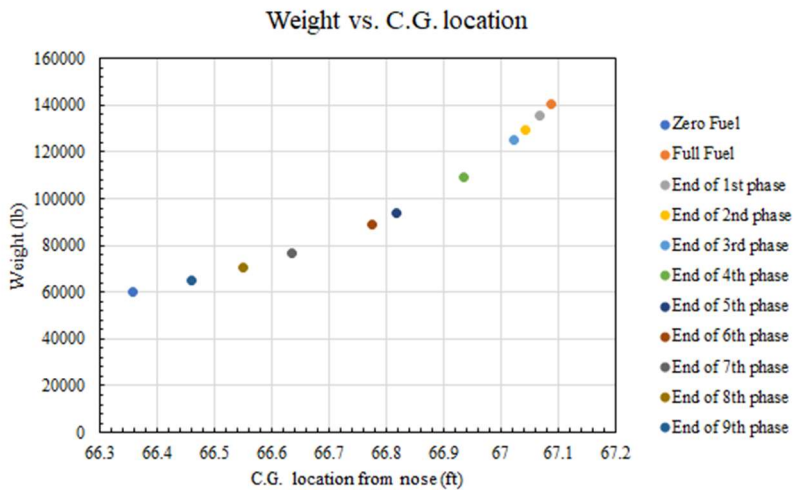


Fig. 41 Weight change with c.g. location for flight phases by Shiori Jo [38].

The following graph above was produced by Weights and Balance member Shiori for each flight phase using the SR-71's weight data in Nicolai Appendix and Wesley Junell's fuel fraction code [5,34]. This graph would be very useful in stability analysis during CE and verification with actual SR-71 weight change.

4.5.1. Phase 1 – Takeoff

Verification: [25]

- For 140,000 lbs: Max fuel load weight = 80,280 lbs
- For 140,000 lbs: Runway needed = 7,600 ft
- Takeoff speed: 210 KIAS

4.5.2. Phase 2 – Subsonic Climb

Verification: [25]

- Climb speed, subsonic: 400 – 450 KEAS.
- For 140,000 lbs: Climb profile = 450 KEAS
- Climb operating limit – 500 KEAS

4.5.3. Phase 3 – Refuel and accelerate to M = 1.5.

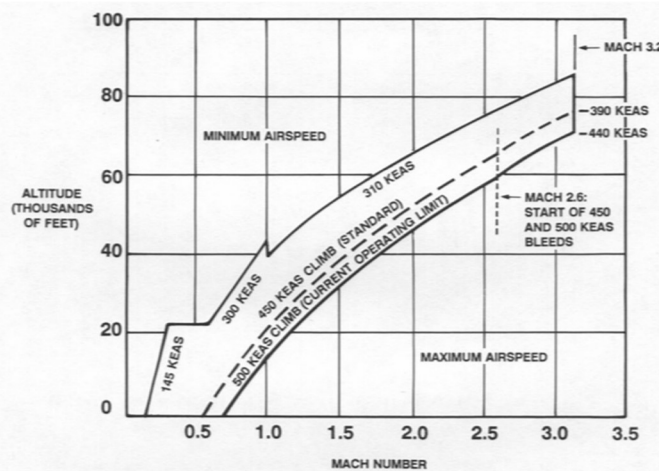


Fig. 42 Climb profiles for various altitudes [25].

This Fig. 42 above will be used to verify climb gradients for the current 25,000 ft refuel and climb phase.



4.5.4. Phase 4 – Accelerated climb to Mach 3

Phase Requirement:

- The thrust required has to be higher than drag during climb.

4.5.5. Phase 5 – Cruise at Mach 3

Verification: [25]

- Max cruise performance: $M = 3.2$, at 74,000 ft to 85,000 ft.
- Supersonic cruise speed range: 310 – 400 KEAS, upto 500 KEA for operational limit.

4.5.6. Phase 6 – Turn 180 degrees

Phase Requirement:

- 180 degrees.
- Level turn.

Verification: [25]

- Bank angle versus turn radius plots in Fig. 43.

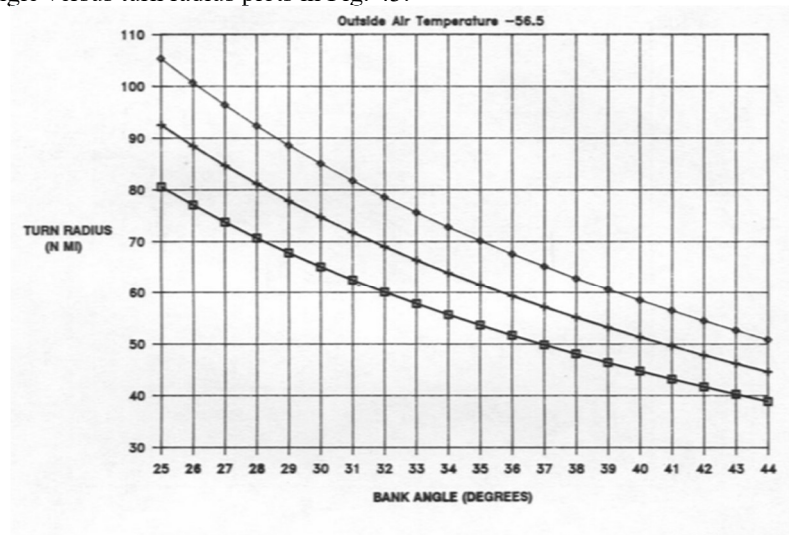


Fig. 43 Bank angle versus turn radius for supersonic speeds verification [25].

4.5.7. Phase 9 – Landing

Phase Requirement:

- For 140,000 lbs: with 10,000 lbs of fuel + chute deployed, landing distance = 4,200 ft.

Verification: [25]

- Landing speed: 155 KIAS
- Landing gross weight: 75,000 lbs (with 10,000 lbs fuel)
- Drag chute deployment, max airspeed = 210 knots

5. Stability and Control

5.1. Understanding the Discipline

In order to get an in-depth understanding of stability and control, three main references are being reviewed initially. For brief descriptions of SR-71 longitudinal and lateral stability features, the textbook “Aircraft Performance and Design” by John D. Anderson was reviewed [21]. To collect input parameters needed from other teams for stability calculations, the course’s main textbook was used [5]. Lastly, to understand the aircraft’s stability characteristics, SR-71’s online flight manual was referenced [22]. In this section, a summary of key elements is given from each reference. The structure of this sub-section will be modified later after reviewing more literature.



5.1.1. John D. Anderson reference [21]: SR-71 Design features

Chapter 9 of this text has clear explanations of features like chines that were added to ensure the Blackbird's stability. The aerodynamic center (neutral point) of an aircraft change substantially when flying from the subsonic to the supersonic regime. This can also be explained from a drag perspective, where the drag coefficient diverges dramatically at sonic speed (Mach 1). These drastic shifts can be a problem for a supersonic aircraft's pitch stability. Chines, a variation of strakes, reduce the movement of the neutral point as the aircraft travels at supersonic speeds. The Fig. 44 shows the effect of chine as a function of Mach number. The case with chine on brings back the neutral point close to its original location after crossing sonic speed.

According to longitudinal stability criteria, the neutral point of an aircraft must always be behind the center of gravity. This ensures that the aircraft does not pitch up too quickly or enter into high angles of attack that guarantee a stall. This concept is illustrated by the "static margin" in Eq. (10). Where X_{np} is the location of the neutral point and $X_{c,g}$ is the center of gravity of the aircraft. A positive SM value means that the neutral point is behind the center of gravity.

$$SM = \frac{X_{np} - X_{c,g}}{\bar{c}} \quad (10)$$

A large positive value indicates that the aircraft is more stable. The faster a plane goes, the farther the neutral point travels from c.g. This causes the plane to become more stable than desired, limiting maneuverability. The elevon will require a higher force to change the vehicle attitude to trim the aircraft. This results in trim drag.

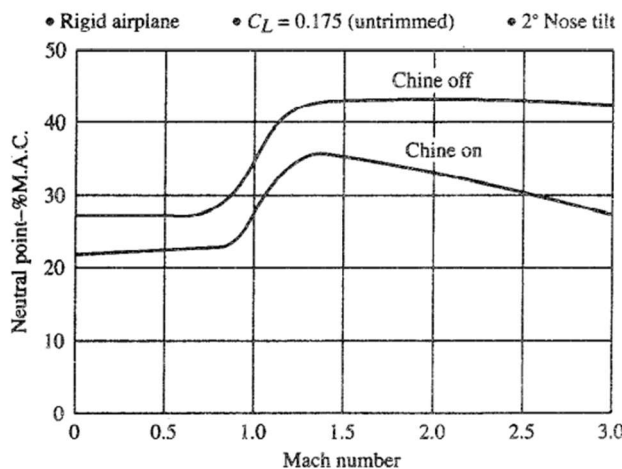


Fig. 44 Neutral point shift from subsonic to supersonic for SR-71 [21].

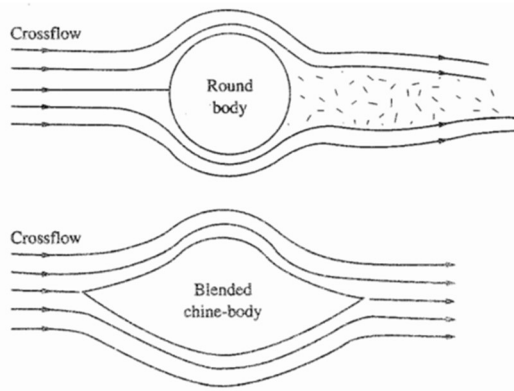


Fig. 45 Crossflow of streamlines for chines versus a cylindrical fuselage [21].



The Fig. 45 above shows the crossflow pattern on a cylindrical fuselage versus a blended-chine body. The crossflow creates a side force on the fuselage that makes it yaw in the flow direction. Cylindrical bodies will experience flow separation for small yaw angles. Having a blended chine as in the case of SR-71 helps a smoother flow resulting in favorable directional stability. This consequently reduces the need for larger vertical tails, thereby reducing weight and skin drag on the aircraft. Chines also aid in producing additional lift. The delta wing was placed at a small negative incidence angle relative to the fuselage centerline due to this.

For directional control, the SR-71 does not have any surfaces. Instead, it is equipped with two all-moving vertical tails that are canted inward by a 15° angle. In the instance of a side force acting on an uncanted vertical tail, the center of pressure for the tail is above the aircraft's longitudinal axis. This caused a rolling moment about the axis, decreasing its lateral stability. By canting the vertical tails, the moment arm is much shorter as seen in Fig. 46. According to the text, the hinges on the rudder surfaces were exposed to high temperatures in supersonic flight tests. They also required large rudder deflection in one engine-out condition. This proved to be very risky in terms of control authority. This was the main reason for using all-moving vertical fins.

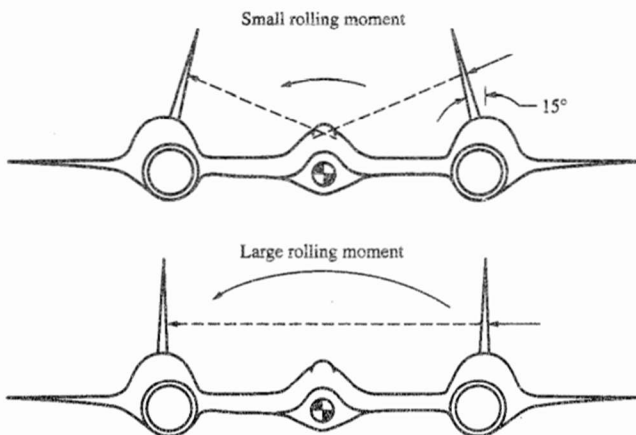


Fig. 46 Rolling moments of the SR-71 vertical tail with and without canting [21].

5.1.2. Nicolai [5]: General tailless aircraft methods

During week 3, the entire design team decided to use course textbook nomenclature as a standard while performing calculations for convergence. The Fig. 47 shows the Stability and Control team nomenclature to be an aircraft axis system to be adapted. Since Stability and Control will be dealing with forces and moments on the aircraft, the use of this text helps to establish the various kinds of derivatives involved. Specifically, Chapters 21 – 23 give detailed methods to calculate these moment coefficients, as a starting point. Other methodologies such as Roskam VII which covers step-by-step calculation procedures based on aircraft type will be reviewed in week 4 [11].

Upon reading these chapters, some important equations and parameters were collected in order to derive a draft IDA. The describes methods for longitudinal and lateral stability for different types of control surfaces. The exact equations are discussed further. The SR-71 would be classified as a tailless aircraft since it has no horizontal stabilizer (an aft tail) or canards, only elevons directly attached to the delta wing. As discussed earlier, elevons are responsible for longitudinal (pitch) and lateral (roll) control. Elevons move up and down together to maintain pitch and move in opposite directions to one another to roll. The force-moments diagram is given in Fig. 48.

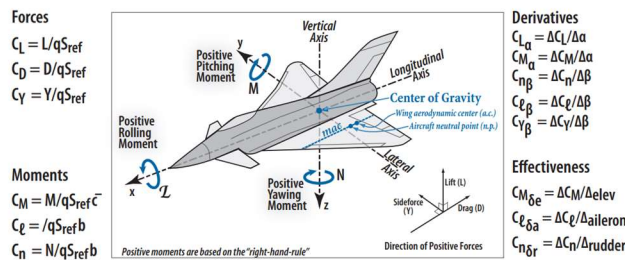
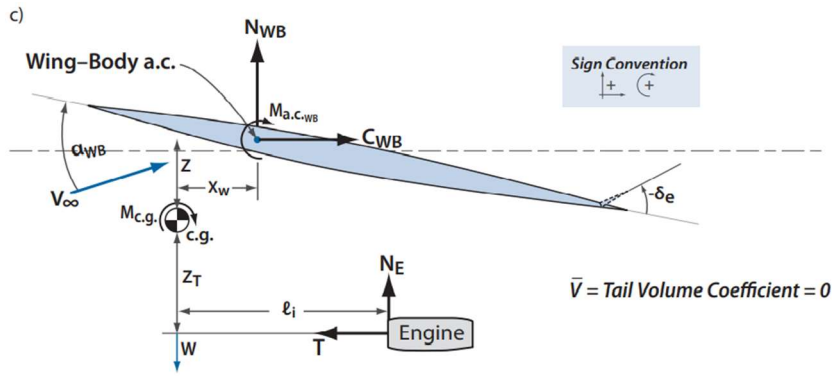


Fig. 47 Important non-dimensional parameters and sign convention [5].



All distances are positive as shown
 ϵ_T = tail downwash angle due to wing downwash w_T at the tail a.c.
For small a we can assume
 N = normal force $= L = C_L q S_{ref}$
 C = chord force $= D = C_D q S_{ref}$

Fig. 48 Freebody diagram of forces and moments acting on a tailless aircraft [5].

There are federal regulations to use as a reference point while making static and dynamic stability criteria in design. Since the SR-71 is a military aircraft, two main documents, MIL-HDBK-1797 and its previous version ML-F-8787C can be referenced. This text outlines some stability criteria from both these documents. The documents state the requirements of aircraft flight operation quality for military aircraft including trans-atmospheric flight where an aircraft uses air-breathing propulsion systems.

5.1.3. SR-71 Flight Manual Reference [22]: Means to verify the methodology

An estimate of all the control surface area was found in the manual. The Fig. 49 specifies the inboard and outboard elevon areas, movable and total rudder area, and tip and root chords for the wing and vertical tail. These values can be used to make rough calculations of the different stability derivatives before the Synthesis team gives out this information. Various references use vertical tail and rudders interchangeably while referring to SR-71's directional stabilizer. However, most of them specify "all-moving" to differentiate from conventional rudder-vertical stabilizer combinations.

This flight manual has abundant information on the flight trim system and Stability Augmentation System (SAS) that can be referenced later for method verification purposes.

SR-71 Specifications	
Manufacturer:	Lockheed Aircraft Corporation
Length:	107' 5"
Length of Nose Probe:	4' 11"
Wing Span:	55' 7"
Wing Area:	1,795 ft. sq.
Wing Aspect Ratio:	1.939
Wing Root Chord:	60.533
Wing Dihedral Angle:	0 degrees
Wing Chord:	0.00
Wing Sweep:	52.629 degrees
Inboard Elevon Area:	39.00 ft. sq.
Outboard Elevon Area:	52.50 ft. sq.
Total Vertical Rudder Area:	150.76 ft. sq.
Moveable Rudder Area:	70.24 ft. sq.
Rudder Root Chord:	14.803 ft.
Rudder Tip Chord:	7.833 ft.
Height:	18' 6"
Empty Weight:	59,000 lbs.
Maximum Weight:	170,000 lbs.
Fuselage Diameter:	5.33 ft.
Service Ceiling:	85,000'+
Maximum Speed:	Mach 3.3+ (Limit CIT of 427 degrees C)
Cruising Speed:	Mach 3.2
Engines:	2 Pratt & Whitney J-58 (JT11D-20A) with 34,000 lbs. of thrust.
Range:	3,200 nautical miles (without refueling)

Fig. 49 Flight geometry data for elevon and vertical tail [22]



5.1.4. Chudoba [9]: Stability coefficients and previous methodologies

Another methodology, mentioned in the book “Stability and Control of Conventional and Unconventional Aircraft Configurations”, known as VORSTAB is a software capable of calculating aerodynamic and stability derivatives using the Vortex Lattice Method (VLM) [9]. This numerical method works for both subsonic and supersonic flow. However, the author has not been able to find this software for free use on the internet.

Another VLM method presented in the same book named VORLAX is also being searched. For now, the current methodology is to write MATLAB scripts to iterate for a range of sideslip angle β , dynamic pressure q_∞ or Mach number. As a baseline calculation setup, a simplified geometry of the delta wing will be used to obtain the yawing and rolling moment coefficients. This process has to be obtained for each flight phase: takeoff, climb, cruise, descent, approach, loiter, and landing. The Fig. 52 shows a clear control surface design process that can be incorporated. The same book lists all the important stability and control derivatives to consider during the Conceptual Design process – boxed in Fig. 50. The derivatives on the upper side of the table show the stability derivatives and the bottom part lists the control derivatives.

TABLE 4-7. Matrix of Translational and Rotary Stability Derivative Coefficients

	X[D,T]	Y	Z[L,W]	L	M	N
u	$C_{D_u} C_{T_u}$	C_{Y_u}	C_{L_u}	C_{I_u}	C_{m_u}	C_{n_u}
v [β]	$C_{D_\beta} C_{T_\beta}$	C_{Y_β}	C_{L_β}	C_{I_β}	C_{m_β}	C_{n_β}
w [α]	$C_{D_\alpha} C_{T_\alpha}$	C_{Y_α}	C_{L_α}	C_{I_α}	C_{m_α}	C_{n_α}
p	$C_{D_p} C_{T_p}$	C_{Y_p}	C_{L_p}	C_{I_p}	C_{m_p}	C_{n_p}
q	$C_{D_q} C_{T_q}$	C_{Y_q}	C_{L_q}	C_{I_q}	C_{m_q}	C_{n_q}
r	$C_{D_r} C_{T_r}$	C_{Y_r}	C_{L_r}	C_{I_r}	C_{m_r}	C_{n_r}
\dot{u}	$C_{D_{\dot{u}}} C_{T_{\dot{u}}}$	$C_{Y_{\dot{u}}}$	$C_{L_{\dot{u}}}$	$C_{I_{\dot{u}}}$	$C_{m_{\dot{u}}}$	$C_{n_{\dot{u}}}$
$\dot{v} [\dot{\beta}]$	$C_{D_{\dot{\beta}}} C_{T_{\dot{\beta}}}$	$C_{Y_{\dot{\beta}}}$	$C_{L_{\dot{\beta}}}$	$C_{I_{\dot{\beta}}}$	$C_{m_{\dot{\beta}}}$	$C_{n_{\dot{\beta}}}$
$\dot{w} [\dot{\alpha}]$	$C_{D_{\dot{\alpha}}} C_{T_{\dot{\alpha}}}$	$C_{Y_{\dot{\alpha}}}$	$C_{L_{\dot{\alpha}}}$	$C_{I_{\dot{\alpha}}}$	$C_{m_{\dot{\alpha}}}$	$C_{n_{\dot{\alpha}}}$
\dot{p}	$C_{D_{\dot{p}}} C_{T_{\dot{p}}}$	$C_{Y_{\dot{p}}}$	$C_{L_{\dot{p}}}$	$C_{I_{\dot{p}}}$	$C_{m_{\dot{p}}}$	$C_{n_{\dot{p}}}$
\dot{q}	$C_{D_{\dot{q}}} C_{T_{\dot{q}}}$	$C_{Y_{\dot{q}}}$	$C_{L_{\dot{q}}}$	$C_{I_{\dot{q}}}$	$C_{m_{\dot{q}}}$	$C_{n_{\dot{q}}}$
\dot{r}	$C_{D_{\dot{r}}} C_{T_{\dot{r}}}$	$C_{Y_{\dot{r}}}$	$C_{L_{\dot{r}}}$	$C_{I_{\dot{r}}}$	$C_{m_{\dot{r}}}$	$C_{n_{\dot{r}}}$
δ_{PC_i}	$C_{D_{\delta_{LoCE_i}}} C_{T_{\delta_{LoCE_i}}}$	$C_{Y_{\delta_{LoCE_i}}}$	$C_{L_{\delta_{LoCE_i}}}$	$C_{I_{\delta_{LoCE_i}}}$	$C_{m_{\delta_{LoCE_i}}}$	$C_{n_{\delta_{LoCE_i}}}$
	$C_{D_{\delta_{DiCE_i}}} C_{T_{\delta_{DiCE_i}}}$	$C_{Y_{\delta_{DiCE_i}}}$	$C_{L_{\delta_{DiCE_i}}}$	$C_{I_{\delta_{DiCE_i}}}$	$C_{m_{\delta_{DiCE_i}}}$	$C_{n_{\delta_{DiCE_i}}}$
	$C_{D_{\delta_{LaCE_i}}} C_{T_{\delta_{LaCE_i}}}$	$C_{Y_{\delta_{LaCE_i}}}$	$C_{L_{\delta_{LaCE_i}}}$	$C_{I_{\delta_{LaCE_i}}}$	$C_{m_{\delta_{LaCE_i}}}$	$C_{n_{\delta_{LaCE_i}}}$
δ_{SC_i}	$C_{D_{\delta_{SC_i}}} C_{T_{\delta_{SC_i}}}$	$C_{Y_{\delta_{SC_i}}}$	$C_{L_{\delta_{SC_i}}}$	$C_{I_{\delta_{SC_i}}}$	$C_{m_{\delta_{SC_i}}}$	$C_{n_{\delta_{SC_i}}}$
δ_{CS_i}	$C_{D_{\delta_{CS_i}}} C_{T_{\delta_{CS_i}}}$	$C_{Y_{\delta_{CS_i}}}$	$C_{L_{\delta_{CS_i}}}$	$C_{I_{\delta_{CS_i}}}$	$C_{m_{\delta_{CS_i}}}$	$C_{n_{\delta_{CS_i}}}$

Fig. 50 Translational and rotational stability and control derivatives [9].



Table 6. Important longitudinal and lateral stability derivatives [9]

Symbol	Parameter Name	Category
$C_{L\alpha}$	Variation of lift coefficient with angle of attack	Longitudinal
$C_{D\alpha}$	Variation of drag coefficient with angle of attack	Longitudinal
$C_{m\alpha}$	Variation of pitching moment coefficient with angle of attack	Longitudinal
C_{Lq}	Variation of lift coefficient with pitch rate	Longitudinal
C_{mq}	Variation of pitching moment coefficient with pitch rate	Longitudinal
$C_{Y\beta}$	Variation of sideforce coefficient with angle of sideslip	Directional
$C_{l\beta}$	Variation of rolling moment coefficient with angle of sideslip	Lateral
$C_{n\beta}$	Variation of yawing moment coefficient with angle of sideslip	Directional
C_{Yp}	Variation of sideforce coefficient with roll rate	Lateral
C_{lp}	Variation of rolling moment coefficient with roll rate	Lateral
C_{np}	Variation of yawing moment coefficient with roll rate	Lateral
C_{Yr}	Variation of sideforce coefficient with yaw rate	Directional
C_{lr}	Variation of rolling moment coefficient with yaw rate	Directional
C_{nr}	Variation of yawing moment coefficient with yaw rate	Directional

5.1.5. Aircraft Design, A systems engineering approach [24]: Control Surface Sizing

This book contains detailed control surface sizing steps, especially for tail design. For a vertical tail design, the book recommends the following parameters shown in Table 7 below.

Table 7. Vertical tail design parameters [24].

Symbol	Parameter Name
S_v	Tail planform area
l_v	Tail arm
AR_v	Tail aspect ratio
λ_v	Tail Taper ratio
C_{tv}	Tail tip chord
C_{rv}	Tail root chord
MAC_v or C_v	Mean aerodynamic chord
-	Airfoil section
b_v	Tail span
Λ_v	Tail sweep angle
Γ_v	Tail dihedral angle
i_v	Tail incidence angle

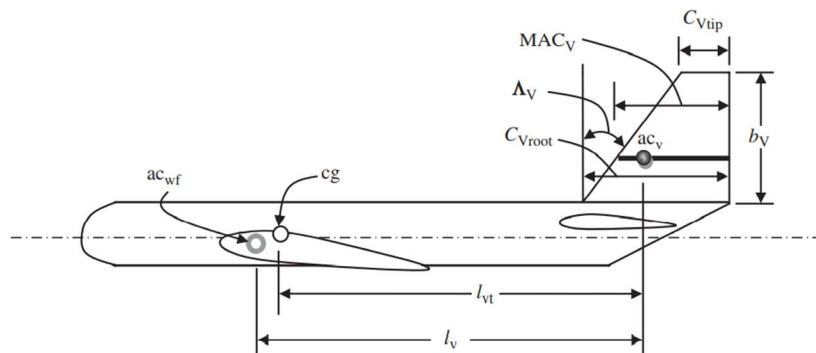


Fig. 51 Typical vertical tail parameters and geometry [24].

The Fig. 51 above can be used as a reference for the exact geometry parameters needed for the vertical tail design. Since the SR-71 does not have a horizontal tail, it can be neglected from the design process. The tail design process is very clearly outlined in this book, seen in Fig. 52 below. The Fig. 53 can be used as a reference for typical values of static and directional stability.

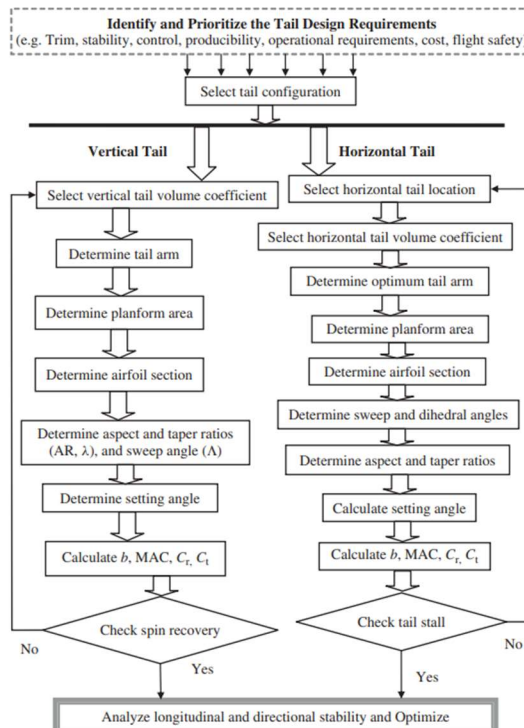


Fig. 52 Control surface design process [24].

Table 6.3 The static and dynamic longitudinal and directional stability requirements

No.	Requirements	Stability derivatives	Symbol	Typical value (1/rad)
1a	Static longitudinal stability	Rate of change of pitching moment coefficient with respect to angle of attack	$C_{m\alpha}$	-0.3 to -1.5
1b	Static longitudinal stability	Static margin	$h_{np} - h_{cg}$	0.1–0.3
2	Dynamic longitudinal stability	Rate of change of pitching moment coefficient with respect to pitch rate	C_{m_q}	-5 to -40
3	Static directional stability	Rate of change of yawing moment coefficient with respect to sideslip angle	$C_{n\beta}$	+0.05 to +0.4
4	Dynamic directional stability	Rate of change of yawing moment coefficient with respect to yaw rate	C_{n_r}	-0.1 to -1

Fig. 53 Typical values for static and dynamic stability of an aircraft [24].

One of the main questions the author has struggled with while researching the tail design of SR-71 was the rotation of the *all-moving* vertical fins. The Fig. 54 below beautifully illustrates the horizontal tail setting configurations that can also be interpreted for the vertical tails. The Fig. 54 shows the fixed (a), adjustable (b), and all-moving (c) variations. The actual rotated vertical fin of the SR-71 is seen in the Fig. 55.

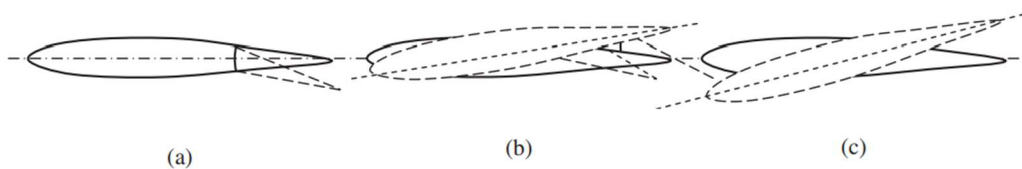


Fig. 54 Horizontal tail setting configurations; (a) Fixed, (b) Adjustable, (c) All-moving [24].



Fig. 55 Vertical fin movement of the SR-71 [39].

5.1.6. Roskam: Methodology search

Since the Synthesis team has chosen Roskam as their sizing methodology, Roskam could be evaluated for methods to size the vertical tail. Roskam Part II sets out an example methodology to size the vertical tail for a fighter aircraft named “*Eris*”. This aircraft has longitudinal instability and lacks a horizontal tail. Upon reading many references, the SR-71 aircraft configuration appears to be a delta-wing with two vertical tails (tailless). Although the level of instability that’s permitted for a fighter is not required for a reconnaissance aircraft, this could be a good starting point for estimating static directional stability. Roskam also outlines methods for calculating One-Engine-Inoperative (OEI) conditions.

5.1.7. USAF DATCOM: Methodology search

The new reference gathered is the USAF Stability and Control DATCOM by the McDonnell Douglas corporation. This document gives extensive equations for stability in the subsonic, transonic, and supersonic regimes. The author is currently considering this reference as a potential methodology since it includes supersonic stability equations. This document gives criteria based on what kind of configuration the aircraft is with ranges for parameters like taper ratio, leading edge sweep angle, thickness-to-chord ratio, Mach number, etc.

DERIVATIVE	CONFIG.	SPEED REGIME	EQUATIONS FOR DERIVATIVE ESTIMATION (Datcom section for components indicated)	METHOD LIMITATIONS ASSOCIATED WITH EQUATION COMPONENTS
C_{n_g} (Contd.)	WBT (Contd.)	SUPSONIC	(Same as subsonic equation)	<ul style="list-style-type: none"> 1. Linear-lift range $(C_{n_g})_{WB}$ 2. Straight-tipped wings 3. Wing tips parallel to free stream 4. Foremost Mach line from wing tip may not intersect remote half-wing 5. $M \geq 1.4$ $(C_{n_g})_D$ (based on expanded vertical-tail geometry) 6. Additional tail limitation is identical to Item 5 immediately above
C_{n_g}	W	SUBSONIC (Low Speed) (Subcritical)	$\frac{C_{n_g}}{C_L^2} = \frac{1}{57.3} \left[\frac{1}{4\pi A} - \frac{\tan \Lambda_{1/4}}{\pi A(A + 4 \cos \Lambda_{1/4})} \left(\cos \Lambda_{1/4} \frac{A}{2} - \frac{A^2}{8 \cos \Lambda_{1/4}} + 6 \frac{x}{\pi} \sin \Lambda_{1/4} \right) \right]$ $\left(\frac{C_{n_g}}{C_L^2} \right)_M = \left(\frac{A + 4 \cos \Lambda_{1/4}}{AB + 4 \cos \Lambda_{1/4}} \right) \left(\frac{A^2 B^2 + 4AB \cos \Lambda_{1/4} - 8 \cos^2 \Lambda_{1/4}}{A^2 + 4A \cos \Lambda_{1/4} - 8 \cos^2 \Lambda_{1/4}} \right) \left(\frac{C_{n_g}}{C_L^2} \right)_{low}$ <p>Eq. 5.1.3.1-a Eq. 5.1.3.1-b 5.1.3.1</p>	1. Linear-lift range
		TRANSOMIC	(No method)	
		SUPersonic	$\frac{C_{n_g}}{\sigma^2} = \frac{1}{\pi A^2 \beta^2} \left[\frac{4M^2}{3} + 8M^2 \frac{x}{\beta} - \# \left \frac{A(1-\beta^2)}{\beta} - \frac{2+\beta^2}{3\beta^2} \right \right] \frac{1}{57.3}$ <p>Eq. 5.1.3.1-c</p>	<ul style="list-style-type: none"> 1. Rectangular planform 2. $A \sqrt{M^2 - 1} \geq 1.0$ (Mach number and aspect ratio parameter for those for which Mach line from LE of tip section intersects TE of opposite tip section)
			$\frac{C_{n_g}}{\sigma^2} = \frac{x}{3} \left[\frac{C_{\mu}(QC)}{7.1.1.1} F_{11}(N) + \left(\frac{A^2}{16} F_{11}(N) + \frac{2}{\pi} \right) M^2 - QC \right] \frac{1}{57.3}$ <p>Eq. 5.1.3.1-d</p>	<ul style="list-style-type: none"> 1. $\lambda = 0$ 2. $\sqrt{M^2 - 1} \cot \Lambda_{1/4} \leq 1.0$ (Mach number and aspect ratio for which wing lies within Mach cones springing from apex and TE at center of wing)

Fig. 56 USAF DATCOM stability equations [26].

 PENGUIN SUPersonic	SENIOR DESIGN: MAE 4351 Project	Ref.: MAE 4351-001-2021 Date: 11. May. 2023 Name: Gayathri Kola Status: In Progress
---	---	---

5.1.8. Static and Dynamic Stability

Stability can be further classified into two more distinct categories: static stability and dynamic stability. When a vehicle's natural tendency is to slowly return to its original position (in equilibrium) after a disturbance, we call that *static stability*. When an aircraft tends to diverge from equilibrium over time, it becomes unstable. This is an undesired effect, and usually, control power is required to trim the aircraft. When the forces and moments on an aircraft balance correctly when performing maneuvers, it is said to have *dynamic stability*. The SR-71 is said to have a slight pitch and yaw divergence, making it laterally unstable. This imposed a heavy load on the pilot to constantly control the aircraft [40]. The conceptual design often involves static stability analysis first. Dynamic stability analysis requires design data; hence it is often performed in Preliminary Design (PD) [5].

Upon reviewing methods presented in Roskam Part VII, the following steps have been determined to be taken initially. According to the text, the designer must first decide whether or not the aircraft would have Inherent Stability or De-facto stability. Inherent stability would be for an aircraft that doesn't require any form of closed-loop stability augmentation system. The de-facto stability aircraft would require such a static or dynamic augmentation system [11]. After reviewing the SR-71 flight manual for stability and control characteristics, it has become apparent that the plane had an onboard Stability-Augmentation-System (SAS) which played a critical role to manage the instability that arises from engine unstarts. Below in Fig. 57 gives a classification of SR-71 from the older regulation document MIL-F-8785C as a class III aircraft. It would mean that it is a low-to-medium maneuverability vehicle. Inverted flight is not permitted for this purpose [22].

Class	General aircraft types	Specific examples
Class I	Light utility	T-41
small, light airplanes	Primary trainer	T-6
	Light observation	O-1, O-2
Class II	Heavy utility/search and rescue	C-21
medium weight; low-to-medium maneuverability airplanes	Light or medium transport/cargo/tanker	C-130
	Early warning/ECM/Command & control	E-2
	Anti-submarine	S-3A
	Assault transport	C-130
	Reconnaissance	U-2
	Tactical bomber	B-66
	Heavy attack	A-6
	Trainer for Class II	T-1A
Class III	Heavy transport/cargo/tanker	KC-10, C-17
large, heavy, low-to-medium maneuverability airplanes	Heavy bomber	B-52, B-1, B-2
	Patrol/Early warning/ECM/Command & control	P-3, SR-71
	Trainer for Class III	TC-135
Class IV	Fighter/Interceptor	F-22, F-15, F-16
high-maneuverability airplanes	Attack	F-15E, A-10
	Tactical reconnaissance	RF-4
	Observation	OV-10
	Trainer for Class IV	T-38

Fig. 57 MIL-F-8785C Aircraft classes [23]



5.1.9. Lateral-Directional Stability

In order to stabilize an aircraft, it is important to have a set criterion. The course textbook outlines a few of these criteria for lateral and directional stability down in Table 8. These criteria come from regulatory documents within the U.S. Column 4 in Table 8 signifies the static stability criterion. The opposite sign for the coefficients would mean that the aircraft will become unstable. The criterion for dynamic stability will be updated upon reviewing the latest MIL-HDBK-1797 military flying qualities document. The MIL-HDBK-1797 is a handbook, not the actual standard qualities listing document. The standard is called MIL-STD-1797, with 3 revisions up till 2012. This is currently a classified document; hence the handbook will be used as guidance only.

Table 8. Lateral-Directional Stability Criteria [5].

Symbol	Parameter	Category	Static Stabilizing	Regulations
$c_{n\beta}$	Yawing moment due to sideslip angle	Directional	> 0 (positive)	MIL-HDBK-1797
c_{l_p}	Roll damping derivative	Lateral	< 0 (negative)	MIL-F-8785C
$c_{l\beta}$	Rolling moment due to sideslip angle	Lateral	< 0 (negative)	MIL-HDBK-1797

Following equations from Nicolai are being considered for an initial analysis of the lateral and directional stability of a tailless aircraft [5].

$$C_{l\beta} = C_{l\beta_{wing}} + C_{l\beta_{vertical stabilizer}} + C_{l\beta_{wing-fuselage}} \quad (11)$$

Where $C_{l\beta}$ is the rolling moment due to sideslip angle β . The terms on the right-hand side of Eq. (11) are the components influencing the derivative. Here, a negative value of $C_{l\beta}$ will cause the aircraft to roll up from the right wing, hence laterally stabilizing it.

For directional stability, the derivative–yawing moment due to the sideslip angle $C_{n\beta}$ is used as seen in Eq. (12) below.

$$\frac{dC_n}{d\beta} = C_{n\beta} = C_{n\beta_{fus}} + C_{n\beta_{wing}} + \bar{V}_{VT} C_{L\alpha_{VT}} \left(1 + \frac{d\sigma}{d\beta} \right) \frac{q_{VT}}{q_\infty} \quad (12)$$

In the last term, \bar{V}_{VT} is the vertical tail volume coefficient. The coefficient $C_{n\beta}$ must be positive for yaw stability. Usually, the rudder size must be modified to affect this derivative. A positive $C_{n\beta}$ value is required to directionally stabilize the aircraft. Plots will have to be made for different values of β and their derivatives, then eventually for the coefficients. Based on the geometry, constraints charts are to be made for each criterion.

Some verification methods that are being looked into are the SR-71 flight manual. The S&C team has agreed to work on producing plots as a function of angle of attack α and sideslip angle β that show whether the aircraft is stable or not as seen in Fig. 58. Here, C_m is the pitching moment coefficient and C_n is the yawing moment coefficient.

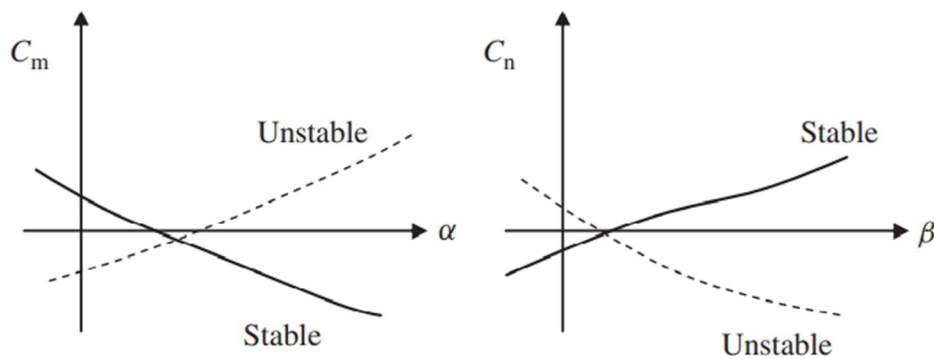


Fig. 58 Stabilizing and de-stabilizing plots with respect to the angle of attack and sideslip [24]



For Stability and Control, the parametric sizing (PS) process is not required since the geometry, weights, and aerodynamics of the supposed aircraft need to be established, shown in the IDA. The control surfaces to be sized for the SR-71 are twin vertical tails and inboard-outboard elevons. A list of possible aircraft configurations similar to the SR-71, in that they have a delta wing and elevons are listed below in Table 9. Aircraft similar to SR-71 with delta wings and elevons..

Table 9. Aircraft similar to SR-71 with delta wings and elevons.

Symbol	Features	Inboard Elevons	Outboard Elevons
Concorde	Delta wing, 6 elevons	2	2 middle, 2 outer
Tupolev 144	Delta wing	0	8
Eurofighter Typhoon	Delta wing, elevons	-	2 middle 2 outer
Vulcan	Delta wing, elevons, flying wing	-	4 middle, 4 outer
XB-70	Delta wing, elevons	0	2 middle

5.1.10. Stability & Control IAO

After reviewing the course text to find equations for calculating stability derivatives, an initial IAO is drafted. This IAO will be revised after finalizing the methodology to use for convergence based on the Synthesis team's needs.

INPUT – ANALYSIS – OUTPUT

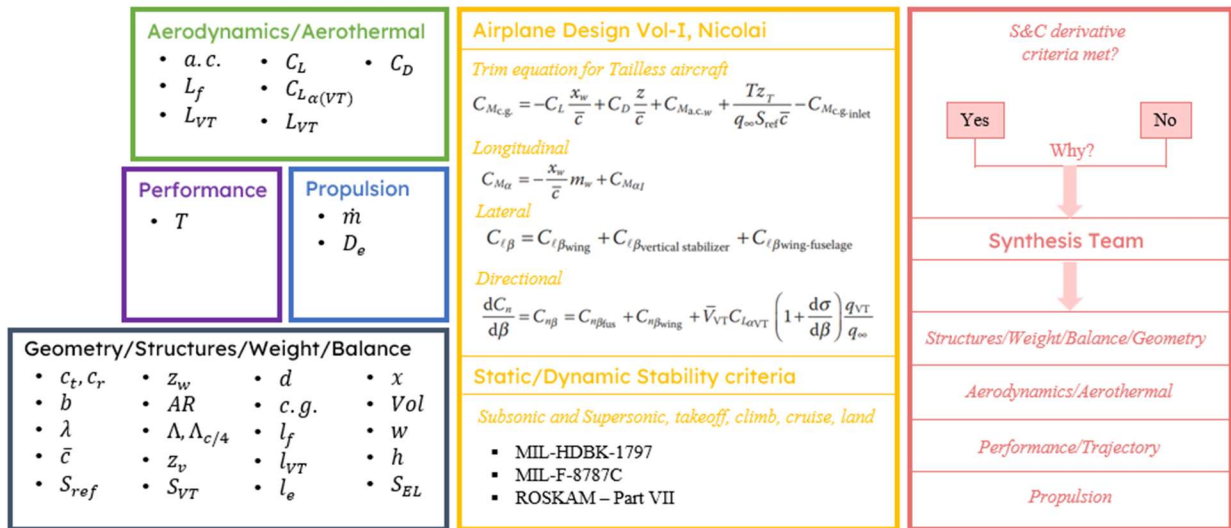


Fig. 59 Initial IAO for Stability and Control.

An IAO for stability and Control was made by the team lead, Austin. Below in Fig. 60 Detailed IAO by the team lead Austin Prior [35]. the IAO outlines the current plots each member is responsible for. After testing the methodology and generating the plots, this team will make an IDA that will show the chronology of the methods being used.



Stability and Control															
Management		Lead		Longitudinal Stability		Member 1		Directional and Roll Stability		Member 2		Controls		Member 3	
• Organize team responsibility		• Pitching moment		• Yawing moment		• Trim		• Side slip		• Elevon deflection		• All stages of flight		• Neutral Point	
• Schedule team meetings		• Effects of AOA		• Vertical Stabilizer effects		• All stages of flight		• C.G. location effects		• All stages of flight		• Full aircraft description		• All stages of flight	
• Monitor and ensure pace of team		• All stages of flight		• All stages of flight				• All stages of flight							
• Define roles															
• Orchestrate individual deliverables															
• Full aircraft description															
Team Deliverable		Lead		Deliverable		Member 1		Deliverable		Member 2		Deliverable		Member 3	
• Full description of aircraft moments		• Pitching moment as a function of angle of attack		• Determine the yaw moment as a function of side slip angle		• Elevon deflection angle as a function of pitch moment		• Yawing capabilities in both subsonic and supersonic flight		• Roll capabilities and requirements during turn		• Landing and takeoff stability behavior		• Elevon deflection as a function of pitch moment	
• Landing and takeoff stability behavior		• Neutral point location during different flight phases		• Yawing moment as a function of side slip angle		• Elevator deflection during takeoff and landing		• Roll capabilities and requirements during turn		• Cruise behavior		• Subsonic and supersonic description		• Trim requirements	
• Cruise behavior		• Elevon effects of pitching moment		• Takeoff and landing moments											
• Climb and decent															
• Subsonic and supersonic description															

Fig. 60 Detailed IAO by the team lead Austin Prior [35].

The thesis written by Stenila Simon gives a clear breakdown of conceptual design parameters necessary for each phase by PS, CL, and CE. For the Configuration Layout stage, this paper will focus on finding the applicable equations governing rolling and yawing moment coefficients, C_l and C_n . It will also detail some aspects of elevon sizing for lateral stability and vertical tail sizing for directional stability.

Categories	PS			CL			CE		
	S. M.	Static Margin	m	C_m	Pitching moment coefficient	-	C_{m_α}	Variation of C_m coefficient with respect to AOA	-
Longitudinal	-	-	-	δ_e	Elevator deflection angle	deg	C_{m_q}	Variation of C_m with respect to pitch rate	-
	-	-	-	-	Elevator Area	m^2	-	-	-
	-	-	-	C_l	Rolling moment coefficient	-	C_{l_β}	Variation of C_l with respect to sideslip angle	-
Lateral	-	-	-	δ_a	Aileron deflection angle	deg	C_{l_p}	Variation of C_l with respect to roll rate	-
	-	-	-	-	Aileron area	m^2	-	-	-
	-	-	-	C_n	Yawing moment coefficient	-	C_{n_β}	Variation of C_n with respect to sideslip angle	-
Directional	-	-	-	δ_r	Rudder deflection angle	deg	C_{n_r}	Variation of C_n with respect to yaw rate	-
	-	-	-	-	Rudder area	m^2	-	-	-
	-	-	-	-	-	-	-	-	-

Fig. 61 Parameter breakdown for each phase of Stability and Control [20].

 PENGUIN SUPERSONIC	SENIOR DESIGN: MAE 4351 Project	Ref.: MAE 4351-001-2021 Date: 11. May. 2023 Name: Gayathri Kola Status: In Progress
---	------------------------------------	---

5.2. Configuration Layout (CL) for Stability and Control

5.2.1. Vertical fins sizing for directional stability – desired outcomes

Once the PS is finished, geometry will be used to size the control surfaces for the SR-71. The variables needed are listed in the IDA for Stability and Control (Fig 12). The methodologies being tested were from Nicolai, Raymer, and USAF Stability and Control DATCOM [5,26,27]. A reasonable range of values was taken into account to generate a plot of the rolling moment coefficient as a function of the vertical tail area.

The following are the assumptions made:

- $C_{L\alpha VT} = 2\pi$ (Symmetrical airfoil for vertical tail)
- $S_{ref} = 1880.918 \text{ ft}$ (Appendix B)
- $AR = 1.851$ (Appendix B)
- $\Lambda_{c/4} = 58.24^\circ$ (Converted to radians, estimate provided by Noah Blakely)
- $z_v = 0 \text{ ft}$ (assumed)
- $d = 5.25 \text{ ft}$ (Estimate provided by Austin Prior based on CAD geometry)
- $z_w = 0 - 10 \text{ ft}$ range with 2 ft increments.
- $b = 59 \text{ ft}$ (Appendix B)
- $S_{vt} = 0 - 600 \text{ ft}^2$ with 100 ft^2 increments

Following were the resources and equations used for the build-up:

Nicolai (Page. 591):

$$\left(1 + \frac{d\sigma}{d\beta}\right) \frac{q_{VT}}{q} = 0.724 + \frac{3.06 \left(\frac{S'_{VT}}{S_{ref}}\right)}{1 + \cos \Lambda_{c/4}} + \frac{0.4 z_v}{d} + 0.009 AR \quad (13)$$

$$(C_{l\beta})_{VT} = -C_{L\alpha VT} \left(1 + \frac{d\sigma}{d\beta}\right) \frac{q_{VT}}{q} \frac{S_{VT}}{S_{ref}} \frac{z_w}{b} \quad (14)$$

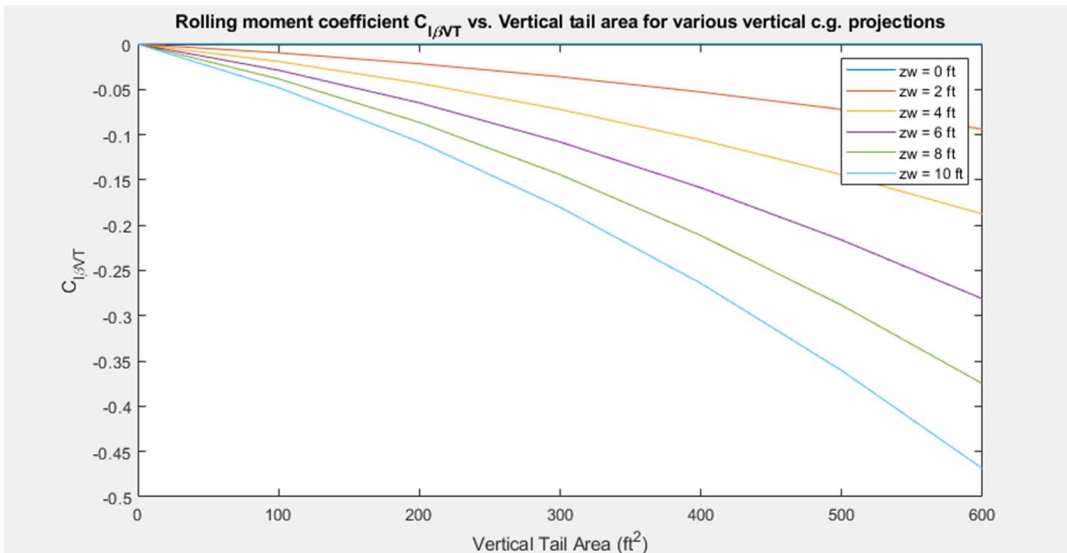


Fig. 62 Rolling moment coefficient $C_{l\beta VT}$ vs. vertical tail area for various vertical c.g. positions.

This plot was made to see how the vertical distance from the fuselage to the vertical tail aerodynamic center would influence the vertical tail area and rolling coefficient of the vertical tail. As the area and vertical displacement increases, the more destabilizing it is for the vertical tail.

 PENGUIN SUPersonic	SENIOR DESIGN: MAE 4351 Project	Ref.: MAE 4351-001-2021 Date: 11. May. 2023 Name: Gayathri Kola Status: In Progress
---	--	---

5.2.2. Vertical Fins Sizing

In Configuration Layout (CL), various configurations of the vertical tails are laid out. For reference, following in Table 10, are the various configurations identified from the book “Stability and Control of Conventional and Unconventional Aircraft Configurations” [Chudoba]. These configurations can be tested for in CL phase. Additionally, the number of vertical fins can be another trade study performed for the CL phase.

Table 10. Airplane Configurations [Chudoba]

Type	Example Aircraft
Tail-Aft Configuration	A380
Tail-First Configuration	XB-70
Three-Surface Configuration	Piaggio P-180
Flying-Wing Configuration	YB-49
Oblique-Wing Configuration	NASA AD-1
Oblique Flying-Wing Configuration	

To size the vertical tail or any control surfaces, the vehicle geometry must be known first. This is why the control surface sizing is not performed in the PS phase. To better layout the control surfaces, similar vehicles like the SR-71 can be referenced. The following supersonic vehicles have been identified to be the most similar to the SR-71 in Table 9. The resource “XB-70, SR-71, & TU-144: Large Supersonic Transports” lists all the geometries of these chosen vehicles. The CL phase lays out various possible configurations and their possible control surfaces. The actual control surface sizing for each flight phase is done in the CE phase with higher fidelity models.

Here is the methodology for vertical tail sizing chosen for each flight phase. First, Chapter 6 of “Aircraft Design: A Systems Engineering Approach” was chosen for various sizing considerations. Additionally, “Aircraft Design: A Conceptual Approach” by Raymer was used for further sizing analysis. The main lateral-directional aspects of sizing include:

- Trim (directional) for this report, OEI (One-Engine-Inoperative) trim condition.
- Aircraft has to be able to trim in yaw by the yawing moments produced by the engine thrust.
- Stability (directional) for this report.

During week 10, the geometry team member Austin Prior provided an approximate rudder geometry that could be used [35]. Once all configurations have been finalized, the rudders will be sized based on stability and propulsion requirements. The engine placement will mainly depend on aerodynamics leading nose shock angle. The engine must be placed inside the shock angle to avoid malfunctions.

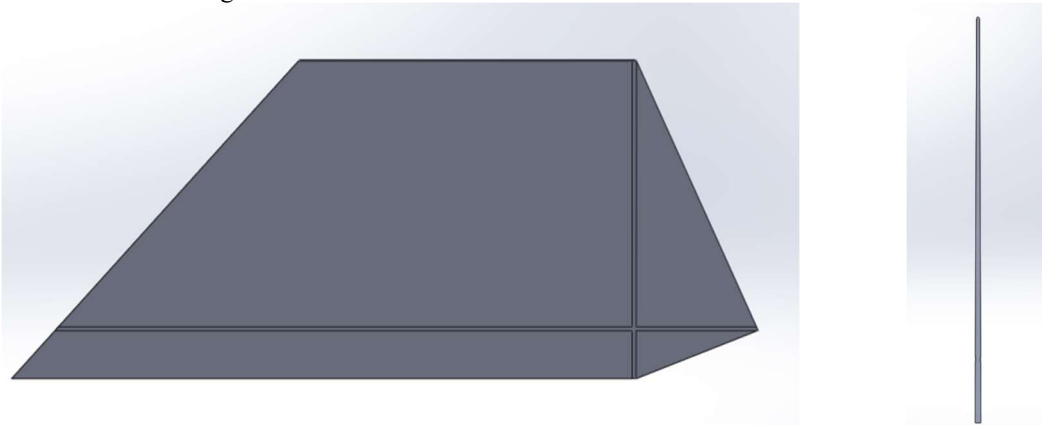


Fig. 63 Vertical tail geometry provided by Austin Prior [35]

5.2.3. Elevons sizing

The following Fig. 64 was produced by team member Noah for sizing the elevon area as a function of the pitching moment coefficient using the methods set out by Raymer [27]. This is the kind of analysis being aimed for lateral stability as a function of the elevon area. Currently, the right set of equations has not been found specifically for elevons. The author is looking into Raymer for further elevon analysis.

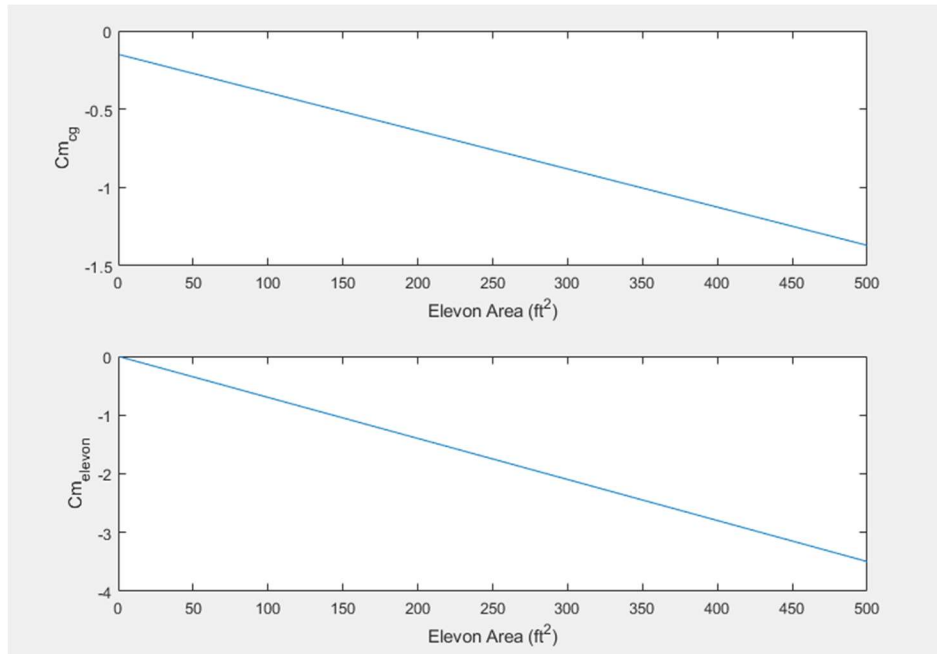


Fig. 64 Elevon sizing for pitch stability by Noah Blakely [41].

The following graph in Fig. 65 is produced by Austin for elevon sizing during the cruise phase.

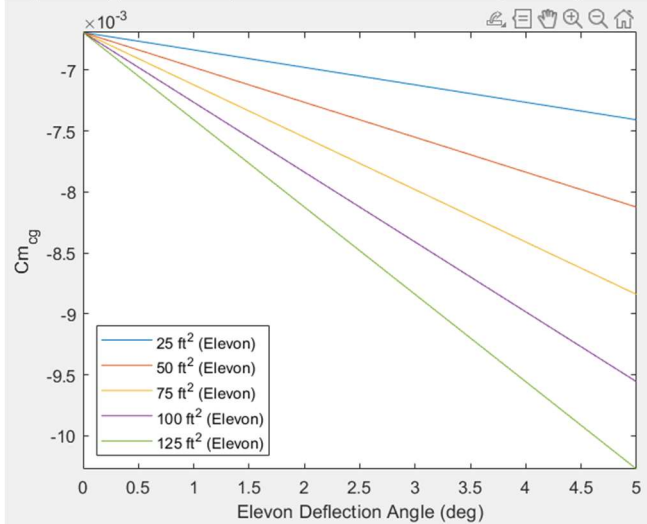


Fig. 65 Elevon sizing for pitch stability during cruise by Austin Prior [35].

5.3. Configuration Evaluation for S&C

For the CE phase, resources such as DATCOM and the software called OpenVSP are being considered. OpenVSP allows for a CAD model to be imported and analyzed for aerodynamics and stability and control. Specifically, analysis pertaining to trim conditions can be performed. The author is currently learning to use this software along with the CAD model provided by Austin.

 PENGUIN SUPERSONIC	SENIOR DESIGN: MAE 4351 Project	Ref.: MAE 4351-001-2021 Date: 11. May. 2023 Name: Gayathri Kola Status: In Progress
---	--	---

Table 11. Literature for Stability and Control Configuration Evaluation.

Title	Author	Year	Application
SR-71 Researcher's Handbook	Et. al	2010	Mission Profile verification numbers
SR-71 Flight Manual	Loftin, L. K	1980	SR-71 Verification data (main source)
Development of the Vehicle Configuration Compendium: A Comprehensive Data-Information-Knowledge System to Aid in High-Speed Vehicle Design [20]	Simon, S.	2021	SR-71 Verification Data

5.3.1. CE – Initial literature testing

Another option being considered is USAF DATCOM. There is an online coded version of the document that can be used to analyze conditions for subsonic, transonic, supersonic, and hypersonic flight based on body configuration. The following assumptions were made to produce the plot in Fig. 66:

- $\beta = 1 - 10^\circ$ (converted to radians)
- $M = 1 - 4$ (Mach number range)
- $\alpha = 1^\circ$ (angle of attack of aircraft)
- $AR = 1.851$ (Appendix B)
- $\bar{c} = 29.504$ ft (Appendix B)

Following are the equations used from DATCOM (Pages. 1-38):

$$\frac{C_{n\beta}}{\alpha^2} = \frac{1}{\pi AR^2 \beta^2} \left[\frac{4M^2}{3} + 8M^2 \frac{x}{\bar{c}} - \pi \left\{ \frac{AR(1 - \beta^2)}{\beta} \frac{3 + \beta^2}{3\beta^2} \right\} \right] \frac{1}{57.3} \quad (15)$$

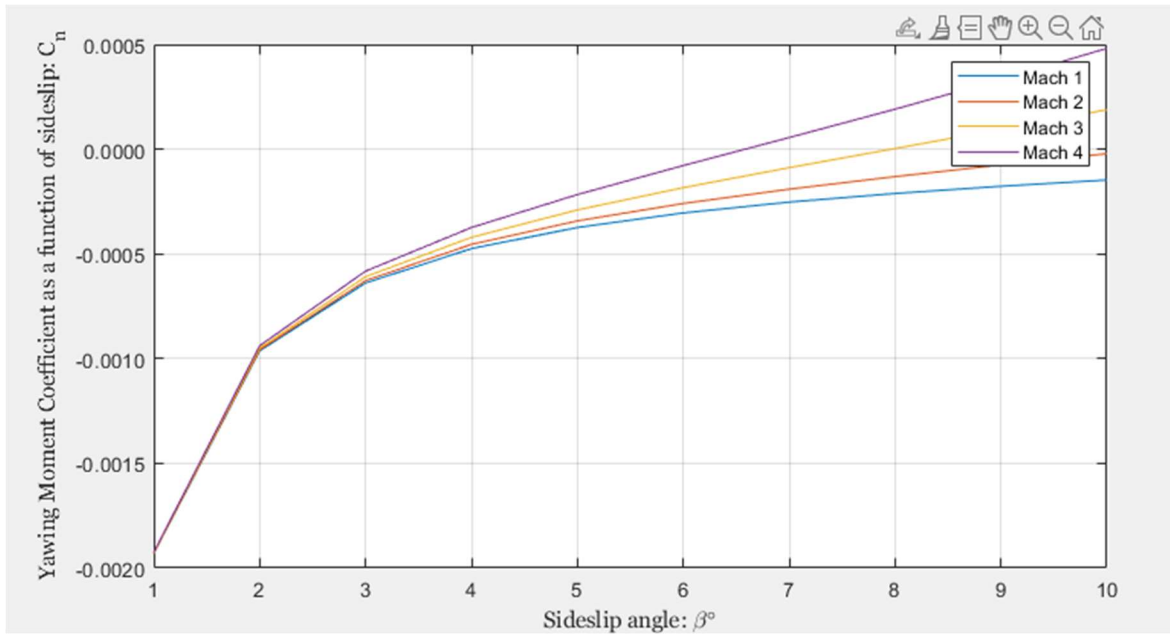


Fig. 66 Yawing moment as a function of sideslip angle for supersonic Mach numbers.

The following in Fig. 67 shows the static margin change as a function of Mach number produced by Austin Prior. This shows for each phase segment.

 PENGUIN SUPersonic	SENIOR DESIGN: MAE 4351 Project	Ref.: MAE 4351-001-2021 Date: 11. May. 2023 Name: Gayathri Kola Status: In Progress
---	--	---

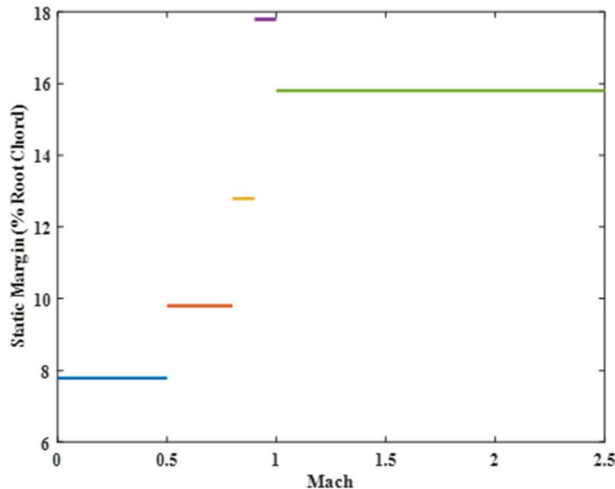


Fig. 67 Static margin as a function of Mach number by Austin Prior [35].

5.3.2. Software Review

Table 12. Software Review for S&C Configuration Evaluation.

Serial No.	Software Name	Benefits	Drawbacks	Application
1.	USAF DATCOM	Applicable for subsonic, supersonic flight, multiple configuration options.	Lower fidelity, too many inputs for coding	Subsonic, supersonic, moment coefficient calculations.
2.	OpenVSP/VSPAero	Trim Drag Calculations for Control Surfaces	Software crashes, needs to be verified	Stability & Control analysis for wing & control surfaces.
3.	AVL (Vortex Lattice Method) from MIT	Stability & Control derivatives, trim drag calculations, dynamic stability	Fortran	Stability and trim drag calculations.
4.	Flow5	Stability derivatives	Planes operating at low Reynolds numbers	Preliminary design of wings,
5.	MATLAB Vortex Lattice Method	Lateral-Directional Stability derivatives	Too many output graphs using meshgrids	Stability derivatives for conventional swept wings.

5.4. Vertical Tail Sizing

This section will cover the buildup of vertical tail sizing for each flight phase. The elevon sizing is performed by team lead, Austin. The textbook “Aircraft Design: A Systems Engineering Approach” has been identified as a suitable resource for twin vertical tail sizing [24]. First, the textbook by Raymer was consulted for a general vertical tail sizing process outlined in Chapter 6.

Raymer’s approach first goes over geometric sizing of the aircraft. Here, the fuselage length is estimated based on the type of aircraft being looked into. After estimating the fuselage length, the vertical tail volume coefficient must be estimated. This can be done by looking into similar aircraft and obtaining an approximate number for the coefficient. Then, the moment arm from the wing quarter-chord to the vertical tail quarter chord is estimated as a function of percent fuselage length. For the original SR-71, the vertical tail moment arm must be small since the tails were mounted on engines which were a part of the delta wing. If twin vertical tails are being used, which is the case of the original SR-71, the sum of the two tail areas will be the total vertical tail area, S_{VT} . Following is the summary of the method obtained from Raymer [27]:

- Estimate fuselage length based on aircraft type – Get from Geometry
- Estimate the vertical tail moment arm, l_{VT} as percent fuselage length.
- Needed numbers: wingspan b_w and wing area S_w .
- For twin vertical tails, S_{VT} is the sum of the two tail areas.
- Calculate the vertical tail area using the equation below:



$$S_{VT} = \frac{C_{VT} b_w S_w}{L_{VT}} \quad (16)$$

Additional considerations:

- For an all-moving tail, Raymer recommends a 10% reduction of the tail volume coefficient.
- For a T-tail configuration, Raymer recommends a 5% reduction in tail volume coefficient.
- For a V-tail configuration, Raymer recommends the tails must be sized for the total tail surface area. So, S_{VT} must be divided by two, and the appropriate distance the tails and their dihedral angles must be taken into account. The tail dihedral must be close to 45 degrees, can be calculated using the equation below:

$$\Gamma = \tan^{-1} \sqrt{\frac{S_{VT}}{S_{HT}}} \quad (17)$$

- The tail taper ratio is often similar to wing taper ratios. The general number for rudders is about 25-50% of tail chord.
- Addition of aerodynamic weight balance before the control surface hinge line reduces flutter tendencies. Flutter tendencies can cause tearing of wing or control surfaces due to weight imbalance.
- “*The hinge axis should not be farther aft than about 20% of the average chord of the control surface*” [27].
- All-moving vertical tails such as in the case of SR-71, are used to increase control authority during supersonic flight. Other aircraft with all-moving vertical tails – F23, North American F-107.

Using the information above and the original SR-71 numbers given in Fig. 49, the following plot was generated for three different tail configurations. Namely, all-moving tails, T-tail, V-tail. From the data in Fig. 49, and recalculating for tail volume coefficient of the original SR-71, it becomes clear that the total vertical tail area mentioned is for one single tail because c_{VT} is 0.0301. The dashed line in the Fig. 68 below accounts for both the vertical tails with a tail volume coefficient of 0.0603. As seen, it is very close to the all-moving tail coefficient of 0.07 which were taken from Raymer for Jet Fighter type aircraft given in Chapter 6. With this information, we can deduce that the total vertical area should range from 200-400 ft². The actual tail volume coefficient numbers used are given in Appendix B.

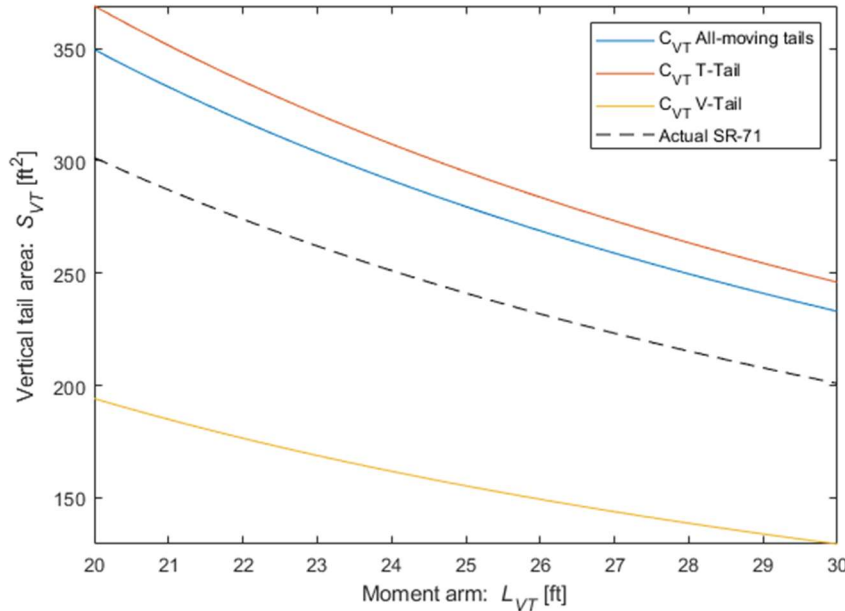


Fig. 68 Vertical tail area for different tail configurations by varying tail volume coefficient.

The reason why the twin vertical tails are mounted on top of the engine is to improve rudder control power, especially at low speeds [42].

Table 13. Summary of vertical tail sizing for CE.

 PENGUIN SUPERSONIC	SENIOR DESIGN: MAE 4351 Project	Ref.: MAE 4351-001-2021 Date: 11. May. 2023 Name: Gayathri Kola Status: In Progress
---	--	---

Phase	Title	Author	Application/Type
1	Aircraft Design: A Systems Engineering Approach	Mohammad. S	Twin vertical tails sizing step-by-step methodology
2	Aircraft Design: A Conceptual Approach	Raymer	Lateral-directional trim equations and build-up
3	Fundamentals of Aircraft Design – Volume 1	Nicolai	Maneuver flight method build-up, OEI, crosswind, trim drag
4	Airplane Flight Dynamics and Automatic Flight Controls	Roskam	Trim equations, uncommon moment coefficients, maneuvers.

5.4.1. Rudder trim calculation

The rudder trim condition is an important aspect of yaw stability. The maximum deflection angle of rudder can be calculated by equating the yawing moment coefficient to zero. The method used here is referenced from Roskam [28].

$$C_n = C_{n_0} + C_{n\beta}\beta + C_{n\delta_e}\delta_e + C_{n\delta_r}\delta_r = 0 \quad (18)$$

The term $C_{n\delta_e}$ is for the outboard elevons that are responsible for roll. Similarly, δ_e is the outboard elevon deflection angle. These terms are included in the equation because control surfaces for roll and yaw affect each other. The term C_{n_0} is the value of C_n when β, δ_e , and δ_r are equal to zero. By equating the above equation to zero, the rudder deflection can be found as follows:

$$\delta_r = \frac{-C_{n_0} - C_{n\beta}\beta - C_{n\delta_e}\delta_e}{C_{n\delta_r}} \quad (19)$$

Where $C_{n\delta_r}$ is the yawing moment due to rudder deflection, can be calculated using the equation below:

$$C_{n\delta_r} \approx 0.9C_L \alpha_{VT} \frac{l_v S_v}{b S_{ref}} \tau \quad (20)$$

The values for vertical tail lift coefficient will be provided by the aerodynamics team based on the airfoil chosen for the rudder. Noah's recommendation was to choose a symmetrical airfoil from the NACA 6 series such as NACA 63-010A. The term τ is the change in yawing moment coefficient due to rudder deflection with a constant angle of attack. This value is taken from the plot given in Nicolai chapter 21 seen below. Since the rudder for SR-71 is all-moving vertical tails, the value of τ is speculated to be equal to 1. However, from Fig. 49, the rudder has a movable area and a total area. The ratio of the movable area to total area is 0.47. This would mean the value of τ could be close to 0.5.

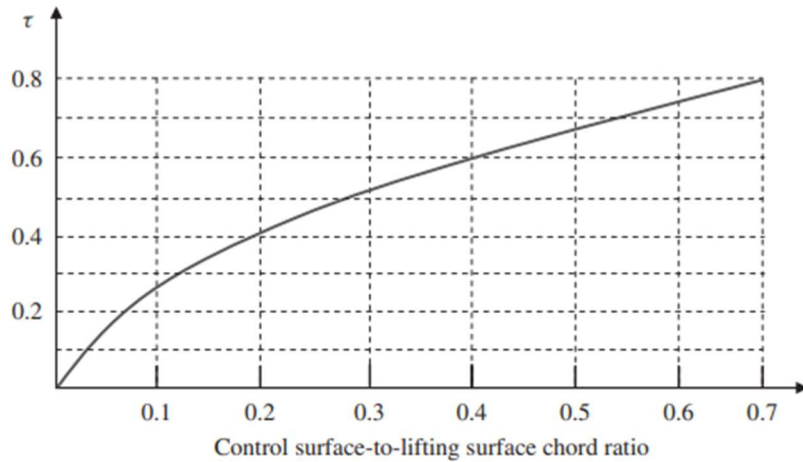


Fig. 69 Rudder effectiveness chart [24].

For lateral (roll) trim, Roskam method was chosen and given below.

$$C_l = 0 = C_{l_0} + C_{l\beta}\beta + C_{l\delta_e}\delta_e + C_{l\delta_r}\delta_r \quad (21)$$

Similar to yawing moments, the term C_{l_0} is the value of C_l for β, δ_e and δ_r are equal to zero. To calculate the rolling moment coefficient due to sideslip $C_{l\beta}$, the following equation build-up from Raymer:



$$C_{l\beta_v} = -C_{F\beta_v} \frac{\partial \beta_v}{\partial \beta} \eta_v \frac{S_v}{S_w} \bar{Z}_v \quad (22)$$

$$(C_{l\beta})_\Gamma = \frac{-C_{L\alpha}\Gamma}{4} \left[\frac{2(1+2\lambda)}{3(1+\lambda)} \right] \quad (23)$$

$$C_{l\beta_{wf}} = -1.2 \frac{\sqrt{A} Z_{wf} (D_f + W_f)}{b^2} \quad (24)$$

$$C_{l\beta_w} = \left(\frac{C_{l\beta_{wing}}}{C_L} \right) C_L + (C_{l\beta})_\Gamma + C_{l\beta_{wf}} \quad (25)$$

The first term in equation 25 can be found using the chart presented in Raymer chapter 16 seen below. A more detailed equation based on wing geometry (for a double-delta wing) has been found in DATCOM to calculate the same term. One drawback with the DATCOM equation given in CE section is that it requires many inputs of wing geometry and sorting through the large empirical data for many other constants. However, the downside of Raymer's method for the first term given the figure below is that the plots are only for taper ratio of 0.5 and 1. The taper ratio for a delta wing of the SR-71 is nearly 0.

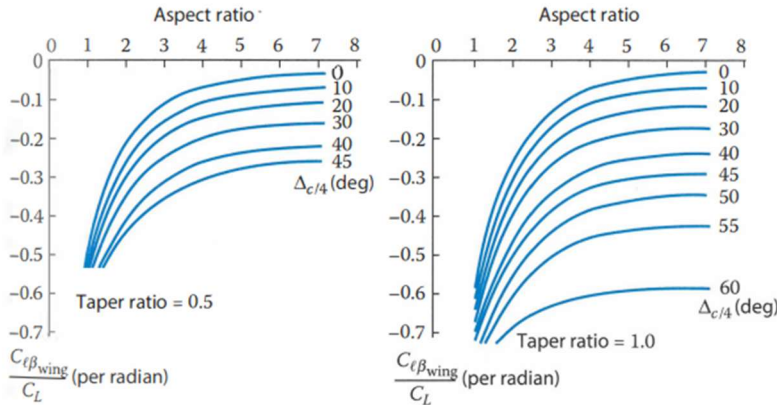


Fig. 70 Dihedral effect of aspect ratio for given taper ratio and wing sweep angles [27].

Then the total rolling moment is just the sum of rolling moment due to wing and vertical tail as seen below. Note, the rolling moment due to fuselage is included as the last term of equation 25.

$$C_{l\beta} = C_{l\beta_w} + C_{l\beta_v} \quad (26)$$

For the rudder rolling moment coefficients $C_{l\delta_r}$:

$$C_{l\delta_r} = C_{l\alpha_{VT}} \tau \frac{S_v l_v}{S_{ref} b} \quad (27)$$

5.4.2. Sizing for One-Engine-Inoperative (OEI)

For asymmetric thrust condition, that is when one engine fails, the methods given Nicolai can be used to size the rudder. The engine thrust T and engine drag D_e can be obtained from the propulsion team for takeoff phase at $1.2V_{TO}$. The rudder must be sized such that it can hold $\beta = 0$ at OEI.

$$C_n = 0 = -\frac{(T + D_e)}{q_\infty S_{ref} b} + C_{n\delta_r} \delta_r \quad (28)$$

From the following parameters obtained from teams, the OEI was calculated.

- Engine thrust from Fig #, $T = 17,000$ lb. (single engine thrust)
- Takeoff velocity, $V_{TO} = 354.44$ ft/s
- Engine (form) drag $D_e = 813.44$ lb (form drag for 2 engines 2 and nacelles) provided by Noah Blakely. The author is waiting for a value of total engine drag from Propulsion team for more accuracy.
- The ratio τ means the rudder effectiveness value seen in Fig # above. It relates the ratio of rudder area to vertical tail area. The author is unsure which value of τ to use since the engine drag value appears to be very



low. For a value of $S_{VT} = 300 \text{ ft}^2$, $l_{VT} = 18 \text{ ft}$, $\delta_r = 10^\circ$, the author solved for the value of $D_e = 15,638.3 \text{ lbs}$. It is 90% of the thrust value of 17,000 lbs.

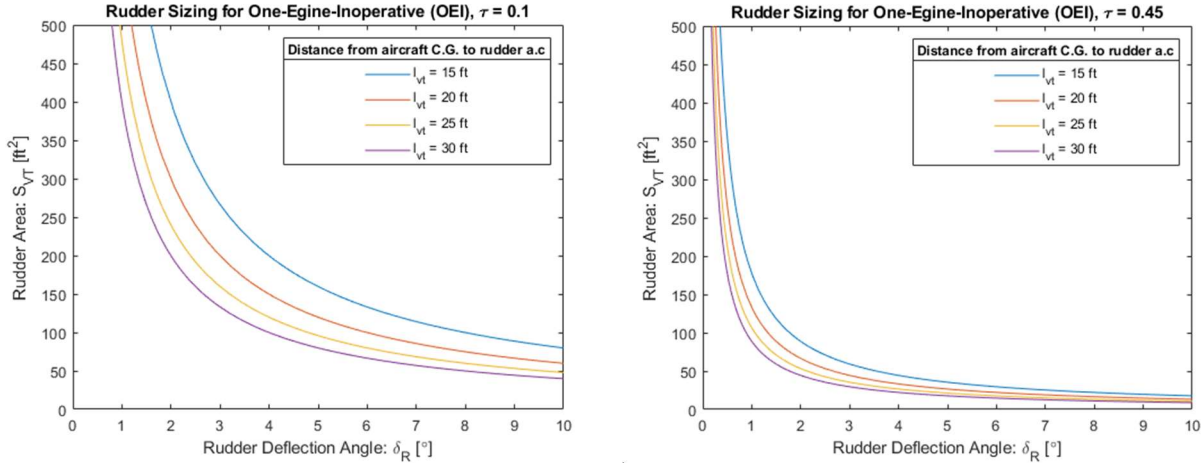


Fig. 71 Rudder Sizing for One-Engine-Inoperative.

Another method from Mohammad Sadraey was used to size the vertical tail for OEI and the tail geometry was determined. This approach appears to be more streamlined and yields the most accurate results. Following are equations used:

$$N_A = -T_L y_T = C_{n_0} + C_{n_\beta} \beta + C_{n_{\delta_e}} \delta_e + C_{n_{\delta_r}} \delta_r \quad (29)$$

Here, T_L is the thrust from both the engines that are equidistant from the fuselage centerline. The term y_T is the total distance between the two engines. The elevon deflection δ_e and the sideslip angle β are assumed to be zero at takeoff. This leaves with the following equation to calculate rudder deflection angle δ_r :

$$\delta_r = \frac{T_L y_T}{-q S b C_{n_{\delta_r}}} \quad (30)$$

In this method, the angle of attack effectiveness parameter is given by $\tau = c_R / c_{VT}$. Instead of the ratio of areas, it's the ratio of chords. This allows for easy calculation of the rudder height and vertical tail height (non-moving part).

$$C_{n_{\delta_r}} = -C_{L_{\alpha VT}} \frac{l_v S_v}{b S_{ref}} n_v \tau \frac{b_R}{b_v} \quad (31)$$

The text defines the variables b_R and b_v as the following given in Fig. # below.

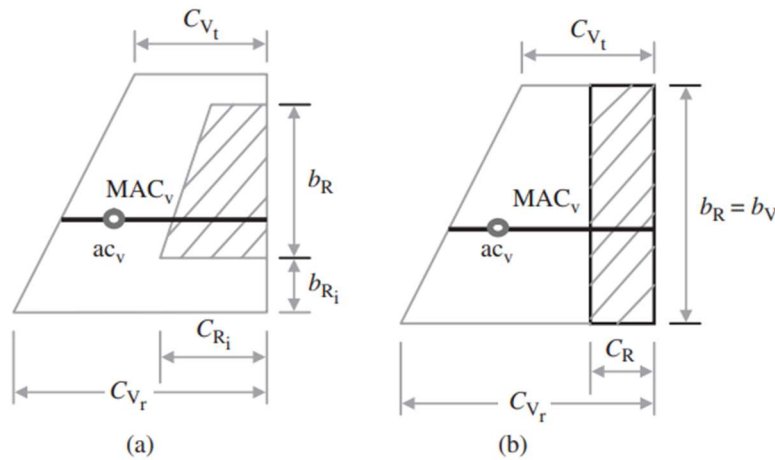


Fig. 72 Vertical tail geometry variables [24].



However, the current geometry being designed for the first configuration is an all-moving vertical tail. The vertical tail lift coefficient $C_{L\alpha_{VT}}$ is taken to be 2π , since the airfoil chosen is the same as the wing airfoil. It is a symmetrical, sharp-edged biconvex airfoil with the maximum thickness at 50% chord. The engine thrust is assumed to be 34,000 lbs. The following was the initial vertical tail geometry provided based on $l_e = 30$ ft.

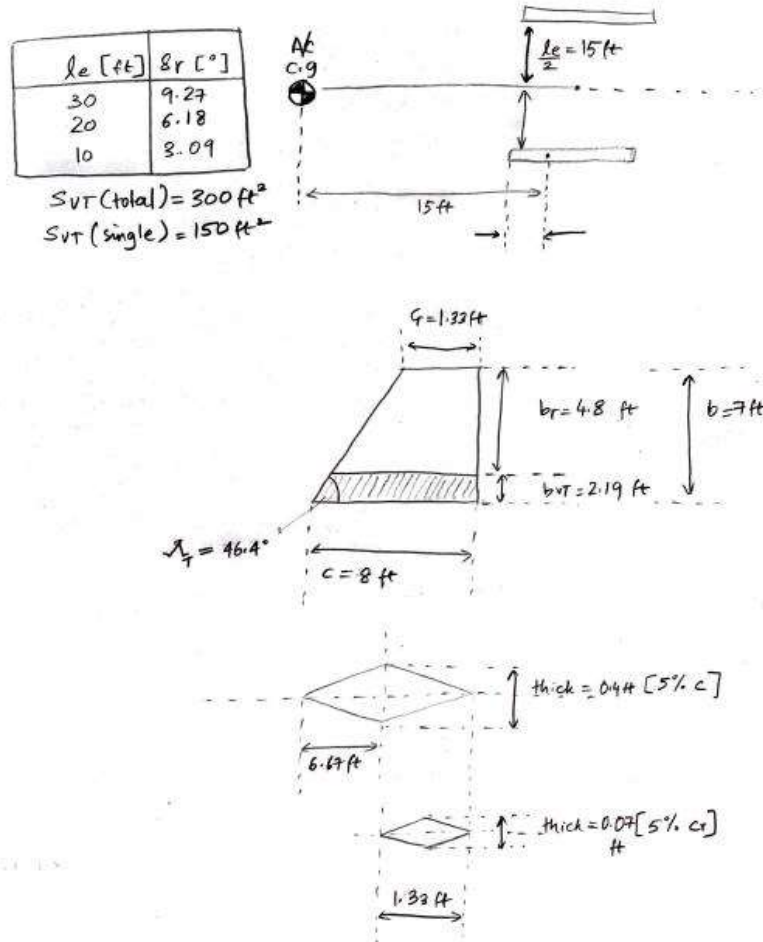


Fig. 73 Initial vertical tail geometry layout.

The vertical tail shape chosen is a right trapezoid, for simplicity. The original SR-71 had a generic trapezoid shape as seen in Fig. # below. The tail sweep angle was calculated using trigonometric relations based on the geometry.

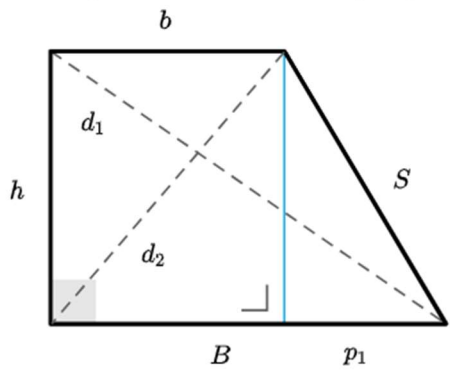


Fig. 74 Right trapezoid for 1st configuration.

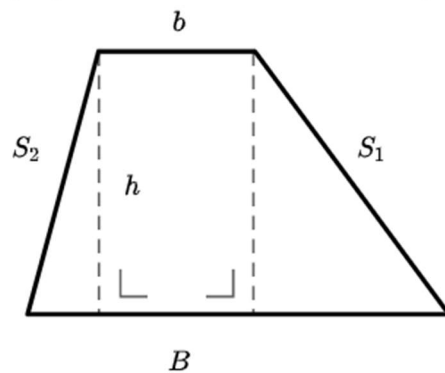


Fig. 75 Generic trapezoid of original SR-71.

Fig. 76 Trapezoid comparisons.



The total chord length at the base was estimated by referencing SR-71 drawings. The span of the tail (vertical height) was estimated as well. A small geometry code was written in MATLAB that calculates the minor geometries based on total chord length of the tail c_t , span of the tail b_t and single tail area S_{vt1} . Based on the engine placement estimate of $l_e = 30$ ft, Fig 77 were the initial estimates given to geometry member, Austin. However, this proved to be too small of vertical tails as seen in Fig. # below.

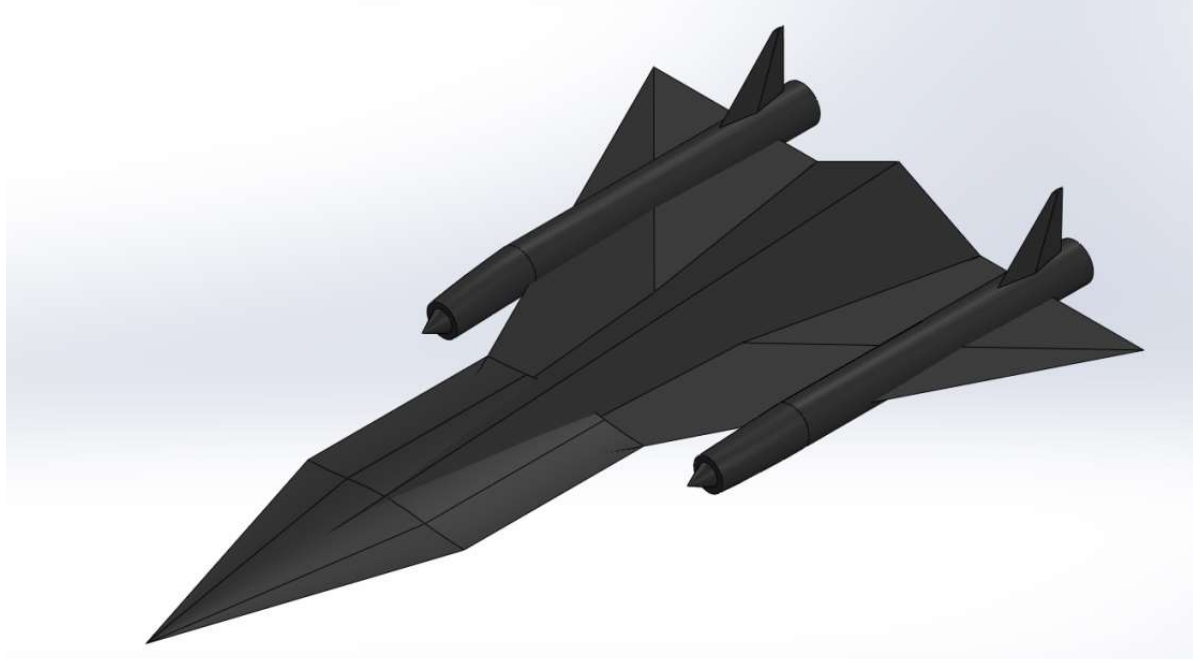


Fig. 77 CAD created by Austin Prior based on given estimates of tail geometry [35].

The engine placement value of $l_e = 16.87$ ft was obtained from Austin, developed based on Propulsion team minimum requirements as seen below in Fig. 78.

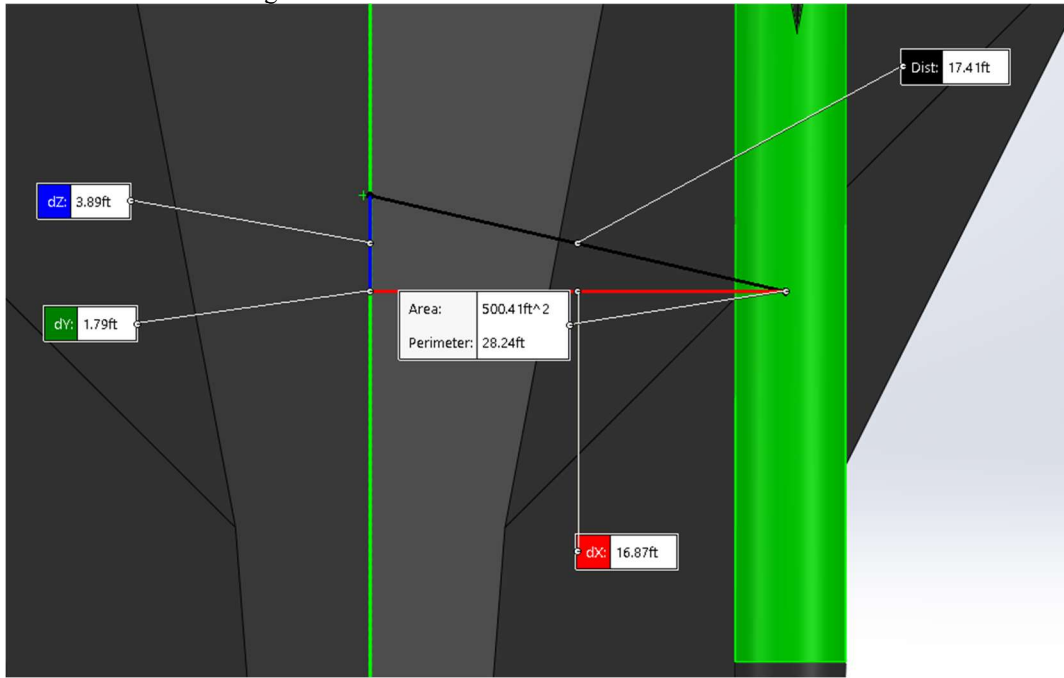


Fig. 78 Engine placement dimension given by Austin Prior [35].



With the new value of l_e and corrections made to the code, the maximum rudder deflection for OEI condition was plotted for a given rudder area range as seen in the Fig. 79 below.

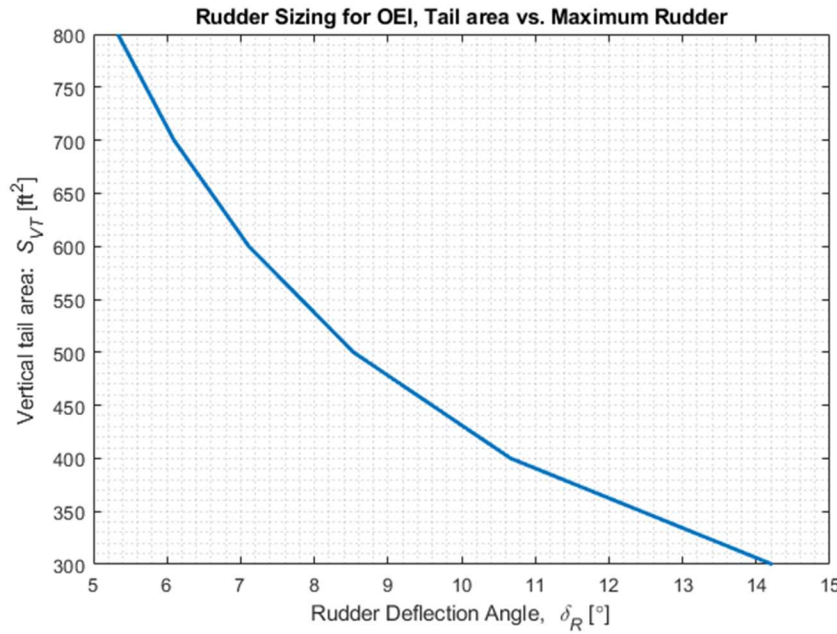


Fig. 79 Rudder Sizing for OEI.

Based on thrust values of cruise phase given by the Propulsion team, the asymmetric thrust due inlet unstart was calculated and plotted as seen below in Fig. 80. A total of 24,353 lb of thrust for 85,000 ft value was given by Propulsion team accounting for both the engines at cruise. A maximum rudder deflection angle of $\delta_r = 2.8^\circ$ can be set for $S_{VT} = 900 \text{ ft}^2$ as seen from the figure below.

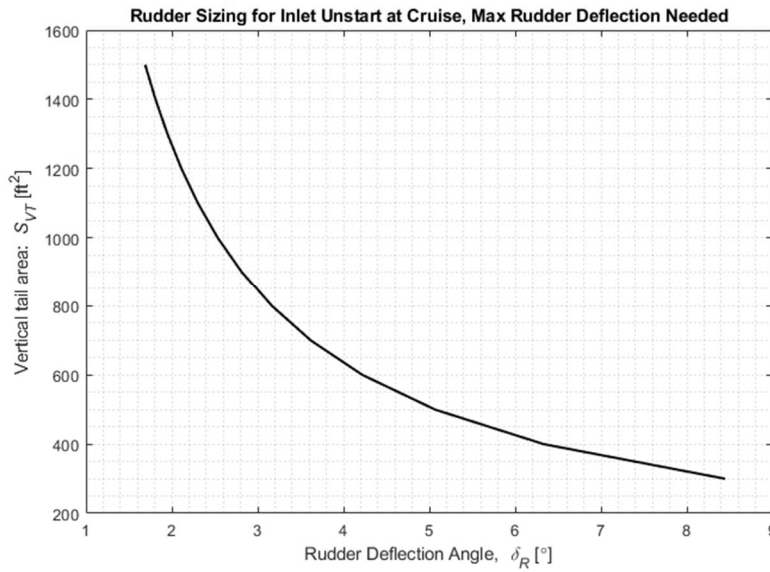


Fig. 80 Rudder sizing for Inlet Unstart at Cruise.

5.4.3. Sizing for crosswind condition

The crosswind condition for rudder sizing is also being taken into account using the methods established in Nicolai. Following the crosswind condition where maximum rudder deflection is $\pm 20^\circ$, same for OEI condition.

$$C_n = 0 = C_{n\beta}\beta + C_{n\delta_r}\delta_r \quad (32)$$

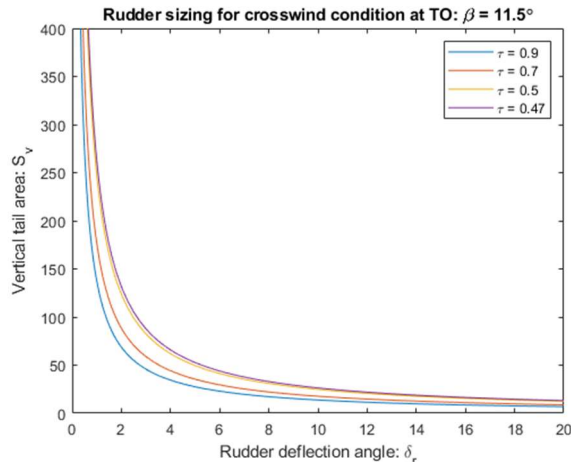


Fig. 81 Rudder sizing for crosswind conditions at takeoff.

For the plot in Fig. 81, the values used are given in the code in Appendix B. These values will change during CE when evaluating an actual configuration. The current values used are based off of SR-71 data and Shiori's C.G. estimates based on flight phase, above was the sizing for takeoff. The plot needs to be verified from SR-71 Flight Manual. Below is Shiori's C.G. estimates table used, and the following figure is the C.G. error based on flight manual.

Mach	Phase #	Weight (lb)	C.G. location from nose (ft)	A.C. location from nose (ft)	C.G. %MAC	C.G. %MAC (Manual)	error (%)
0.4	1	135412.5	67.06827153	68.23702195	22.97279076	21	9.394241691
0.8	2	129438.5	67.04229948	69.37446058	23.04636596	22	4.756208929
1.5	3	125381.5	67.02325052	72.81960681	23.10032903	23	0.43621316
2.5	4	109426.5	66.93463617	72.64667908	23.35136118	24.25	3.705727088
3	5	93857.5	66.81912275	72.56021521	23.67859467	24.4	2.956579222
3	6	89114.5	66.77591128	72.56021521	23.80100675	24.5	2.853033669
3	7	76507.5	66.63500752	72.56021521	24.20016755	24.85	2.615019926
0.8	8	70598.5	66.55164368	69.37446058	24.43632574	24.1	1.395542501
0.4	9	65162.5	66.46160078	68.23702195	24.69140477	21.65	14.04805898

Fig. 82 Weight estimate and C.G. location estimates per flight phase by Shiori Jo [38].

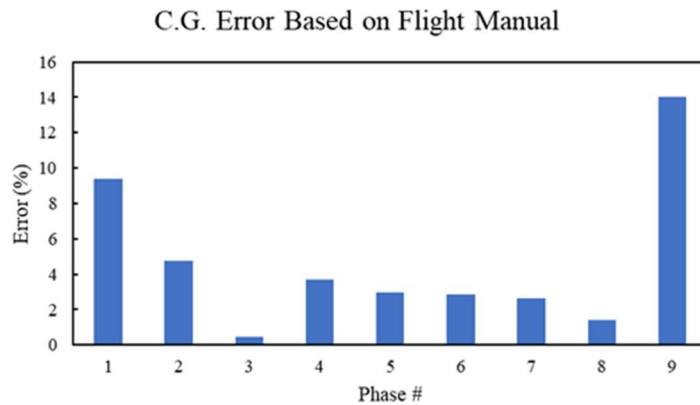


Fig. 83 C.G. error based on SR-71 Flight Manual by Shiori Jo [38].

 PENGUIN SUPersonic	SENIOR DESIGN: MAE 4351 Project	Ref.: MAE 4351-001-2021 Date: 11. May. 2023 Name: Gayathri Kola Status: In Progress
---	--	---

5.4.4. Rudder trim drag calculation.

Trim drag is produced when a control surface deflects to trim the aircraft. The total trim drag calculations are being performed by Controls member Noah. This section will go over the necessary coefficients that can be calculated when a rudder is deflected that produce drag.

5.5. Lateral-Directional Stability Derivatives for CE

Another aspect of lateral stability analysis is the calculation of stability derivatives that initially tell whether the aircraft is stable during flight. In CE phase, higher fidelity analysis methods can be employed for calculating these stability derivatives. One main method that can be initially employed is through the use of Stability and Control DATCOM by USAF (United-States-Air-Force). The full document gives methods and equations for calculating these derivatives based on the type of aircraft configuration used, i.e., wing (W), wing-body (WB), wing-body-tail (WBT), etc. DATCOM gives these equations for subsonic, supersonic, transonic, and hypersonic regimes. However, not all configurations have methods for all speed regimes. The full Stability and Control DATCOM was found with full descriptions and references of equations mentioned within the document. DATCOM will be utilized until a higher fidelity, computerized programs prove to be usable by the author within the time constraints. Computerized programs that employ Vortex-Lattice-Methods (VLM) are known to produce reasonable results for lateral-directional values. For the purpose of simplicity, only the following configurations are considered: W, WB, WBT.

5.5.1. Subsonic Description [26]

Since the main focus of this paper is on lateral stability, only yawning, rolling and sideforce coefficients will be focused in the evaluation process. MATLAB functions will be written and tested for any feasibility using generic geometry inputs. The effects of chine on the original SR-71 cannot be included in this analysis since the geometries used are either delta wings or double-delta wings. This could introduce significant errors in the calculations that need to be verified using original SR-71 results.

Following are the equations deemed usable for subsonic description along with their assumptions:

Assumptions for $C_{n\beta}$

- linear range, wing configuration (W)

$$\frac{C_{n\beta}}{C_L^2} = \frac{1}{57.3} \left[\frac{1}{4\pi AR} - \frac{\tan \Lambda_{0.25c}}{\pi AR(AR + 4 \cos \Lambda_{0.25c})} \left(\cos \Lambda_{0.25c} - \frac{AR}{2} - \frac{AR^2}{8 \cos \Lambda_{0.25c}} + 6 \frac{\bar{x} \sin \Lambda_{0.25c}}{\bar{c}} \right) \right] \quad (33)$$

Assumptions for $C_{l\beta}$

- DATCOM (Pg. 1484) wing configuration (W)
- Double-delta wings, A_i = inboard panel aspect ratio, A_o = outboard panel aspect ratio
- No twist
- No wing dihedral
- Below Mach 0.6, A_i and $A_o \geq 1$,
- Sideslip angle range: $\beta = \pm 5^\circ$

Note, there are many inputs needed to calculate this variable and the inputs are currently being sorted through from the DATCOM document. The author was unable to configure the DATCOM online software and has to rely on coding this term using MATLAB. A simpler way was found in methods given by Raymer which has been discussed on CL section.

Moment due to sideforce as a function of sideslip angle, $C_{Y\beta}$:

- From DATCOM (Pg. 40), wing configuration, subsonic, constant chord swept wings, not so applicable.

$$C_{Y\beta} = C_L^2 \left[\frac{6 \tan \Lambda \sin \Lambda}{\pi AR(AR + 4 \cos \Lambda)} \right] \frac{1}{57.3} \text{ per deg} \quad (34)$$

For subcritical speeds, Prandtl-Glauert correction factor needs to be applied:

$$\left(\frac{C_{Y\beta}}{C_L} \right)_M = \frac{AR + 4 \cos \Lambda}{ARB + 4 \cos \Lambda} \left(\frac{C_{Y\beta}}{C_L} \right)_{\text{low speed}} \quad (35)$$

Where,

$$B = \sqrt{1 - M^2 \cos^2 \Lambda} \quad (36)$$

 PENGUIN SUPERSONIC	SENIOR DESIGN: MAE 4351 Project	Ref.: MAE 4351-001-2021 Date: 11. May. 2023 Name: Gayathri Kola Status: In Progress
---	------------------------------------	--

The previous mentions of $C_{Y\beta}$ calculation for twin vertical tails from DATCOM has been removed due to its complexity in calculation.

5.5.2. Supersonic Description [26]

Yawing moment due to sideslip angle, $C_{n\beta}$:

- DATCOM, yawing moment coefficient due to sideslip angles as a function of angle of attack, rectangular planform, supersonic, wing configuration.

$$\frac{C_{n\beta}}{\alpha^2} = \frac{1}{\pi AR^2\beta^2} \left[\frac{4M^2}{3} + 8M^2 \frac{x}{c} - \pi \left\{ \frac{AR(1-\beta^2)}{\beta} \frac{3+\beta^2}{3\beta^2} \right\} \right] \frac{1}{57.3} \quad (37)$$

The previous mentions of $C_{n\beta}$ for a sweptback planform for wing, wing-body configurations has been removed to due many inputs needed. Instead, the rectangular planform equation has been chosen for simplicity. This method may not yield accurate results. Similarly, methods listed for $C_{l\beta}$ and $C_{Y\beta}$ from DATCOM for supersonic regime calculations have been removed from this buildup due to their high complexity. Methods set out Raymer have been used instead for $C_{l\beta}$.

5.5.3. Stability Derivatives Verification

Not many verification numbers have been found for the original SR-71 to compare rolling and yawing moment coefficient values. However, an experiment performed by NASA in 2009 named Linear Aerospike SR-71 Experiment (LASRE) documented it's longitudinal, lateral and directional stability calculations.

$$\begin{aligned} C_Y &= C_{Y_b} + C_{Y_\beta} \beta + \frac{b}{2V} (C_{Y_p} p + C_{Y_r} r) \\ &\quad + C_{Y_{\delta a}} \delta a + C_{Y_{\delta r}} \delta r \\ C_l &= C_{l_b} + C_{l_\beta} \beta + \frac{b}{2V} (C_{l_p} p + C_{l_r} r) \\ &\quad + C_{l_{\delta a}} \delta a + C_{l_{\delta r}} \delta r \\ C_n &= C_{n_b} + C_{n_\beta} \beta + \frac{b}{2V} (C_{n_p} p + C_{n_r} r) \\ &\quad + C_{n_{\delta a}} \delta a + C_{n_{\delta r}} \delta r \end{aligned}$$

Fig. 84 Equations used by NASA LASRE experiment for lateral-directional stability [14].

Possible equations for method verification obtained from NASA LASRE experiment. This experiment was conducted to allow access to space for a single-stage-to-orbit (SSTO) mission using a linear aerospike engine. This project aimed to further development of the X-33 demonstrator program. A modified payload was mounted on SR-71A, and flight stability, control and performance tests were conducted. The experiment first conducted a baseline SR-71A configuration flight test, wind tunnel tests, flight simulations, before conducting a flight test with the LASRE pod mounted on SR-71A. The baseline SR-71A stability flight test results can be used for method verification. One limitation is that the test results presented are only upto Mach 1.8 – 2.0.

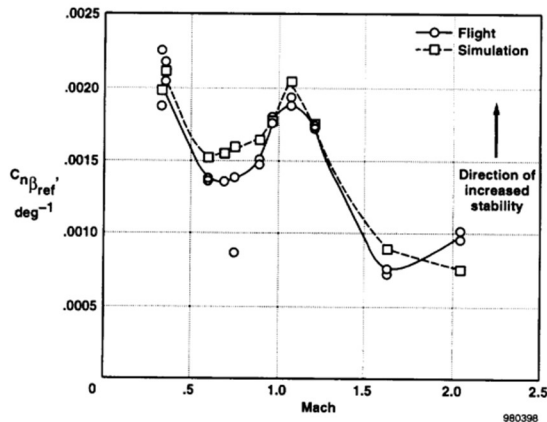


Fig. 85 Baseline SR-71 directional stability derivative for LASRE experiment.

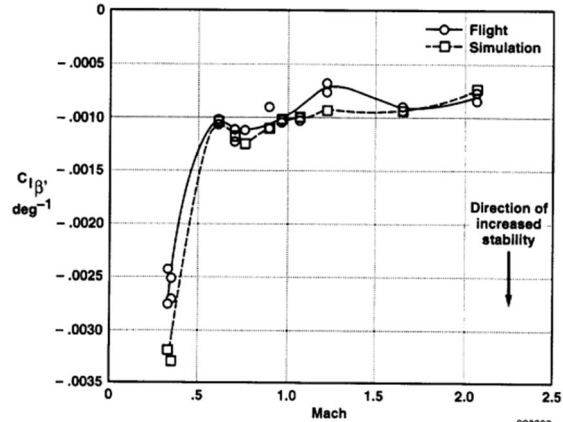


Fig. 86 Baseline SR-71 dihedral stability derivative for LASRE experiment.

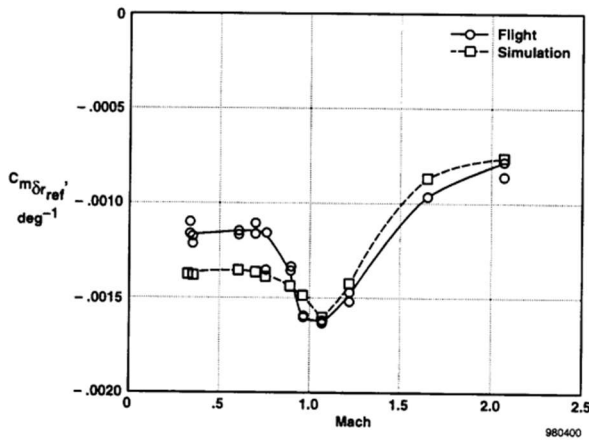


Fig. 87 Baseline SR-71 rudder effectiveness derivative for LASRE experiment.

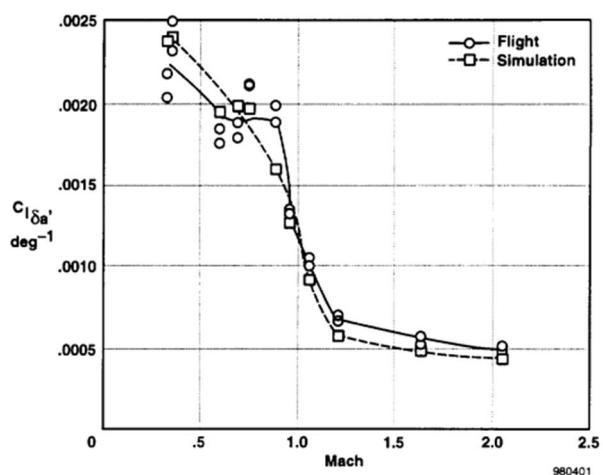


Fig. 88 Baseline SR-71 aileron effectiveness derivative for LASRE experiment.

Fig. 89 Stability derivatives verification from the LASRE Experiment [14].

5.6. Lateral-Directional Stability – Mission Profile Description

Following are phase requirements breakdown based on the chosen mission profile for a single-legged mission. Many of the requirements listed are for the full Stability & Control team, not just lateral-directional stability. For this report, only static stability is being considered. The main verification resources come from the SR-71 Researcher's Handbook and SR-71 Flight Manual. Verification numbers from SR-71 Researcher's Handbook are based on the original SR-71's operational limits for each flight phase [22,25].

5.6.1. Phase 1 – Takeoff Description

Phase Requirement:

- Subsonic Mach range: $M = 0$ to 0.4 .
- Maximum elevon deflection δ_r
- Maximum rudder deflection δ_e
- C.G. range for takeoff (needed from Weights & Balance)
- Maximum angle of attack at takeoff (needed from Performance)
- Flight stability: $C_{n\beta} > 0$, and $C_{l\beta} < 0$.
- Varied S_{VT} based on maximum rudder deflection angle δ_r
- Takeoff thrust required from both engines (needed from Propulsion)

 PENGUIN SUPersonic	SENIOR DESIGN: MAE 4351 Project	Ref.: MAE 4351-001-2021 Date: 11. May. 2023 Name: Gayathri Kola Status: In Progress
---	--	---

Methods:

- Subsonic DATCOM, Nicolai, Raymer methods for $C_{n\beta}$, $C_{l\beta}$, $C_{Y\beta}$

Verification:

- Critical angle of attack α for uncontrollable pitch = 18°
- Sideslip angle β (subsonic) = 12°
- Maximum angle of attack α subsonic, above FL 250: 10°
- Maximum angle of attack α subsonic below FL 250: 14°
- The C.G. has to be 22% forward
- Max rudder deflection δ_r for trim = 10° (all phases)
- LASRE Experiment data up to Mach 1.

5.6.2. Phase 2 – Subsonic Climb

Phase Requirement:

- Subsonic climb: Mach range: $M = 0.4$ to 0.8 .
- Maximum rudder deflection δ_r
- Maximum elevon deflection δ_e
- Angle of attack α at climb (needed from Performance)
- Flight stability: $C_{n\beta} > 0$, and $C_{l\beta} < 0$.
- C.G. during climb (needed from Weights & Balance)

Methods:

- Subsonic, supersonic DATCOM and Nicolai methods for $C_{n\beta}$, $C_{Y\beta}$ and Raymer for $C_{l\beta}$

Verification:

- Below 25,000 ft (Subsonic), AOA = 14°
- Above 25,000 ft (Subsonic), AOA = 10°
- The C.G. can be upto 24% aft for normal climb, refuel and supersonic acceleration.
- Sideslip angle = 12 deg (subsonic) and climb at 350 KEAS = 4.5°
- LASRE experiment data upto Mach 1.8

5.6.3. Phase 3 - Refuel and accelerate to Mach 1.5

- Accelerate from $M = 1$ to 1.5
- Angle of attack during acceleration
- Max elevon deflection δ_e
- Max rudder deflection δ_r
- C.G. during flight (needed from Weights & Balance)
- Flight stability: $C_{n\beta} > 0$, and $C_{l\beta} < 0$.

Methods: Same as phase 2 and 4.

Verification: Same as phase 4.

5.6.4. Phase 4 – Accelerated climb to Mach 3

Phase Requirement:

- Supersonic: Mach range: $M = 1$ to 3.2
- Maximum rudder deflection to trim
- Maximum elevon deflection to trim (laterally)
- Angle of attack range at supersonic climb
- Flight stability: $C_{n\beta} > 0$, and $C_{l\beta} < 0$.
- C.G. during acceleration (needed from Weights & Balance)

Methods: supersonic DATCOM methods for $C_{n\beta}$, and Raymer for $C_{l\beta}$

Verification:

- Above 25,000 ft (Supersonic, automatic inlet operation), $\alpha = 8^\circ$
- Above 70,000 ft (Supersonic, manual inlet operation), $\alpha = 6^\circ$
- Sideslip angle $\beta = 3^\circ$ (450 KEAS)
- Supersonic aft C.G. limit is 25% below $M = 3.2$



5.6.5. Phase 5 – Cruise at Mach 3

Phase Requirement:

- Flight stability: $C_{n\beta} > 0$, and $C_{l\beta} < 0$.
- Mach range: 3.0 – 3.2
- Angle of attack α for cruise, level flight (needed from Performance)
- C.G. during cruise (needed from Weights & Balance)

Methods:

- supersonic DATCOM methods for $C_{n\beta}$, and Raymer for $C_{l\beta}$

Verification:

- Not more than 1.5° nose-down trim for trimmed flight at 25% C.G.

5.6.6. Phase 6 – Turn 180.

Phase Requirement:

- Flight stability: $C_{n\beta} > 0$, and $C_{l\beta} < 0$.
- Supersonic Mach 3.0 turn
- Turn radius (needed from Performance)
- Max rudder deflection δ_r for turn
- Max outboard elevon deflection δ_e
- C.G. range (needed from Weights & Balance)
- Bank angle needed: 32 deg, max is 51.54 deg (given by performance). Following are the graphs provided by Wesley Junell for this phase [34]. The values for load factor n which is a function of bank angle ϕ are needed to calculate the outboard elevon deflection for a level turn. A table for the same was also provided by Wesley.

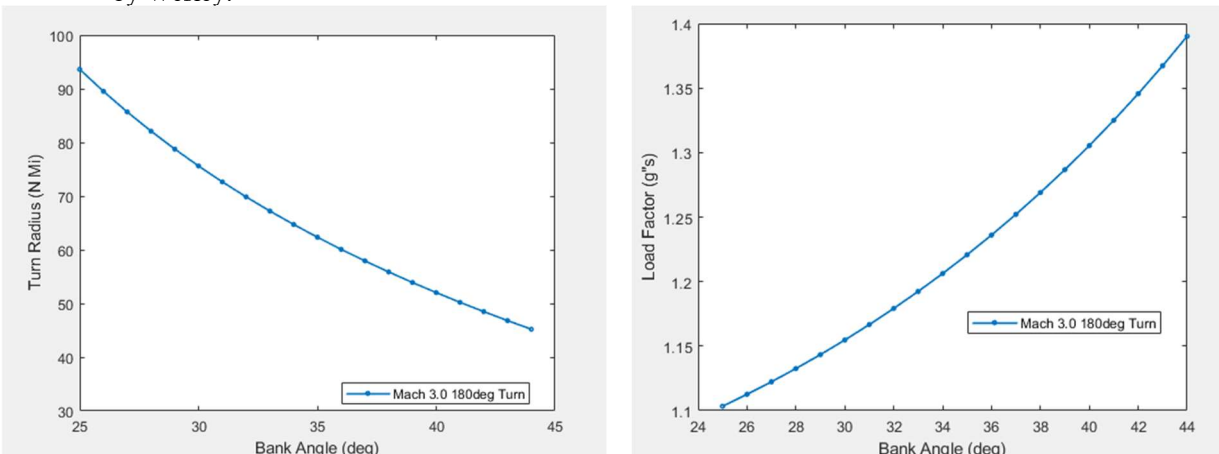


Fig. 90 SR-71 Turn radius, load factor versus bank angle level 180 turn, provided by Wesley Junell [34].

Methods:

- supersonic DATCOM methods for $C_{n\beta}$, and Raymer for $C_{l\beta}$, Bank angle and turn radius methods needed, LASRE Bank angle determination method.

Verification:

- The aircraft should descend to 83,000 ft before performing turn maneuvers. Since the maximum altitude of the aircraft is 85,000 ft and it is not recommended to perform turns at maximum altitude cruise profile.
- Prohibited maneuvers are stalls, spins, inverted flight (SR-71FM).
- Fig. 43 Bank angle versus turn radius for supersonic speeds verification .

5.6.7. Phase 7 – Cruise Back

Phase Requirement:

 PENGUIN SUPERSONIC	SENIOR DESIGN: MAE 4351 Project	Ref.: MAE 4351-001-2021 Date: 11. May. 2023 Name: Gayathri Kola Status: In Progress
---	--	---

- Flight stability: $C_{n\beta} > 0$, and $C_{l\beta} < 0$.
- Mach range = 3.0 – 3.2
- Angle of attack α for cruise, level flight (needed from Performance)
- C.G. during cruise (needed from Weights & Balance)

Methods: Same as phase 5.

Verification: Same as phase 5.

5.6.8. Phase 8 – Descent

Phase Requirement:

- Flight stability: $C_{n\beta} > 0$, and $C_{l\beta} < 0$.
- Supersonic to subsonic descent Mach range: Mach 3.0 to 0.2.
- Descent angle of attack (needed from Performance)
- Elevon deflection range δ_e
- Max rudder deflection δ_r to maintain trim at descent.

Methods:

- supersonic DATCOM methods for $C_{n\beta}$, and Raymer for $C_{l\beta}$
- Rate of descent should support positive fuel tank pressure at speeds higher than M = 2.6.
- For maximum rate of descent above M = 1.8, the speed should not go down 1 Mach in 3 minutes. No limit for below M = 1.8

5.6.9. Phase 9 – Landing

Phase Requirement:

- Flight stability: $C_{n\beta} > 0$, and $C_{l\beta} < 0$.
- Subsonic: Mach 0.5 to 0.
- Landing α (needed from Performance)
- Elevon deflection δ_e for landing
- Rudder deflection δ_r

Methods:

- supersonic DATCOM methods for $C_{n\beta}$, and Raymer for $C_{l\beta}$

Verification:

- “Single engine approaches at 200 KIAS and less than 25,000 lbs of fuel is prohibited” [22]

Table 14. Stability and Control Phase Methodology Summary.

Phase	Title	Application
1	SR-71 Researcher's Handbook	Operation Limits for verification
2	SR-71 Flight Manual	Control surface ranges for verification
3	NASA Flight Stability and Control Performance Results for Linear Aerospike SR-71 Experiment (LASRE).	Lateral-Directional coefficients verification upto Mach 1.8

5.6.10. Results and Discussion

Based on the numbers given by the performance, aerodynamics, weights and balance and geometry teams, the following plots are generated for different flight phases. Due to time constraints, simpler methods have been adopted for yawing moment calculations. This reduces its accuracy. However, it can be seen that there is significant directional stability for the aircraft. This can be due to the increased weight and size of the vertical fins. The original SR-71 had one-third the area of this configuration’s total tail area. The main disadvantage is that it increases the weight of the aircraft. With the increased vertical tail area, smaller rudder deflection angles are needed to trim the aircraft. For the plots presented below, equations for rectangular wing were used since they required fewer inputs and sorting through empirical data. So, this is a large exaggeration of its directional stability. With more time and method refinements, an accurate representation of directional stability can be made.

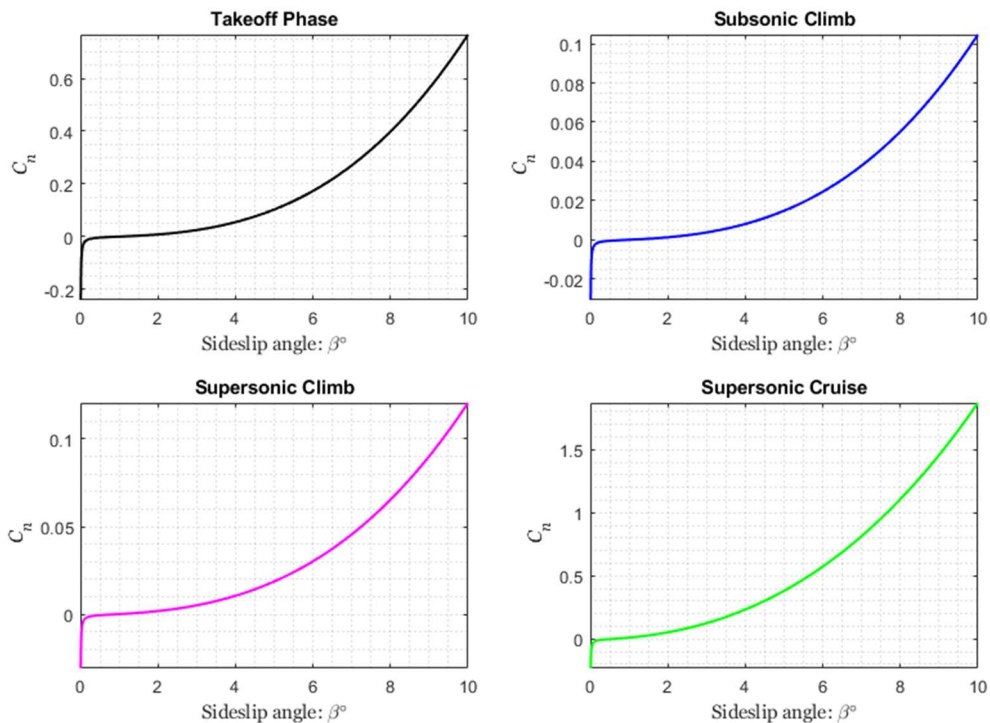


Fig. 91 Yawing moment as a function of sideslip angle for flight phases.

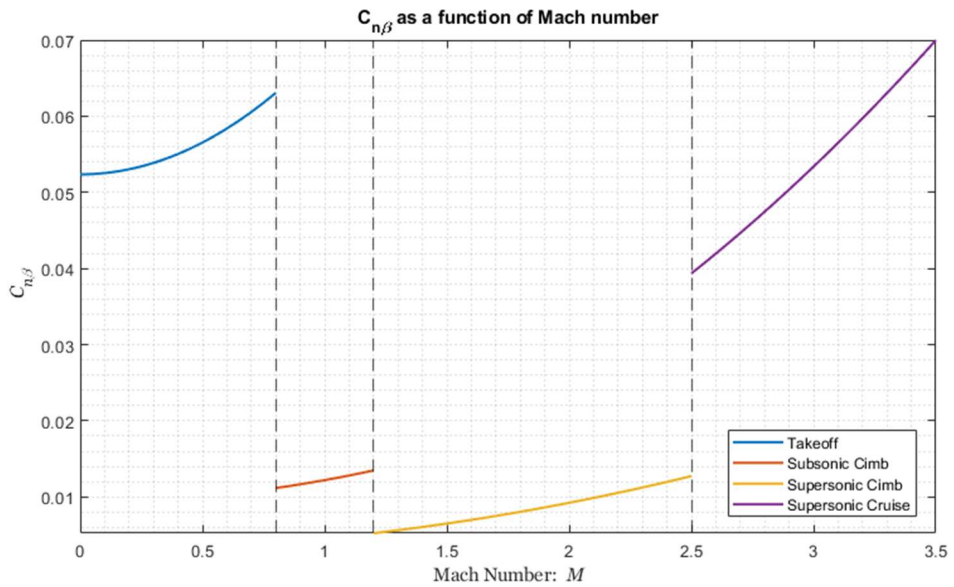


Fig. 92 Yawing moment as a function of Mach number for flight phases.

If compared with LASRE experiment's plots, it is clear that this configuration has higher directional stability in supersonic cruise conditions. One explanation could be due to the large cruise angle of attack value of 7.03 degrees obtained from performance team. However, since this method mainly applies to rectangular wings, this makes the method unreliable for supersonic cruise phase. Due to its higher values of directional stability, the engines can be placed further apart from the fuselage centerline. The next steps would be to use a higher fidelity method for directional stability calculations to improve its accuracy.



The following Table 15 below are the values used for plotting the value graphs.

Table 15. Aircraft similar to SR-71 with delta wings and elevons [37,38].

Phase	Mach Number	Angle of Attack [°]	C.G. from nose [ft]	A.C. from nose [ft]
Takeoff	0.0 - 0.4	7.83	59.87	68.23
Subsonic Climb	0.4 - 0.8	2.57	59.91	69.37
Supersonic Climb	1.2 - 3.0	2.75	59.93	72.82
Supersonic Cruise	2.5 - 3.0	7.07	60.18	72.56

Based on the inputs given by Aerodynamics, Geometry and Performance teams, the following graphs for rolling moment due to sideslip angle have been plotted. The rolling moment graphs agree with the lateral stability criteria where $C_{l\beta}$ must be negative for all flight phases.

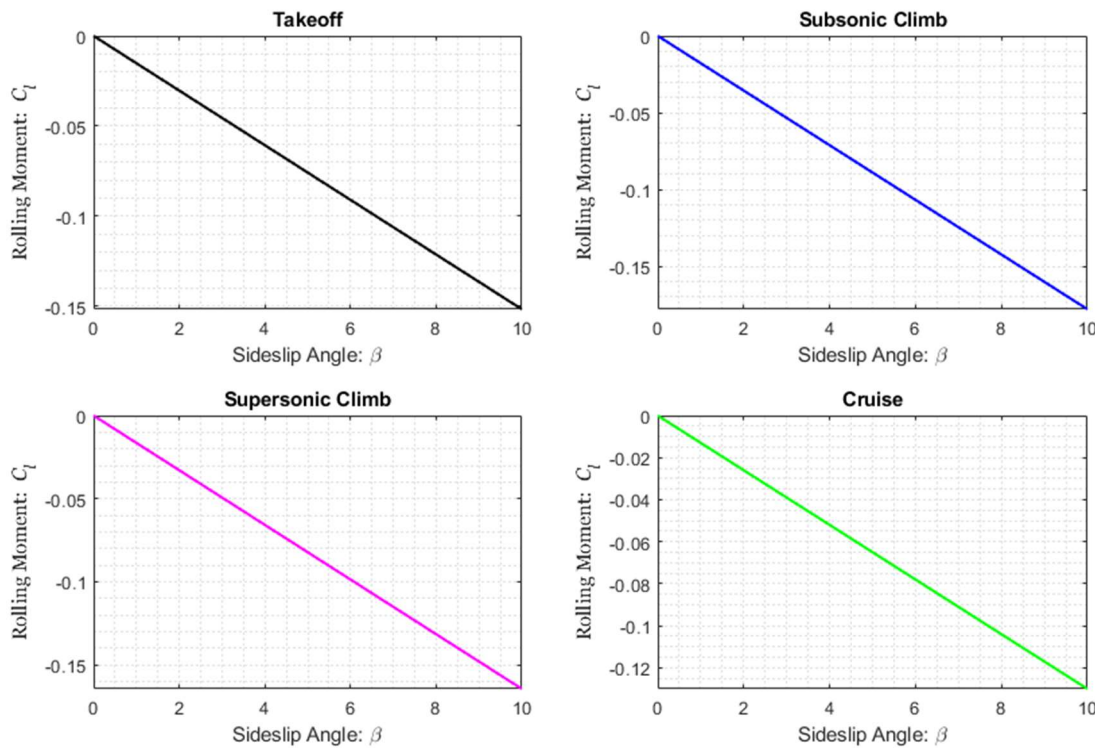


Fig. 93 Rolling moment coefficient as a function of sideslip angle

Historical Development

Week 1

The week was spent segregating the team into various disciplines and working with other teams to decide the disciplines requirements to ensure uniformity between all teams. A literature review was performed to first understand the features of the SR-71 and gather important resources. Team leads were chosen.

Week 2

The week was spent compiling important resources, literature, books pertaining to Costs and Stability and Control sections. A list of useful literature was made for each discipline. During the team meetings, an attempt was made to distinguish needed constraints based on range, altitude, speed, endurance and takeoff/landing distances. The Stability and Control team was further broken down into longitudinal, lateral-directional and control sub-sections with each member covering one aspect.

 PENGUIN SUPersonic	SENIOR DESIGN: MAE 4351 Project	Ref.: MAE 4351-001-2021 Date: 11. May. 2023 Name: Gayathri Kola Status: In Progress
---	---	---

Week 3

Due to a team member dropping out, the Costs team was being covered by two members. A literature review was performed based on conceptual design phases, namely PS, CL, and CE. The Hypersonic Lecture was introduced during this time, and efforts were made to understand the sizing methodology. Time was spent in reading the gathered Stability and Control literature to have a buildup of the many features of SR-71 that contribute to its overall stability. A basic methodology buildup was made for lateral-directional stability and draft IAOs were created to visualize the inputs and outputs. Many references were used to learn about the vehicle and the disciplines. The Costs team was focused on reviewing the main textbook for Life-Cycle-Costs information, as well as trying to obtain suitable verification data for SR-71.

Week 4

The week's team meeting consisted of finding interconnectivity between disciplines and writing down a chronological order of inputs and outputs needed between teams. Each discipline was focused on building their own methodology while Synthesis team chose a convergence method. The Costs team focused on reviewing the literature gathered and building a methodology as outlined in Roskam.

Week 5

During this week, the author was moved to the Synthesis team from the Costs team due to a team member dropping the course. This time was spent trying to catch up with the different sizing methodologies being considered by Synthesis. Upon weighing between AVD Sizing and Roskam Sizing, the Synthesis team had chosen Roskam as the parametric sizing methodology due to its initial simplicity.

Week 6

The chief engineer was changed to Wesley Junell during this week and the team was advised to utilize hypersonic convergence for parametric sizing methodology instead. The Roskam Sizing is difficult to converge, it was learned. With this information, the team focused on finding the right literature for hypersonic convergence and focused to understand the sizing logic. A list of constants and variables needed from disciplines was produced and notified to disciplines. Simultaneously, a baseline MATLAB script was made housing all the constants variables and equations needed for convergence. The Synthesis team began looking into functions that can solve equations such that they equal each other within a specified tolerance.

The remaining time was spent on preparing materials for the midterm presentations and studying for midterm examination. The teams were already working on developing their methodologies, so IDA templates were made on PowerPoint and sent to teams by the author. However, due to the time-consuming nature of the software, the IDA templates were later produced using online websites for ease. The Synthesis team decided to have one member of the team focus on one phase of conceptual design process. The author was responsible for the Configuration Evaluation (CE) phase. Initial MDAs were produced by the Chief engineer Wesley for PS and CL, and CE MDA was produced by the author.

For Stability and Control, the team focused on developing a sizing methodology for control surfaces – elevons and vertical tails to be utilized in the CL phase. MATLAB functions were made to produce the lateral and directional coefficients for supersonic flight by the author. The author was facing challenges interpreting the format laid out in USAF DATCOM.

Week 7

This week was spent on developing the convergence code for Parametric Sizing. The chief engineer Wesley was able to develop the convergence code without any iterations. The challenge then came while incorporating embedded loops to iterate both slenderness ratio and planform area. A previous senior design report by Valkyrie Supersonics was referred to clearly understand the convergence logic.

Week 8

The week was focused on refining the Parametric Sizing code for Synthesis. The issue run into was developing the solution space by iterating planform area and slenderness ratio. The convergence code was fully functional and was made into a function to produce several design points for values of tau. The issue here is plotting the results as a carpet plot showing all converged design points. Functions on MATLAB like meshgrid() were tested to generate these

 PENGUIN SUPersonic	SENIOR DESIGN: MAE 4351 Project	Ref.: MAE 4351-001-2021 Date: 11. May. 2023 Name: Gayathri Kola Status: In Progress
---	------------------------------------	--

carpet plot, but unsuccessful. After the midterm presentation, it was evident that our team lacked verification methods and data. Time was spent gathering the right verification data and establishing methodology for each flight phase for both teams. The full Stability and Control DATCOM was found and was being considered for lateral-directional moment coefficient buildup for subsonic and supersonic regimes.

Week 9

The week was spent on obtaining appropriate solution space results to being Configuration Layout. A basic configuration was obtained by the Synthesis team and the geometry was being developed alongside. Time was spent of gathering CE resources and reviewing them. A detailed mission profile was made again due to a minor error in the previous one. Weights and Balance provided with C.G. location estimates for the original SR-71 for all flight phases. Time was spent on vertical tail sizing buildup and refining gathered SR-71 verification data.

Week 10

The majority of the week was spent on getting the information needed from teams to complete the configuration layout phase. Most of the teams have given appropriate ranges for important variables needed in CL phase to the geometry member. One configuration has been nearly made for sizing through PS again. The Aerodynamics team has given requirements for minimum fuselage length, aspect ratio, and sweep angle. The aspect ratio was chosen by a compromise between aerodynamics and performance in order for ensuring takeoff. The propulsion requirement was to have the engines be placed inside the leading nose shock angle. The vertical tails we made by the geometry member for lateral stability. The performance team provided Stability and control with minimum and maximum values of bank angles needed for 180 degrees turn. Most teams have filled out Excel provided for CE inputs and outputs for each flight phase for Synthesis team. The presentation outline and design layout was discussed and finalized by the author and Jared Coultron after the weekly team meeting.

Week 11

The week was spent working on configuration layout, assembling geometries for different aircraft parts. A 3D solution space was created by chief engineer, Wesley. An initial final presentation template was prepared by the author and sent to the entire team. This week was busy for many members due to exams and projects. The engine placements were done based on the Propulsion team's input. A code for the vertical tail geometry was made by the author and sized for One-Engine-Out condition at takeoff. The first configuration was made by Geometry member Austin along with the vertical tails and engine placements.

Week 12

The week was spent interacting with many teams to obtain needed values to perform analysis for each flight phase. Performance team provided with angle of attacks up to cruise phase. Stability and control were focused on completing stability analysis based on the data obtained from Geometry, Aerodynamics, Performance and Propulsion. Not all phases evaluated due to time constraints. The vertical tails and elevons were sized for the first configuration. Since the geometry keeps changing based on each phase's major disciplines' requirements, it is difficult fully make the first configuration until as phases are evaluated and necessary sizing is completed. This makes it challenging to come to a single answer since if stability is not met at the end of each flight phase, the process for sizing and analysis needs to be repeated until satisfied.

Appendix

1. Costs and Market Estimates Appendix

Table 16. Literature Review for Costs and Market Estimates.

Serial No.	Title	Author	Year	Category
1	Airplane Design Part VIII: Cost Estimation: Design, Development, Manufacturing, and Operating [43]	Jan Roskam	2015	Book
2	US Military Aircraft Cost Handbook [44]	DePuy, W. E. Moyer, R.	1983	Book
3	The Minimization of Combat Aircraft Life-Cycle-Cost through Conceptual Design Optimization [45]	Woodford, S.	1999	Thesis

 PENGUIN SUPERSONIC	SENIOR DESIGN: MAE 4351 Project	Ref.: MAE 4351-001-2021 Date: 11. May. 2023 Name: Gayathri Kola Status: In Progress
---	--	---

4	Statistical-Analytical Model for Cost Estimation and Economic Optimization of Launch Vehicles [46]	Koelle, D. E.	2013	Book
5	The Lockheed SR-71 Blackbird – A Senior Design Capstone Re-Engineering Experience [13]	Mixon, B. Chudoba, B.	2007	Article
6	DAPCA: A Computer Program for Determining Aircraft Development and Production Costs [47]	Boren, H. E.	1967	Book
7	Fundamentals of Aircraft and Airship Design Volume II – Airship Design & Trade Studies [48]	Carichner, G Nicolai, L. M	2013	Book
8	An Estimation of USAF Aircraft Operating and Support Cost Relations [49]	Hildebrandt, G. Sze, M.	1990	Report
9	Aircraft Airframe Cost Estimating Relationships Study Approach and Conclusions [50]	Hess, R. Romanoff, H.	1987	Book
10	Commercial Airplane Design Principles [51]	Sforza, P. M.	2014	Book

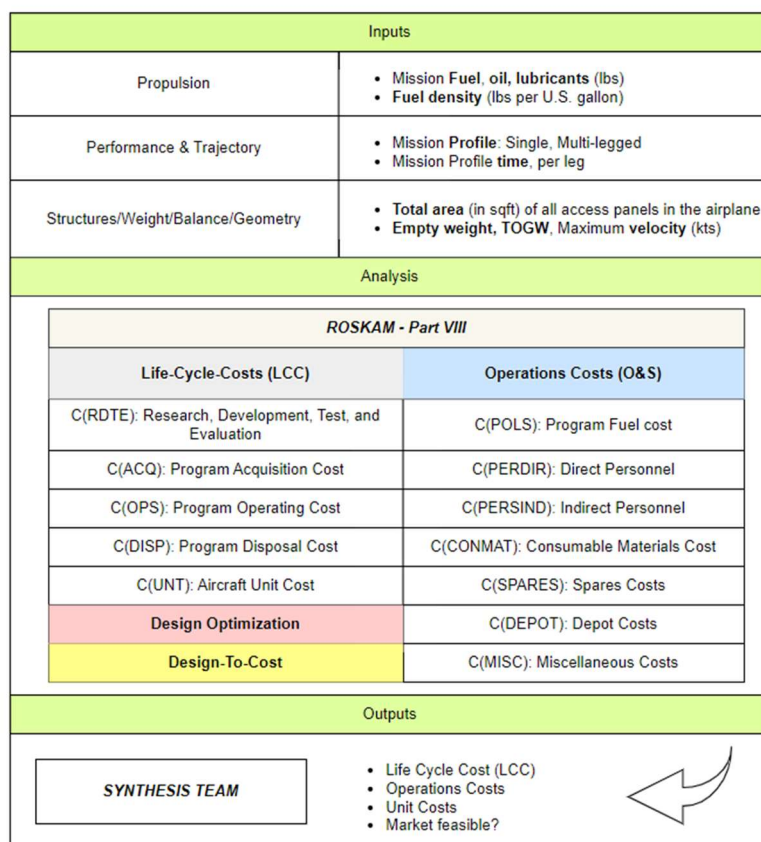


Fig. 94 Initial IAO for Costs and Market Estimates.

Stability and Control Appendix

Lateral-directional coefficients as a function of sideslip angle codes.

```
%% STABILITY AND CONTROL: DIRECTIONAL STABILITY
%% CONFIGURATION: Wing
```

```
% INPUTS:
```

```
% _____Geometry_____
% 1 - length of fuselage [ft]
```



```
% lf      - distance from c.g to fuselage sideforce [ft]
% lvt     - distance from c.g to vertical tail c.g [ft]
% Sref    - wing reference area [ft^2]
% Svt     - vertical tail area [ft^2]
% b       - span [ft]
% Nwing   - Wing moment [lb-ft]
% zw      - distance along aircraft z axis from the wing root chord to the fuselage centerline [ft]
% d       - max fuselage depth [ft]

% _____Aerodynamics_____
% CL      - Lift coefficient [-]
% AR      - Aspect Ratio [-]
% Sweep   - Leading Edge Sweep [deg]
% SWEEPc4 - Sweep at quarter chord [deg]
% Cbar    - mean aero chord [ft]
% CLavt   - lift-curve-slope of vertical tail [-]

% _____Propulsion_____
% Npower  - Engine Moment [lb-ft]

% _____Weights_____
% xcg     - center of gravity of aircraft [ft]
% xcgVT   - center of gravity of vertical tail [ft]

% q       - dynamic pressure
% qvt     - dynamic pressure on vertical tail
% mach    - mach number [-]
% alt     - altitude [ft]
% -----
clc
clear all

% GEOMETRY
xcg = input('Aircraft C.G. location [ft]: ');
Sideforce = input('Sideforce location on fuselage from fuselage start line in %: ');
Tailac = input('Tail a.c. locaiton from fuselage start line in %: ');
l = 105.373;
lf = xcg - (Sideforce*l);
lvt = (Tailac*l) - xcg;
Sref = 1880.918;
Svt = 106.593;
b = 59;
Vol = 1325.71;
h = 5.42;
w = 12;
Wingac = input('Wing a.c [ft]: ');
x = xcg - Wingac;

% AERODYNAMICS
CL = 0.9;
AR = 1.851;
Sweep = 60;
SWEEPc4 = 58.24;
Cbar = 29.504;
CLavt = 2*pi; % Symmetric tail airfoil

% PROPULSION
Npower = 0;
Nwing = 0;
% -----
% OTHER
xcg = 0.55*l;
xcgVT = 0.78*l;
```



```
zw = 0; %[ft]
d1 = 1; %[ft]

LF = input('Sideforce on the fuselage [lb]: '); %[lb]
alt = input('Altitude [ft]: '); %[ft]
Mach = input('Mach number [-]: ');
[Temp,Press,rho,SOS] = FeetStandardAtmosphere(alt);
velocity = Mach * SOS;
q = 0.5 * rho * velocity^2;
% -----
```



```
beta = 1:1:15;
CN = zeros(length(beta),1);

for i = 1:length(beta)
    CN(i,1) = Cn(lf,LF,lvt,Svt,b,Sref,CLavt,SweepC4,zw,d1,AR,Npower,Nwing,q,beta(i));
end

SweepC4i = [30:5:70] * (pi/180);
CNBeta = zeros(length(SweepC4i),1);

for j = 1:length(SweepC4i)
    CNBeta(j,1) = CnBeta(Vol,Sref,b,h,w,CL,AR,SweepC4(j),Cbar,x,lvt,Svt,CLavt,zw,d1);
end

figure(1)
plot(beta(:,1),CN(:,1))
xlabel('Sideslip angle: \beta\circ');
ylabel('Yawing moment coefficient: C_n');
```



```
figure(2)
plot(SweepC4i(:,1),CNBeta(:,1))
xlabel('Sideslip angle: \beta\circ');
ylabel('Yawing moment coefficient: C_n');
```

```
% Function file: (1)-----
function Cn = Cn(lf,LF,lvt,Svt,b,Sref,CLavt,SweepC4,zw,d,AR,Npower,Nwing,q,beta)

    % SweepC4 >> radians
    % beta >> radians

    % NICOLAI 21.15: Downwash term - (1+dsdbeta)*(qvt/q)
    K1 = 0.724 + ( (3.06 * (Svt/Sref))/(1+cos(SweepC4)) ) + (0.4*(zw/d)) + (0.009*AR);

    % NICOLAI: BetaVT - (1+dsdbeta)*beta
    betaVT = K1 * beta;

    % NICOLAI 21.19: Cn
    Cn = -(lf*LF/(q*Sref*b)) + ((lvt*Svt/b*Sref)*Clavt*betaVT) + (Npower/(q*Sref*b)) + (Nwing/(q*Sref*b));
end

% Function file: (2)-----
function CNBeta = CnBeta(Vol,Sref,b,h,w,CL,AR,SweepC4,Cbar,x,lvt,Svt,CLavt,zw,d)

    % SweepC4 >> radians

    % NICOLAI 21.15: Downwash term - (1+dsdbeta)*(qvt/q)
    K1 = 0.724 + ( (3.06 * (Svt/Sref))/(1+cos(SweepC4)) ) + (0.4*(zw/d)) + (0.009*AR);

    % NICOLAI 21.23: Cn fuselage
    CnFuselage = -1.3 * (Vol/(Sref*b)) * (h/w);

    % NICOLAI 21.22: Cn wing
```



```

CnWing = CL^2 * ( (1/4*pi*AR) - (tan(SweepC4) / (pi*AR*(AR+(4*cos(SweepC4))))) * (cos(SweepC4) -
(AR/2) - (AR^2/(8*cos(SweepC4))) * ((6*x/Cbar)*(sin(SweepC4)/AR))) );

% NICOLAI: Vertical tail coefficient Vvt
Vvt = (lvt*Svt/(b*Sref));

% NICOLAI 21.21: CnBeta Vertical tail
CnBetaVT = Vvt * Clavt * K1;

% NICOLAI 21.20: Directional stability derivative
CnBeta = CnFuselage + CnWing + CnBetaVT;

end

```

Code segment for $C_{n\beta}$ as a function of sideslip angle and Mach number:

```

M = 1:1:4;
beta2 = [1:1:10] .* (pi/180);
alpha = 1 * (pi/180);
for j = 1:length(M)
    for k = 1:length(beta2)
        CnBeta(k,j) = alpha^2 * (1/pi*AR^2*beta2(k)^2)*(1/57.3)*( (4*M(j)^2/3) + (8*M(j)^2*Cbar) -
pi*(AR*(1-beta2(k)^2)*(3+beta2(k)^2))/(beta2(k)*3*beta2(k)^2));
    end
end
fig2 = {'Mach 1', 'Mach 2', 'Mach 3', 'Mach 4'};
figure(2)
plot(beta2,CnBeta(:,1))
hold on
plot(beta2,CnBeta(:,2))
hold on
plot(beta2,CnBeta(:,3))
hold on
plot(beta2,CnBeta(:,4))
xlabel('Sideslip angle: \beta\circ', 'FontName', 'georgia');
ylabel('Yawing Moment Coefficient as a function of sideslip: C_n', 'FontName', 'georgia');
legend(fig2)
grid on
ax = gca;
ytickformat('%.4f');
% Remove exponent
ax.YAxis.Exponent = 0;

```

Synthesis Appendix

Synthesis base code (iteration 1)

```

%% SYNTHESIS BASE CODE
clc
clear
%=====
% INPUTS VARIABLES
%=====

% SWBG
Istr = 37; %[kg/m^2]
Kw = 2.7; % Wing-body

```



```

Spln = 222.6; %[m^2] -- 2396.114 ft^2
tau = 0.05;
geoOEW = [Istr,Kw,Spln];
geoOWE = [tau,Spln];

% Aero: L/D-MAX @ Mach 12 should be around 4.71
F = (tau^0.333)*(Kw^0.75);
M1 = 12;
A = 4;
B = 3;
LDMAX = (A / M1) * (M1 + B);

% Systems
Ncrw = 1; %[-]
Cun = 1.9 * 1000; %[kg]
Fmnd = 1.45 * 1000; %[ton/person]
Csys = Cun + Fmnd + Ncrw;
fsys = 0.16; %[-]
Kvv = 0.10; %[-]
Kvs = 0.02; %[-]
Vun = 5.0; %[m^3]
fcrw = 11; %[m^3/person]
Vfix = Vun + (fcrw*Ncrw);
SystemsOEW = [Csys,fsys];
SystemsOWE = [Kvv,Kvs,Vfix];

% Propulsion
TWMAX = 0.75;
WR = 3;
ETW = 11; %[kg thrust/kg weight]
Kve = 0.25 * 1000; %[ton thrust]
M = 3.2; %[-] Mach number
Ip = 107.6*(10^(-0.081*M));
rhoppl = Ip * (WR - 1);
ICI = 10 * (Ip/Istr);
propOEW = [TWMAX,WR,ETW];
propOWE = [WR,rhoppl,TWMAX,Kve];

% Mission Requirements
Wpay = 1360.777; %[kg]
Wcrew = 90.7185; %[kg/person]
Wcprv = 0.45 * 1000; %[kg/person]
Vpcrv = 6.0; %[m^3/person]
Kcrw = 0.9; %[m^3/person]
Vcrw = (Vpcrv+Kcrw)*Ncrw;
rhopay = 48; %[kg/m^3]
missreqOEW = [Wpay,Wcrew,Wcprv];
missreqOWE = [Ncrw,Vcrw,Kcrw,Wpay,rhopay];

muATERM = 0.63;

%=====
% WEIGHT BUDGET: W_OEW
%=====

W_OEW = ((Istr*Kw*Spln) + Csys + (((TWMAX*WR)/ETW) * (Wpay+Wcrew)) + Wcprv) / ( (1/(1+muATERM)) - fsys - ((TWMAX*WR)/ETW) );

%=====
% VOLUME BUDGET: W_OWE
%=====

W_OWE = ( ((tau*(Spln^1.5))*(1-Kvv-Kvs)) - Vfix - (Ncrw*(Vcrw-Kcrw)) - (Wpay/rhopay) ) / ( ((WR-1)/rhoppl) + (Kve*TWMAX*WR) );

```

 PENGUIN SUPERSONIC	SENIOR DESIGN: MAE 4351 Project	Ref.: MAE 4351-001-2021 Date: 11. May. 2023 Name: Gayathri Kola Status: In Progress
---	--	---

```
W_OWE1 = W_OEW + Wpay + Wcrew;
```

```
%=====
% CONVERGENCE
=====
```

Synthesis Convergence Code: By Wesley Junell (Iteration 2)

```
%% Synthesis Parametric Sizing
```

```
%Adapted and Based On: Roman Renazco, Noah Park, and Alex Plihon's Convergence Code in
%Valkyrie Hypersonics, Design of Hypersonic Aircraft of the Hermeus-Quarterhorse Mission (Chief Engineer's
Report),
%UT Arlington, Arlington TX, 2021, pp. 87-89
```

```
%Based on: Hypersonic Convergence Lecture, By. Thomas Ledford and Cody Harris
```

```
%This Code has been Adapted For Reverse Engineering The SR71, Following Hypersonic
%Convergence, AVD Sizing, and Valkyrie Hypersonics Methods. This is done by
%adapting variables found and verified for our mission, as well as
%researching how to use MATLABS fzero function for solving the weight and
%volume budget for PlanformArea.
```

```
%Written By: Wesley Junell, Distributed to Synthesis Team
%3/25/23
```

```
clc
clear
```

```
%% Inputs
tau = 0.05;
Spln = 2396; %ft^2 from geometry
TOGWi = 140000; %lbs
Wpay = 3000; % Payload Weight
Wcrew = 258; %lbs
TReq = 19318; %lbs (refine)
Ncrw = 1;
```

```
%% Weight and Volume Budget Inputs
```

```
% Geometry
Vtot = tau*(Spln)^1.5; % Total Volume
Kw = 2.6; % Diamond Body
S_wet = Kw*Spln; % Wetted Area, ft^2
```

```
% Trajectory
rho_fuel = 50.31; % lbs/ft^3
Ip = 36.1; % Propulsive Index based on Simons Thesis
WR = rho_fuel/Ip + 1; %Weight Ratio
%WR = 1 / (1 - 0.573); %from perf code
ff = 1 - 1/WR; % Fuel Fraction
```

```
% Convergence Constants
fsys = 0.16; % lbs/lbs Variable System Weight Coefficient
```

```
Istr = 3.9; % lb/ft^2 Material Strength
```

```
Cun = 3306; % lbs Unmanned System Weight
```

```
fmnd = 2500; %lbs/person crew system specific weight
```

```
fcrw = 300; %ft3/person crew member specific weight
```



```
ETW = 5.416; % lbs/lbs (J58 Engine Thrust Ratio)

rho_pay = 2.60; % lbs/ft^3 payload density based on fuselage size of SR71

kvs = 0.05; % ft^3/ft^3 System volume coefficient

kvv = 0.3; % ft^3/ft^3 void volume coefficient

Vun = 176; %ft^3 Unmanned fixed Systems Volume

kve = 0.04; % ft^3/lbs Engine Volume Coefficient

mu = 0.1; % Weight Margin

fcprv = 992;%lb/person

% Convergence Variables
Wstr = Istr*S_wet; % Structural Weight

Csys = (Cun + fmnd) * Ncrw; % Constant System Weight

Weng = ((TReq/TOGWi)*WR)/ETW; % Engine Weight

Wcprv = fcprv * Ncrw; %Provisions Weight (Possibly not needed)

Vfix = (Vun + fcrw) * Ncrw; % Fixed System Volume

Vfuel = (WR-1) / rho_fuel; % Fuel Volume

Vpay = Wpay/rho_pay; % Payload Volume

Vcrew = 31.7; %crew volume ft3/person

%% Convergence Initial Guess (Weight and Volume Budget Equations)

%Weight Budget
OEW = (Wstr + Csys + (Weng * Wpay + Wcrew)) / ( (1/(1+mu)) - fsys - Weng);

%Volume Budget
OWE = (Vtot * (1-kvv-kvs) - Vfix - Vpay - Vcrew)/((Vfuel + kve * (TReq/TOGWi)*WR)) - Wpay - fcrw;

%NEW TOGW
TOGW_new = (OEW + Wpay)*WR;

%% Convergence Logic Modified Hypersonic (AVD Variables)

i = 1;
Spln_new = Spln;
while abs(TOGW_new - TOGWi) > 0.005*TOGWi && abs(OWE-OEW) > 0.005*OEW

    Vtot = tau*(Spln_new)^1.5; % Total Volume

    Kw = 2.4; %diamond body

    S_wet = Kw*Spln_new; % Wetted Area, ft^2

    Wstr = Istr*S_wet; % Structural Weight

    Weng = ((TReq/TOGW_new)*WR)/ETW; % Engine Weight / OWE

    % Weight Budget
    OEW = (Wstr + Csys + (Weng * (Wpay + Wcrew))) / ( (1/(1+mu)) - fsys - Weng);

    % Volume Budget
    OWE = (Vtot * (1-kvv-kvs) - Vfix - Vpay - Vcrew)/((Vfuel + kve * (TReq/TOGW_new)*WR)) - Wpay - fcrw;
```



```
% Convergence using fzero
if abs(OEW-OEW) <= 0.005*OEW
    TOGW_old = (OEW + Wpay + Wcrew)*WR;
    TOGW_new = fzero(@(n) n./WR-OEW, TOGWi);

    if abs(TOGW_new - TOGW_old) <= 0.005*TOGW_old
        break
    end

    else
        TOGW_new = OEW*WR;
        Spln_new = ((OEW*(Vfuel + kve*(TReq/TOGW_new)*WR) + Vfix + Vpay + Vcrew)/(tau*(1-kvv-kvs)))^(2/3);
        i = i + 1;
    end

end

%Outputs
TOGW = TOGW_new;
PlanformArea = (Vtot/tau)^(2/3);

fprintf('For given tau: %0.2f \n\nThe TOGW is: %0.0f lbs and the Planform Area is: %0.0f ft^2 \n\n', tau,
TOGW, PlanformArea)
```

Synthesis Solution Space Code: (Iteration 3)

```
%% SYNTHESIS BASE CODE: Version 3
% Written by: Wesley Junell
% Edited by: Gayathri Kola
% Updates: Added loops for solution space
% Gross Configuration: Diamond Body
% Also credited to "Valkyrie Hypersonics, MAE 4350, 15.Dec.2021"
```

```
clc
clear
%=====
% INPUTS VARIABLES

%[-] slenderness ratio
tau_i = 0.05;

%[ft^2] planform area
Spln_i = 2396;

%[lb] Initial Takeoff gross weight
TOGWi = 140000;

%[lb] Payload weight
Wpay = 3000;

%[lb] Crew weight
Wcrew = 258;

%[lbs] Thrust Required
TReq = 19318;

%[-] No. of Crew
Ncrew = 1;

%% Weight and Volume Budget Inputs

% GEOMETRY
```



```
%=====
Vtot = taui*(Splni)^1.5; % Total Volume
Kw = 2.6; % Diamond Body
S_wet = Kw*Splni; % Wetted Area, ft^2

% TRAJECTORY
%=====
rho_fuel = 50.31; % lbs/ft^3
Ip = 36.1; % Propulsive Index based on Simons Thesis
WR = rho_fuel/Ip + 1;
%WR = 1 / (1 - 0.573); %from perf code
ff = 1 - 1/WR; % Fuel Fraction

% CONVERGENCE CONSTANTS
%=====

% lbs/lbs Variable System Weight Coefficient
fsys = 0.16;

% lb/ft^2 Material Strength
Istr = 3.9;

% lbs Unmanned System Weight
Cun = 3306;

%lbs/person crew system specific weight
fmnd = 2500;

%ft3/person crew member specific weight
fcrw = 300;

% lbs/lbs (J58 Engine Thrust Ratio)
ETW = 5.416;

% lbs/ft^3 payload density based on fuselage size of SR71
rho_pay = 2.60;

% ft^3/ft^3 System volume coefficient
kvs = 0.05;

% ft^3/ft^3 void volume coefficient
kvv = 0.3;

%ft^3 Unmanned fixed Systems Volume
Vun = 176;

% ft^3/lbs Engine Volume Coefficient
kve = 0.04;

% Weight Margin
mu = 0.1;

%lb/person
fcprv = 992;

% CONVERGENCE VARIABLES
%=====

% Structural Weight
Wstr = Istr*S_wet;

Csyst = (Cun + fmnd) * Ncrew; % Constant System Weight
Weng = ((TReq/TOGWi)*WR)/ETW; % Engine Weight
Wcprv = fcprv * Ncrew;
```

 PENGUIN SUPERSONIC	SENIOR DESIGN: MAE 4351 Project	Ref.: MAE 4351-001-2021 Date: 11. May. 2023 Name: Gayathri Kola Status: In Progress
---	--	---

```

Vfix = (Vun + fcrw) * Ncrew; % Fixed System Volume
Vfuel = (WR-1) / rho_fuel; % Fuel Volume
Vpay = Wpay/rho_pay; % Payload Volume
Vcrew = 31.7; %crew volume ft3/person

%% CONVERGENCE INITIAL GUESS

%Weight Budget
OEWi = (Wstr + Csys + (Weng * Wpay + Wcrew)) / ( (1/(1+mu)) - fsys - Weng);

%Volume Budget
OWEi = (Vtot * (1-kvv-kvs) - Vfix - Vpay - Vcrew)/((Vfuel + kve * (TReq/TOGWi)*WR)) - Wpay - fcrw;

%TOGW = OWE*WeightRatio;
TOGWnew = (OEWi + Wpay)*WR;

%% ARRAY ALLOCATIONS

Converged = [];
Unconverged = [];
CONVERGED = [];
UNCONVERGED = [];
TOGWGuess = [];
GUESSED = [];
TOGW = [];
SPLN = [];
OEWW = [];

%% cCONVERGENCE LOGIC MODIFIED HYPERSONIC (AVD VARIABLES)

% ranges
tau = 0.04:0.001:0.06;
Spln = 2200:100:2600;

for i = 1:length(tau)
    for j = 1:length(Spln)

        while abs(TOGWnew - TOGWi) > 0.005*TOGWi && abs(OWEi - OEWi) > 0.005*OEWi

            %[ft^3] Total volume
            Vtot = tau(i)*(Spln(j))^1.5;

            %[ ] Swet per Spln: Diamond Body
            Kw = tau(i)*(exp(0.081*((log(tau(i)))^2)-(.461*log(tau(i)))+1.738));

            %[ft^2] Wetted area
            Swet = Kw*Spln(j);

            %[lbs] Structural weight
            Wstr = Istr*Swet;

            %[lbs] Enigne Weight
            Weng = ((TReq/TOGWnew)*WR)/ETW;

            %[lbs] Weight Budget
            OEW = (Wstr + Csys + (Weng * (Wpay + Wcrew))) / ( (1/(1+mu)) - fsys - Weng);

            %[lbs] Volume Budget
            OWE = (Vtot * (1-kvv-kvs) - Vfix - Vpay - Vcrew)/((Vfuel + kve * (TReq/TOGWnew)*WR)) - Wpay - fcrw;
    end
end

```

 PENGUIN SUPERSONIC	SENIOR DESIGN: MAE 4351 Project	Ref.: MAE 4351-001-2021 Date: 11. May. 2023 Name: Gayathri Kola Status: In Progress
---	--	---

```
% convergence
if abs(OEW - OEW) <= 0.005*OEW

%[lbs] Old TOGW
TOGWold = (OEW + Wpay + Wcrew)*WR;

%[lbs] New TOGW
TOGWnew = fzero(@(n) n./WR-OEW, TOGWi);
%
TOGWGuess = [TOGWnew];
GUESSED = [GUESSED; TOGWGuess];
Splnnew = ((OEW*(Vfuel + kve*(TReq/TOGWnew)*WR) + Vfix + Vpay + Vcrew)/(tau(i)*(1-kvv-
kvs)))^(2/3);
%
Converged = [TOGWnew Splnnew OEW];
CONVERGED = [CONVERGED; Converged];
if abs(TOGWnew - TOGWold) <= 0.005*TOGWold
    break
end

else

TOGWnew = OEW*WR;
Splnnew = ((OEW*(Vfuel + kve*(TReq/TOGWnew)*WR) + Vfix + Vpay + Vcrew)/(tau(i)*(1-kvv-
kvs)))^(2/3);
Unconverged = [TOGWnew Splnnew OEW];
UNCONVERGED = [UNCONVERGED; Unconverged];
end
end
end

% scatter3(CONVERGED(:,3), CONVERGED(:,2), CONVERGED(:,1),"filled","black")

% hold on
scatter3(UNCONVERGED(:,3), UNCONVERGED(:,2), UNCONVERGED(:,1))
hold on
scatter3(Unconverged(:,3), Unconverged(:,2), Unconverged(:,1),"Filled","black")
xlabel('Operating Empty Weight: OEW [lbs]');
ylabel('Planform Area: S_p_l_n [ft^2]');
zlabel('Takeoff Gross Weight: TOGW [lbs]')

```

Synthesis Code (Iteration 4)

```
%% SYNTHESIS BASE CODE: Version 4
% Written by: Wesley Junell, Gayathri Kola
% Updates: Added loops for solution space
% Gross Configuration: Diamond Body
% Also credited to "Valkyrie Hypersonics, MAE 4350, 15.Dec.2021"

% !! to WES: I made your code into a function HCPSV3.m and varied initial tau_i and initial Spln_i
% I also added a break point in your code of i >= 100000, to stop the loop. Without it, it went over a
million times

%to Gayathri: I added the Empty Weights and Volumes as an output as well for HCPSV3 Code.

clc
clear
close all

tic; %Starts Program Timer

fprintf('Starting Program Timer...\n\n')
=====
%% INPUTS VARIABLES

%[-] slenderness ratio
```



```
tauui = linspace(0.04, 0.06, 25);

%[ft^2] planform area
Splni = linspace(2000, 2600, 25);

%[lb] Initial Takeoff gross weight
TOGWi = 140000;

%[lb] Payload weight
Wpay = 3000;

%[lb] Crew weight
Wcrew = 258;

%[lbs] Thrust Required: works upto 41,000 lbs, fails at 45,000 lbs
TReq = 32500;

%[-] No. of Crew
Ncrew = 1;

%[-] Allocate Space
DPS = [];
DesignPoints = [];

for i = 1:length(tauui)
    for j = 1:length(Splni)
        [TOGW, Spln, EmptyWeight, Volume, AreaRatio] =
        HCPSV3(tauui(i), Splni(j), TOGWi, Wpay, Wcrew, TReq, Ncrew);
        [WS, Vs] = LandingV4(TOGW, Spln);
        %[WS, Vs] = LandingV3(TOGW, Spln);

        %Va = 1.3*Vs;
        %Vtd = 1.15*Vs;
        %LandingSpeeds = [Vs Va Vtd];

        DPS = [TOGW Spln tauui(i) Splni(j) EmptyWeight Volume AreaRatio WS Vs];
        DesignPoints = [DesignPoints; DPS];
    end
end

%% PLOTS
%figure(1)

%Plot 3axis plot of TOGW,SPln,Wing Loading
yyaxis left
plot(DesignPoints(:,2), DesignPoints(:,1), '-ob', 'MarkerFaceColor', 'b')
ylabel('TOGW (lbs)', 'FontWeight', 'bold')
yyaxis right
%hold on
plot(DesignPoints(:,2), DesignPoints(:,8), '-or', 'MarkerFaceColor', 'r')
xlabel('Spln (ft^2)')
ylabel('Wing Loading (lbs/ft^2)', 'FontWeight', 'bold')
legend('Hypersonic Convergence Results', 'Wing Loading (lb/ft^2)')

figure(2)
%Plots Spln vs Wing Loading
plot(DesignPoints(:,2), DesignPoints(:,8))
xlabel('Spln (ft^2)', 'FontWeight', 'bold')
ylabel('Wing Loading (lb / ft^2)', 'FontWeight', 'bold')
```

Code segment for vertical tail sizing:

```
%% RAYMER
clc
clear
```

 PENGUIN SUPERSONIC	SENIOR DESIGN: MAE 4351 Project	Ref.: MAE 4351-001-2021 Date: 11. May. 2023 Name: Gayathri Kola Status: In Progress
---	--	---

```

close all

%[] Vertical tail volume coefficient: Table 6.4-Jet fighter
CVT = 0.07;

% All-moving tail:
CVTAllMoving = CVT - (0.10*CVT);
% T-tail:
CVTTTail = CVT - (0.05*CVT);
% V-tail:
CVTVTail = CVT / 2;

%[ft] fuselage length (from Austin's geo)
lf = 105.373;

%[ft] Vertical tail moment arm
% lvt = 0.20 *lf

%[ft] wingspan (from Austin's geo)
bw = 59;

%[ft^2] Wing area (from Austin's geo)
Sw = 1880.918;

%[] Calculate vertical tail area
SVT1 = @(lvt) (CVTAllMoving * bw * Sw) / lvt;
SVT2 = @(lvt) (CVTTTail * bw * Sw) / lvt;
SVT3 = @(lvt) (CVTVTail * bw * Sw) / lvt;

%% VERIFICATION

%[ft] SR-71 fuselage length
Vlf = 107.5;

%[ft] SR-71 wing span
Vbw = 55.7;

%[ft^2] SR-71 wing area
VSw = 1795;

%[ft^2] SR-71 total Vertical rudder area (single-check)
% VSVT = 150.76 * 2;

%[] Vertical tail volume coefficient of SR-71: (recalculated)
VCVT = 0.0603;

%[] Calculate SR-71 tail area
VSVT = @(lvt) (VCVT * Vbw * VSw) / lvt;

legs = {'C_V_T All-moving tails','C_V_T T-Tail','C_V_T V-Tail','Actual SR-71'};
figure(1)
fplot(SVT1,[20 30])
hold on
fplot(SVT2,[20 30])
hold on
fplot(SVT3,[20 30])
hold on
fplot(VSVT,[20 30],'k','LineStyle','--')
xlabel('Moment arm: {\it l_V_T} [ft]')
ylabel('Vertical tail area: {\it S_V_T} [ft^2]')
legend(legs)
set(gcf,'color','w')

```

Code segment for crosswind condition during takeoff for rudder sizing:

 PENGUIN SUPERSONIC	SENIOR DESIGN: MAE 4351 Project	Ref.: MAE 4351-001-2021 Date: 11. May. 2023 Name: Gayathri Kola Status: In Progress
---	--	---

```
%> Rudder Deflection for crosswind condition

clc
clear
close

%[-] Yawing moment due to sideslip
CnBeta = -0.01;

%[deg] Sideslip angle
beta = 11.5 * (pi/180);

%[-] lift coefficient for vertical tails: NACA 63-010
CLalphavt = 0.1;

%[ft] moment arm from aircraft c.g. to vertical tail a.c.
lv = 20;

%[ft] wingspan
b = 59;

%[ft^2] wing area
Sref = 1880;

%[-] change in yawing moment due to rudder deflection for a constant angle of attack.
tau1 = 0.9;
tau2 = 0.7;
tau3 = 0.5;
tau4 = 0.47;

%[-] yawing moment due to rudder deflection angle
Sv1 = @(DeltaR) (-CnBeta*beta*b*Sref)/(0.9*CLalphavt*tau1*lv*DeltaR);
Sv2 = @(DeltaR) (-CnBeta*beta*b*Sref)/(0.9*CLalphavt*tau2*lv*DeltaR);
Sv3 = @(DeltaR) (-CnBeta*beta*b*Sref)/(0.9*CLalphavt*tau3*lv*DeltaR);
Sv4 = @(DeltaR) (-CnBeta*beta*b*Sref)/(0.9*CLalphavt*tau4*lv*DeltaR);

% Plot the varying ranges
legs = {'\tau = 0.9', '\tau = 0.7', '\tau = 0.5', '\tau = 0.47'};
fplot(Sv1,[0 20])
hold on
fplot(Sv2,[0 20])
hold on
fplot(Sv3,[0 20])
hold on
fplot(Sv4,[0 20])
ylabel('Vertical tail area: S_v')
xlabel('Rudder deflection angle: \delta_r')
ylim([0 400])
legend(legs)
title('Rudder sizing for crosswind condition at T0: \beta = 11.5\circ')
set(gcf, 'color', 'w')
```

Script for yawing moment calculation (Ongoing)

```
%> Raymer Cn Beta calculation
```

```
clc
clear
close all

% -----
%[deg] Sweep at wing quarter-chord (aero)
Sweepc4 = ;

%[-] Aspect ratio
AR = ;
```

 PENGUIN SUPERSONIC	SENIOR DESIGN: MAE 4351 Project	Ref.: MAE 4351-001-2021 Date: 11. May. 2023 Name: Gayathri Kola Status: In Progress
---	--	---

```
%[-] Lift coefficient at flight phase
CL = ;

%[-] Non-dimensional a.c. of the wing (aero)
Xacw = ;

%[-] Non-dimensional a.c. of the vertical tail (me)
Xacv = ;

%[ft^3] Fuselage volume (Geo)
fusVol = ;

%[ft^2] wing area
Sw = ;

%[ft^2] Vertical tail area
Sv = ;

%[ft] wingspan
b = ;

%[ft] fuselage depth
df = ;

%[ft] fuselage width
wf = ;

%[rad] sideslip angle
beta = 1 * (pi/180);

%[ft] Vertical tail area extended to the fuselage centerline
SvsP = ;

%[ft] Vertical height of the wing above the fuselage centerline
Zwf = ;

%[IDK] Downwash term + dynamic pressure ratio
dBvdBnv = 0.724 + ((3.06*(SvsP/Sw))/(1+cos(SweepC4))) - (0.4 * (Zwf/df)) + (0.009*AR);

%[lb] Lateral lift-force
Fv = ;

%[-] tail efficiency
nv = 0.98;

%[IDK] Dynamic pressure on vertical tail
qv = ;

%[-] Tail lateral lift-force derivative
CFBetaav = Fv / (qv * Sv * (dBvdBnv/nv) * beta);

%-----%
%[-] Wing yawing moment due to sideslip angle
CnBeta_wing = CnBetaWing(CL,AR,SweepC4,Xacw,Xcg);

%[-] fuselage yawing moment due to sideslip angle
CnBeta_fus = -1.3 * (fusVol/(Sw * b)) * (df/wf);

%[-] vertical tail yawing moment due to sideslip
CnBeta_vt = CFBetaav * dBvdBnv * (Sv/Sw) * (Xacv - Xcg);
```



```
%[-] total yawing moment due to sideslip
CnBeta = CnBeta_wing + CnBeta_fus + CnBeta_vt;

%-----
% Trim calculations [Roskam - Flight Dynamics & Auto-Control 1, Pg. 114]

%[-] Value of Cn for beta = deltaE = deltaR = 0
Cno = ;

%[-] Yawing moment due to Elevon deflection: close of 0 or slightly positive
CnDeltaE = ;

%[rad] Elevon deflection angle
deltaE = 1 * (pi/180);

%[-] lift coefficient on the vertical tails
CLavt = ;

%[rad] angle-of-attack effectiveness term
alphadeltaR = ;

%[ft] moment-arm
Xvs = ;

%[-] Yawing moment due to Rudder deflection
CnDeltaR = -CLavt * alphadeltaR * nv * ((Sv * Xvs)/(Sw * b));

%[rad] Rudder deflection angle
deltaR = 1 * (pi/180);

% Trim condition for zero total yawing moment, find the rudder deflection angle
deltaRTrim = (-Cno - (CnBeta * beta) - (CnDeltaE * deltaE)) / CnDeltaR;
```

Code Segment for Rolling moment due to sideslip for vertical tail placement.

```
clc
clear all

CLavt = 2*pi; % symmetric airfoil
Sref = 1880.918; % [ft]
AR = 1.851;
SweepC4 = 58.24 * (pi/180); %[rad]
zw = 0; %[ft]
d = 5.25; %[ft]
zv = 0:2:10; %[ft]
b = 59; %[ft]

Svt = 0:100:600; %[ft^2]

for i = 1:length(Svt)
    for j = 1:length(zv)
        K1(i) = 0.724 + ( (3.06 * (Svt(i)/Sref))/(1+cos(SweepC4)) ) + (0.4*(zw/d)) + (0.009*AR);
        CLB_VT(j,i) = -CLavt * K1(i) * (Svt(i)/Sref) * (zv(j)/b);
    end
end

% figure (1)
% fplot(CLB_VT, [0 600])
```



```
% xlabel('Vertical Tail Area (ft^2)')
% ylabel('C_lVT')

legs = {'zw = 0 ft', 'zw = 2 ft', 'zw = 4 ft', 'zw = 6 ft', 'zw = 8 ft', 'zw = 10 ft'};
figure(1)
plot(Svt,CLB_VT)
title('Rolling moment coefficient C_l\beta_V_T vs. Vertical tail area for various vertical c.g. projections')
xlabel('Vertical Tail Area, S_V_T (ft^2)')
ylabel('C_l\beta_V_T')
legend(legs);
```

Code Segment for One-Engine-Inoperative (OEI) at takeoff:

```
% ONE-ENGINE OUT / ASYMMETRIC THRUST AT TAKEOFF : By Nicolai

 %[ft] y-axis distance from engine cetnerline to fuselage centerline (geo)
 le = 15;

 %[lbs] Engine thrust (perf)
 Thrust = 34000/2;

 %[lbs] Engine drag (prop)
 De = 813.33/2;

 %[ft/s] Velocity at takeoff (aero)
 Vto = 354.44;

 %[slugs/ft^3] Density at takeoff for Edwards Airforce Base
 Den = 0.002571;

 %[lbs/ft^2] freestream dynamic pressure (for takeoff at sea level)
 qinf = 0.5 * Den * (Vto^2);

 % %[rad] rudder deflection to overcome asymmetric thrust: Cn = 0; Max rudder deflections should be +- 20 deg
 % deltaRAsym = (Thrust + De) / (CnDeltaR * qinf * Sw * b);

 % Vary and Plot
 lvt1 = 15;
 lvt2 = 20;
 lvt3 = 25;
 lvt4 = 30;

 %[-] from Nicolai
 tau = 0.1;

 % lvt : the x-distance from c.g. of aircraft to a.c of vertical tail
 SVT1 = @(deltaR) (Thrust + De) / (qinf * 0.9 * CLavt * lvt1 * deltaR * tau);
 SVT2 = @(deltaR) (Thrust + De) / (qinf * 0.9 * CLavt * lvt2 * deltaR * tau);
 SVT3 = @(deltaR) (Thrust + De) / (qinf * 0.9 * CLavt * lvt3 * deltaR * tau);
 SVT4 = @(deltaR) (Thrust + De) / (qinf * 0.9 * CLavt * lvt4 * deltaR * tau);

 legs = {'l_v_t = 15 ft','l_v_t = 20 ft','l_v_t = 25 ft','l_v_t = 30 ft'};
 fplot(SVT1, ([0 10]))
 hold on
 fplot(SVT2, ([0 10]))
 hold on
 fplot(SVT3, ([0 10]))
 hold on
 fplot(SVT4, ([0 10]))
 hold on
 xlabel('Rudder Deflection Angle: {\delta_R} [\circ]');
 ylabel('Rudder Area: {S_V_T} [ft^2]')
 ylim([0 500])
```



PENGUIN
SUPERSONIC

SENIOR DESIGN:
MAE 4351 Project

Ref.: MAE 4351-001-2021
Date: 11. May. 2023
Name: Gayathri Kola
Status: In Progress

```
legend(legs)
title('Rudder Sizing for One-Engine-Inoperative (OEI), {\tau} = 0.1')
leg = legend('show');
title(leg,'Distance from aircraft C.G. to rudder a.c')
set(gcf,'color','w')
```

```
% ONE-ENGINE OUT / ASYMMETRIC THRUST AT TAKEOFF : By Systems
```

```
%[lbs] Engine thrust (2 engines combined)
Te = 34000;

%[-] Vertical tail lift coefficient
Clavt = 2*pi;

%[ft] Distance between two engines
le = 10;

%[ft^2] Reference area
Sref = 2580;

%[ft^2] Vertical tail area
Svt = 300;

%[ft] Wing Span
bw = 61.2;

%[ft] distance from aircraft c.g. to vertical tail a.c.
lv = 15;

%[-] rudder chord to vertical tail chord ratio
CrCv = 0.20;

%[-] tail efficiency
nv = 0.98;

%[ft/s] Stall Speed
Vstall = 339.47;

%[-] Minimum controllable speed requirement
Vcm = 0.8;

%[ft/s] Minimum controllable speed
VCM = Vcm * Vstall;

%[-] Vertical tail volume coefficient
Vvt = (lv * Svt) / (bw * Sref);

%[-] angle of attack effectiveness
tau = 0.4;

%[slugs/ft^3] air density standard
rho = 0.00257;

%[ft] Vertical tail span, rudder span
% bv = 5:1:10;
br = 2.73;
BrBvt = 2.2;
bvt = (1/BrBvt)*br;
b = br + bvt;

VerticalTailHeight = table(b, br, bvt, BrBvt)

%[1/rad] Rudder control derivative
CNdeltaR = -Clavt * Vvt * nv * tau * (br/bvt);
```

 PENGUIN SUPERSONIC	SENIOR DESIGN: MAE 4351 Project	Ref.: MAE 4351-001-2021 Date: 11. May. 2023 Name: Gayathri Kola Status: In Progress
---	--	---

```
%[rad] Rudder deflection to balance asymmetric thrust at sea level
DeltaR = (Te * (le/2)) / (-0.5 * rho * (VCM^2) * Sref * bw * CNDeltaR)

%[deg] Rudder deflection to balance asymmetric thrust at sea level
DeltaRDeg = DeltaR * (180/pi)

%[deg] tail sweep angle
tailSweep = atan(BrBvt/(1-CrCv))

%[ft] Vertical tail root chord
cvt = (2 * (Svt/2)) / (b * (2 - CrCv));

%[ft] Vertical tail tip chord
cr = CrCv * cvt;

%[ft] total vertical chord length
c = cr + cvt;

VerticalTailChords = table(c, cr, cvt, CrCv, Clavt)
```

Vertical Tail geometry code:

```
% PURELY TAIL GEOMETRY
```

```
C = 8;
CrCvt = 0.2;
B = 6.5;
BrBvt = 2.2;
S = 150;
Cvt = C / (1+CrCvt);
Cr = CrCvt * Cvt;
bvt = B / (1 + BrBvt);
br = BrBvt * bvt;
sweep = atan(B / Cvt);
```

Rolling moment codes:

```
%% Rolling Moment - All phases
clc
clear
close

% Inputs
SVTP = 450; % [ft^2]
Sref = 2580; % [ft^2]
SweepC4 = 64.3 * (pi/180); % [rad]
Zw = 0; % [ft]
d = 3.24; % [ft]
AR = 2.0; % [-]
CLAlphaVT = 2*pi; % [-]
SVT = 900; % [ft^2]
Zv = 5; % [ft]
b = 61.3; % [ft]
CLalpha_takeoff = 0.53 / (7.83*pi/180);
CLalpha_Subclimb = 0.33 / (2.57*pi/180);
CLalpha_Supclimb = 0.25 / (2.57*pi/180);
CLalpha_cruise = 0.13 / (7.07*pi/180);
Die = 15 * (pi/180); % [rad]
lambda = 0; % [-]
CLBasic = -0.5; % [-]

% Downwash term
Down = 0.724 + ((3.06 * (SVTP / Sref)) / (1+cos(SweepC4))) + (0.4 * Zw / d) + (0.009 * AR);
```

 PENGUIN SUPERSONIC	SENIOR DESIGN: MAE 4351 Project	Ref.: MAE 4351-001-2021 Date: 11. May. 2023 Name: Gayathri Kola Status: In Progress
---	--	---

```
% Vertical stabilizer Contribution
CLvt = -CLAlphaVT * Down * (SVT / Sref) * (Zv / b);

% Dihedral contribution
CLDie1 = ((-CLalpha_takeoff * Die )/4) * ((2*(1+2*lambda)/(3*(1+lambda)))); 
CLDie2 = ((-CLalpha_Subclimb * Die )/4) * ((2*(1+2*lambda)/(3*(1+lambda)))); 
CLDie3 = ((-CLalpha_Supclimb * Die )/4) * ((2*(1+2*lambda)/(3*(1+lambda)))); 
CLDie4 = ((-CLalpha_cruise * Die )/4) * ((2*(1+2*lambda)/(3*(1+lambda))));

% Wing contribution
CLBBasic = CLBasic + CLDie1;
CLBWing2 = CLBasic + CLDie2;
CLBWing3 = CLBasic + CLDie3;
CLBWing4 = CLBasic + CLDie4;

% total
CLB1 = CLBWing1 + CLvt;
CLB2 = CLBWing2 + CLvt;
CLB3 = CLBWing3 + CLvt;
CLB4 = CLBWing4 + CLvt;

% Just C1
C11 = @(beta) CLB1 * (pi/180) * beta;
C12 = @(beta) CLB2 * (pi/180) * beta;
C13 = @(beta) CLB3 * (pi/180) * beta;
C14 = @(beta) CLB4 * (pi/180) * beta;

% Plotting
figure(1)
subplot(2,2,1)
fplot(C11, [0 10], '-','LineWidth',1.5,'color','k');
grid minor
xlabel('Sideslip Angle: \beta');
ylabel('Rolling Moment: {\it C_1}', 'FontName', 'georgia')
title('Takeoff')
set(gcf, 'color', 'w');
hold on
subplot(2,2,2)
fplot(C12, [0 10], '-','LineWidth',1.5,'color','b');
grid minor
xlabel('Sideslip Angle: \beta');
ylabel('Rolling Moment: {\it C_1}', 'FontName', 'georgia')
title('Subsonic Climb')
hold on
subplot(2,2,3)
fplot(C13, [0 10], '-','LineWidth',1.5,'color','m');
grid minor
xlabel('Sideslip Angle: \beta');
ylabel('Rolling Moment: {\it C_1}', 'FontName', 'georgia')
title('Supersonic Climb')
hold on
subplot(2,2,4)
fplot(C14, [0 10], '-','LineWidth',1.5,'color','g');
grid minor
xlabel('Sideslip Angle: \beta');
ylabel('Rolling Moment: {\it C_1}', 'FontName', 'georgia')
title('Cruise')
```

References

- [1] How the X-Men's X-Jet Blackbird Compares to the SR-71. *Lockheed Martin*. <https://www.lockheedmartin.com/en-us/news/features/2017/how-the-x-men-blackbird-compares-to-the-original-sr-71.html>. Accessed Feb. 12, 2023.



- [2] Moes, T. R. *Stability and Control Estimation Flight Test Results for the SR-71 Aircraft With Externally Mounted Experiments*. National Aeronautics and Space Administration, Dryden Flight Research Center, 2002.
- [3] *Airport Master Record, Edwards AFB*. Publication FAA FORM 5010-2 (3/96). U.S. Department of Transportation Federal Aviation Administration, Edwards Air Force Base, California, 2023, p. 6.
- [4] Kucher, P. R. SR-71 Online - SR-71 Reconnaissance Profile. *SR-71 Reconnaissance Profile*. <https://www.sr-71.org/blackbird/diagrams/reconprofile.php>. Accessed Feb. 12, 2023.
- [5] Nicolai, L. M., and Carichner, G. E. *Fundamentals of Aircraft and Airship Design*. American Institute of Aeronautics and Astronautics, Inc., Reston, Virginia, 2010.
- [6] Loftin, L. K. Subsonic Aircraft: Evolution and the Matching of Size to Performance. NASA Reference Publication, Aug 01, 1980.
- [7] Chudoba, B. Parametric Sizing Process, Lab #2, MAE 4350 Aerospace Vehicle Design I. AVD Laboratory, Jan, 2023.
- [8] Ledford, T., and Harris, C. Hypersonic Convergence. Background and Methodology. Aerospace Vehicle Design (AVD) Laboratory, Feb 08, 2023.
- [9] Chudoba, B. *Stability and Control of Conventional and Unconventional Aerospace Vehicle Configurations: A Generic Approach from Subsonic to Hypersonic Speeds*. Springer International Publishing, Cham, 2019.
- [10] Coleman, G., and Chudoba, B. A Generic Stability and Control Tool for Conceptual Design, Prototype Styem Overview. In *45th AIAA Aerospace Sciences Meeting and Exhibit*, American Institute of Aeronautics and Astronautics, 2007.
- [11] Roskam, D. J. *Airplane Design Part VII: Determination of Stability, Control and Performance Characteristics*. Design, Analysis and Research Corporation, Lawrence, Kansas, 2017.
- [12] Merlin, P. W. Design and Development of the Blackbird: Challenges and Lessons Learned. Presented at the 47th AIAA Aerospace Sciences Meeting, Florida, 2009.
- [13] Mixon, B. D., and Chudoba, B. "The Lockheed SR-71 Blackbird – A Senior Capstone Re-Engineering Experience." *45th AIAA Aerospace Sciences Meeting and Exhibit, Reno, Nevada*, 2007, p. 35. <https://doi.org/10.2514/6.2007-698>.
- [14] Moes, T., Cobleigh, B., Cox, T., Conners, T., Iliff, K., and Powers, B. Flight Stability and Control and Performance Results from the Linear Aerospike SR-71 Experiment (LASRE). Presented at the 23rd Atmospheric Flight Mechanics Conference, Boston, MA, U.S.A., 1998.
- [15] Cox, T. H., and Jackson, D. Supersonic Flying Qualities Experience Using the SR-71. Presented at the Atmospheric Flight Mechanics, New Orleans, LA, 1997.
- [16] Corda, S., Moes, T. R., Mizukami, M., Hass, N. E., Jones, D., Monaghan, R. C., Ray, R. J., Jarvis, M. L., and Palumbo, N. The SR-71 Test Bed Aircraft: A Facility for High-Speed Flight Research. Jun 01, 2000.
- [17] Malvestuto, F. S., and Kuhn, R. E. *Examination of Recent Lateral-Stability-Derivative Data*. Publication NACA RM L53I08a. National Advisory Committee for Aeronautics, Washington, 1953, p. 28.
- [18] Cox, T. H., and Marshall, A. "Longitudinal Handling Qualities of the Tu-144LL Airplane and Comparisons With Other Large, Supersonic Aircraft." *National Aeronautics and Space Administration, Dryden Flight Research Center*, 2000, p. 44.
- [19] Czysz, P., Bruno, C., and Chudoba, B. *Future Spacecraft Propulsion Systems and Integration: Enabling Technologies for Space Exploration*. Springer, Berlin, Heidelberg, 2018.
- [20] Simon, S. *Development of the Vehicle Configuration Compendium: A Comprehensive Data-Information-Knowledge System to Aid in High-Speed Vehicle Design*. University of Texas at Arlington, 2022.
- [21] Anderson, J. D. *Aircraft Performance & Design*. McGraw-Hill Education, 1999.
- [22] SR-71 Online - SR-71 Flight Manual: Section 6, Page 6-2. <https://www.sr-71.org/blackbird/manual/6/6-2.php>. Accessed Feb. 18, 2023.
- [23] Yechout, T. R., Hallgren, W. F., Morris, S. L., and Bossert, D. E. *Introduction to Aircraft Flight Mechanics Performance, Static Stability, Dynamic Stability, and Classical Feedback Control*. American Institute of Aeronautics and Astronautics, Reston, UNITED STATES, 2003.
- [24] Aircraft Design: A Systems Engineering Approach | Wiley. <https://www.wiley.com/en-us/Aircraft+Design%3A+A+Systems+Engineering+Approach-p-9781119953401>. Accessed Feb. 26, 2023.
- [25] *Lockheed SR-71 Researcher's Handbook: Supersonic/Hypersonic Research Facility*. Lockheed Advanced Development Company, Sunland, CA.
- [26] *USAF (United States Air Force) Stability and Control DATCOM (Data Compendium)*.

 PENGUIN SUPERSONIC	SENIOR DESIGN: MAE 4351 Project	Ref.: MAE 4351-001-2021 Date: 11. May. 2023 Name: Gayathri Kola Status: In Progress
---	--	---

- [27] Raymer, D. P. *Aircraft Design: A Conceptual Approach*. American Institute of Aeronautics and Astronautics, Inc, Reston, VA, 2018.
- [28] Roskam, J. *Airplane Flight Dynamics and Automatic Flight Controls*. DARcorporation, 1998.
- [29] Roskam, J. *Airplane Design - Part I: Preliminary Sizing of Airplanes*. 1997.
- [30] Coleman, G. *AIRCRAFT CONCEPTUAL DESIGN – AN ADAPTABLE PARAMETRIC SIZING METHODOLOGY*. Dissertation. University of Texas at Arlington, Arlington, TX, 2010.
- [31] Torenbeek, E. *Synthesis of Subsonic Airplane Design: An Introduction to the Preliminary Design of Subsonic General Aviation and Transport Aircraft, with Emphasis on Layout, Aerodynamic Design, Propulsion and Performance*. Delft University Press, Delft, 1976.
- [32] Gudmundsson, S. *General Aviation Aircraft Design: Applied Methods and Procedures*. Elsevier Science & Technology, Saint Louis, UNITED STATES, 2013.
- [33] Musielak, D., Seabridge, A., Radaei, M., Marshall, D. M., Fahlstrom, P. G., Gleason, T. J., Sadraey, M. H., Gregory, J. W., Liu, T., Tewari, A., Torenbeek, E., Farokhi, S., Yedavalli, R. K., CEng, G. D. P., Kluever, C. A., Young, T. M., Keane, A. J., Sóbester, A., Scanlan, J. P., Marqués, P., and Ronch, A. D. “Scramjet Propulsion.”
- [34] Junell, W. *Reverse Engineering the SR-71: Detailed Analysis of Vehicle Synthesis, Performance ,and Trajectory*. University of Texas at Arlington, Arlington, TX, 2023.
- [35] Austin Prior. *Analysis, Description, and Forecast of the SR-71*. University of Texas at Arlington, Arlington, TX, 2023.
- [36] Nguyen, P. *SR-71 Blackbird SR-71 Reverse Engineering Project*. University of Texas at Arlington, Arlington, TX, 2023.
- [37] Mohanty, E. *Reverese Engineering the SR-71 Blackbird*. University of Texas at Arlington, Arlington, TX, 2023.
- [38] Jo, S. *Reverese Engineering the SR-71 Blackbird*. University of Texas at Arlington, Arlington, TX, 2023.
- [39] Lockheed YF-12A. *National Museum of the United States Air Force™*. <https://www.nationalmuseum.af.mil/Visit/Museum-Exhibits/Fact-Sheets/Display/Article/195777/lockheed-yf-12a>[https%3A%2F%2Fwww.nationalmuseum.af.mil%2FVisit%2FMuseum-Exhibits%2FFact-Sheets%2FDisplay%2FArticle%2F195777%2Flockheed-yf-12a%2F](https://www.nationalmuseum.af.mil/Visit%2FMuseum-Exhibits%2FFact-Sheets%2FDisplay%2FArticle%2F195777%2Flockheed-yf-12a%2F). Accessed Mar. 5, 2023.
- [40] Carpenter, B., and Docent, U. Kelly’s Greatest Challenge – The Blackbirds Amazing Achievement – Visionary Tight Leadership. Washington/Northern Virginia, Nov 30, 2016.
- [41] Blakely, N. *Reverse Engineering The SR-71 by Penguin Supersonic Aero and Stability and Control*. University of Texas at Arlington, Arlington, TX, 2023.
- [42] Phillips, W. Aircraft Performance. In *Mechanics of Flight*, John Wiley & Sons, Inc., New Jersey, 2004, pp. 259–367.
- [43] Roskam, J. *Airplane Design Part VIII: Airplane Cost Estimation: Design, Development, Manufacturing and Operating*. Design, Analysis and Research Corporation (DARcorporation), 2015.
- [44] DePuy, W. E., Moyer, R., Palmer, P. R., McKinney, B. J., and Kreisel, G. R. *US Military Aircraft Cost Handbook*. ANALYTIC SCIENCES CORP, Reading, Massachusetts, 1983.
- [45] Woodford, S. *The Minimisation of Combat Aircraft Life Cycle Cost through Conceptual Design Optimisation*. Ph.D. Thesis. Cranfield University, Munich, Germany, 1999.
- [46] Koelle, D. E. *Statistical-Analytical Model for Cost Estimation and Economic Optimization of Launch Vehicles*. TransCostSystems, Liebigweg, Germany.
- [47] Boren, H. E. *DAPCA A Computer Program for Determining Aircraft Development and Production Costs*. RAND Corporation, Santa Monica, California, 1967.
- [48] Carichner, G. E., and Nicolai, L. M. Fundamentals of Aircraft and Airship Design: Volume 2 - Airship Design and Case Studies. In *Fundamentals of Aircraft and Airship Design: Volume 2 - Airship Design and Case Studies*, American Institute of Aeronautics and Astronautics, Inc., 2013, p. 963.
- [49] Hildebrandt, G. G., and Sze, M. *An Estimation of USAF Aircraft Operating and Support Cost Relations*. Publication N-3062-ACQ. RAND Corporation, Santa Monica, California, 1990, p. 78.
- [50] Hess, R., and Romanoff, H. P. *Aircraft Airframe Cost Estimating Relationships Study Approach and Conclusions*. RAND Corporation, Santa Monica, California, 1987.
- [51] Sforza, P. M. *Commercial Airplane Design Principles*. Elsevier Science, 2014.